Laser-driven fusion

Keith A. Brueckner and Siebe Jorna

KMS Fusion, Inc., Ann Arbor, Michigan 48106

The use of intense laser light to bring about thermonuclear reactions in a plasma is of considerable current interest. We present detailed analytical and computational studies which show the feasibility of laser-driven fusion. The required laser technology and the presently anticipated practical difficulties are discussed in outline.

CONTENTS

I. INTRODUCTION

The interest in lasers as a possible source of energy arises from the characteristics of pulsed energy release from a fuel pellet with no external confinement, for which the time available for thermonuclear reactions is determined by the time required for hydrodynamic motion in the pellet. This approach is, therefore, quite different from the quasi steady-state approach with magnetic field confinement which has been studied for about twenty years in laboratories in many countries. For a pulsed system, the time available is set by the pellet dimension and temperature. Crude considerations show that the time is of the order of 10^{-9} sec and the energy in the range of tens of kilojoules, giving a power requirement of millions of megawatts (although only for 10^{-9} sec). The only sources presently known which may yield such enormous peak powers are pulsed lasers (or possibly pulsed electron beams). This possible application of lasers was discussed about a decade ago by Basov (1963) and Dawson (1964), and in more detail by Daiber, Hertzberg and Wittliff (1966). Much work has since been devoted to a study of its feasibility (Nuckolls *et al.* 1972).

The theoretical and computational results reviewed in this paper predict that laser-driven fusion can be experimentally studied at the energetic breakeven level with lasers well within the state of the art. This offers the possibility of relatively early experimental study of the phenomena to test the critically important predictions of the theory. In addition, estimates of requirements for a practical power-producing reactor show that although the technological problems are substantial, no significant difficulty is anticipated in designing and building the necessary laser driver. The field has been studied intensively for a relatively short time; nevertheless, it was felt that there is now a need for a review which discusses the various aspects of laser fusion in quantitative detail, and which collates the widely scattered results of other work. We have chosen to concentrate on the theory of the laser-driven process and the presently anticipated difficulties. In an article of this size, it is clearly impossible to discuss every phenomenon that might occur in a laser–plasma system. We have, therefore, only discussed phenomena which we consider significant to laser-driven fusion. The experimental situation and the laser technology required for the experimental study of the various important phenomena will be briefly reviewed.

Although laser fusion is rapidly acquiring the status of an independent specialty, it is currently still a composite based on such diverse fields as plasma physics, statistical physics, hydrodynamics, nuclear physics, thermodynamics, and numerical analysis. This is reflected in the present treatment where we have found it convenient to separate the subject into four broad categories. In Sec. II, the basic energetic scaling laws of the fusion process are analyzed for an inertially confined DT pellet by traditional methods familiar in the controlled fusion field. This analysis, which is essentially a scaling law study,

exhibits clearly the critical parameters of the process. These are the coupling efficiency of the laser to the plasma, the density at which the plasma reacts, the initial temperature produced by the laser-driven heating processes, the temperature at which the plasma reacts following the start of the thermonuclear reactions, and the energy multiplication required for useful energy output. Each of these parameters can strongly affect the laser energy requirement (and hence the feasibility of the process) both for the early demonstration experiments and for the eventual development of economic power plants.

The effectiveness of the laser in heating the plasma is governed by the coupling mechanisms. These are discussed in Sec. III, together with an extensive review of laser-induced plasma instabilities and their potential benefits or drawbacks. A brief appraisal is also given of the experimental evidence for these instabilities, supplemented by results from numerical simulation studies. In Sec. IV, hydrodynamic compression is analyzed using a simple model which shows how an unavoidable inefficiency of energy transfer results. Section V presents the principal features of the hydrodynamics of shock compression and also considers in some detail the stability of pellet hydrodynamics and the problems of pellet preheat.

The discussions in Secs. II, III, IV, and V are largely analytic and are based on schematic models. The possible sources of difficulty which arise from the various laser–plasma and hydrodynamic instabilities are reviewed at length in these sections. Although substantial uncertainties exist in any description of these phenomena, an idealization of the process is of great interest since a complete calculation has shown that the laser-driven process, *in principle* at least, warrants further theoretical and experimental study. A highly useful idealization results from the assumption that the unstable processes do not significantly perturb the symmetry of the implosion and hence that calculations can be carried out with spherical symmetry in the motion. The major question of the laser–plasma coupling efficiency can be studied parametrically by the introduction of *ad hoc* corrections in describing laser–plasma interaction.

The basic characteristics of computer methods for studying the problem are given in Sec. VI. Section VII first provides numerical results for the ignition and burning sequences in compressed pellets and then presents some numerical results for complete implosion calculations. Section VIII comments briefly on the choice of laser wavelengths and laser characteristics. In Sec. IX, the results of this paper are summarized and a prognosis is given for the further development of laser fusion.

II. ANALYTIC ESTIMATES OF ENERGY PRODUCTION

A. Scaling laws

In this section, we analyze the scaling laws for energy requirements and fusion energy production using simplified models. This analysis is intended to clarify the dominant phenomena, which are somewhat obscured in complete computer studies.

The methods used in this section are intended to be only semiquantitative and hence in several instances we use approximations which are plausible without further discussion. In these cases the reader is invited to consider more accurate methods if increased precision is desired. We do not wish in this section to imply that quantitative results can be obtained by rather simple methods. Our purpose is pedagogical, to clarify the main features of the phenomena. We will return to the detailed computer results in Sec. VI, which also contains the equations of the computer code and summarizes the important features of this code.

The thermonuclear fuel which is most readily brought to reaction is deuterium–tritium. It reacts by the process

$$\begin{aligned} \mathrm{D} + \mathrm{T} &\rightarrow n + \alpha + W, \\ W &= 17.6\ \mathrm{MeV}\ . \end{aligned} \tag{2.1}$$

About 80% of this energy goes into the neutron and the balance to the 3.6 MeV α particle. The nuclear crosssection has a resonance near zero energy with the effect of the Coulomb barrier included, and it reaches a peak of about 5 b at 125 keV. According to Wandel *et al.* (1959), this yields an appreciable reaction rate at a temperature of several kilovolts (1 keV $= 1.16 \times 10^7\,^\circ$K). In contrast to the D–T reaction, the D–D reaction, producing $\mathrm{T} + p$ and $n + \mathrm{He}^3$ through two equally probable reactions has a reaction rate about a factor of 30 lower at several kilovolts, and hence is much harder to bring to the condition at which significant fusion energy is produced.

For DT fuel, the dimension, time scale, and laser energy requirement can be readily estimated for a specified level of multiplication of the laser energy by the fusion process. To obtain the appropriate relationship, we define an energy multiplication factor by

$$M = E_{\mathrm{fusion}}/E_{\mathrm{laser}}(\mathrm{output}), \tag{2.2}$$

and an efficiency for coupling of laser energy into the thermal energy of the DT

$$\varepsilon_L = E_{\mathrm{plasma}}(\mathrm{thermal})/E_{\mathrm{laser}}(\mathrm{output}). \tag{2.3}$$

The first factor M which measures over-all energy gain in a practical application depends on the external laser characteristics and on the system for converting laser energy into fusion energy. The second factor ε_L is determined by the laser–plasma interaction and by the mechanism of energy transfer into hydrodynamic motion and DT compression. The rate of fusion energy production is

$$\begin{aligned} (dE/dt)_{\mathrm{fusion}} &= (\tfrac{4}{3}\pi r^3) n_D n_T \overline{\sigma v}(\theta_i) W \\ &= (\tfrac{4}{3}\pi r^3)(n^2/4)\overline{\sigma v}(\theta_i) W, \end{aligned} \tag{2.4}$$

with $n = n_D + n_T =$ total ion density, and $\overline{\sigma v}$ the reaction rate averaged over the thermal ion distribution. The initial thermal energy is

$$E_{\mathrm{thermal}} = \tfrac{4}{3}\pi r^3 \tfrac{3}{2} n[\theta_e(0) + \theta_i(0)], \tag{2.5}$$

where θ_e and θ_i are, respectively, the electron and ion temperatures times Boltzmann's constant. To proceed, we first need an estimate of the ratio of the electron-to-ion temperature. The laser energy deposition is almost entirely to the electrons which subsequently heat the ions. In the absence of hydrodynamic and nonlinear effects, the energy transfer is by electron–ion collisions, and for Maxwellian distributions is given by the well-known equation

$$d\theta_i/dt = (\theta_e - \theta_i)/\tau_{\rm th}\,, \tag{2.6}$$

with the thermalization time according to Spitzer (1961)

$$\tau_{\rm th} = [3m_e m_i/8(2\pi)^{1/2} ne^4 \ln\Lambda](\theta_e/m_e)^{3/2}. \tag{2.7}$$

For the temperature and density range of interest we set $\ln\Lambda = 5$, and m_i equal to the average ion mass, giving

$$n\tau_{\rm th} = 5.0\theta_e^{3/2}\,10^{12}\,\text{sec cm}^{-3}. \tag{2.8}$$

with θ_e in keV. The ions and electrons reach the same temperature if the time available for the reaction is considerably greater than $\tau_{\rm th}$, giving the condition

$$\begin{aligned} nt &\gg 5.0\times10^{12}\theta_e^{3/2}\,\text{cm}^{-3}\,\text{sec} \\ &= 1.58\times10^{14}\,\text{cm}^{-3}\,\text{sec}, \end{aligned} \tag{2.9}$$

where $\theta_e = 10$ keV. For the moment, we assume that this condition is satisfied and set $\theta_e = \theta_i$ in Eq. (2.5). We will at the end of this section determine the conditions for which this assumption is valid.

For the case of weak heating, the temperature does not increase appreciably during the reaction, and the reaction constant in Eq. (2.4) can be evaluated at the initial temperature. Setting $\theta_e(0) = \theta_i(0) = \theta_0$ in Eq. (2.4) and Eq. (2.5), we find

$$\begin{aligned} E_{\rm fusion} &= \tfrac{4}{3}\pi r^3 n^2 \overline{\sigma v}(\theta_0) Wt, \\ E_{\rm thermal} &= 4\pi r^3 n\theta_0\,. \end{aligned} \tag{2.10}$$

The condition for energy multiplication is then

$$E_{\rm fusion} = (M/\epsilon_L) E_{\rm thermal} \tag{2.11}$$

giving

$$nt = (M/\epsilon_L)[12\theta_0/W\overline{\sigma v}(\theta_0)]. \tag{2.12}$$

Equation (2.12) now allows us to estimate the energy requirements. To relate the time to the pellet dimension, we use the time for a rarefaction wave to move from the surface to the center of the pellet,

$$t = r/v_{\rm sound}\,. \tag{2.13}$$

The sound velocity is

$$\begin{aligned} v_{\rm sound} &= v_0\theta^{1/2} \qquad \theta \text{ in keV}, \\ v_0 &= 3.5\times10^7\,\text{cm/sec}\,. \end{aligned} \tag{2.14}$$

The laser energy then is

$$\begin{aligned} E_L &= (1/\epsilon_L) E_{\rm thermal} \\ &= 4\pi(M^3/\epsilon_L^4 n_0^2)\theta_0[12\theta_0^{3/2} v_0/W\overline{\sigma v}(\theta_0)]^3. \end{aligned} \tag{2.15}$$

If the coupling efficiency ϵ_L is assumed to be independent of temperature, the laser energy given by Eq. (2.15) has a broad minimum at 10 keV. At this temperature

$$\begin{aligned} nt &= 5.7\times10^{13} M/\epsilon_L\,\text{cm}^{-3}\,\text{sec} \\ E_L &= (M^3/\epsilon_L^4)(n_s/n_0)^2\,1.6\text{MJ} \\ n_s &= 4.5\times10^{22}/\text{cm}^3, \qquad \text{(solid density)}\,. \end{aligned} \tag{2.16}$$

The nt product for $M/\epsilon_L \approx 2$ is the often quoted "Lawson condition" for energy breakeven to be reached (cf. Lawson, 1965). We note for $M/\epsilon_L = 2$, that the thermalization condition of Eq. (2.9) is not satisfied and the derivation of Eq. (2.12), therefore, not valid. We turn next to a further discussion of the conditions under which the assumption of thermalization is correct.

B. Direct laser heating of uncompressed spheres

The results of Eq. (2.16) show the strong dependence of the laser energy on the parameters M and ϵ_L, and on the pellet density. Similar results have been obtained by, among others, Krokhin (1965), Dawson (1964), Basov and Krokhin (1964), Caruso, Bertotti, and Guipponi (1966), Raizer (1965), Caruso and Gratton (1968), Mulser and Witkowski (1969), and Haught and Polk (1966), and have been the cause of much discussion on realistic values for the parameters. The laser requirement for $M = 1$ (fusion energy equal to thermal energy) and for $\epsilon_L = 1$ (perfect coupling) and for a pellet at solid density is 1.6 MJ with a pulse length of less than one nanosecond. This is a very formidable technological requirement, the largest present laser in this pulse length range giving about 600 J (Basov *et al.* 1972). The assumption of perfect coupling is, of course, highly optimistic under most conditions, since perfect coupling cannot occur unless no energy is reflected at the pellet surface or lost through blowoff in producing hot, low-density plasma that expands from the pellet surface. Coupling sufficient to heat the pellet at solid density is in fact possible only if the laser energy can easily penetrate into the pellet interior. This can occur if the laser wavelength is sufficiently short so the critical density of the plasma is slightly above the solid density. In this case, the laser light directly penetrates and heats the solid pellet, and essentially complete energy deposition can result. This requires a laser wavelength of about 1500 Å. For such a laser, the assumptions of $\epsilon_L = 1$ and uniform heating of the electrons are reasonable. Lasers in this wavelength region have not operated successfully with a significant energy output. The technological problems, therefore, are even more severe than those at wavelengths of $1\mu m$ or longer; work continues on development of lasers of this type.

Detailed numerical calculations relevant to the model of efficient pellet heating were made by Chu (1972) who assumed an energy source in the electrons of the pellet corresponding to classical laser heating, but did not study the actual problem of energy deposition. He did correctly follow the electron–ion energy exchange, the hydrodynamic motion of the pellet, and the fusion reactions. He showed that the estimate based on Eq. (2.15) was very optimistic, the correct laser energy requirement for breakeven being increased by a factor of about 600, or to about 1000 MJ. The large increase was due in part to numerical factors arising from the actual details of the hydrodynamic expansion, but was mainly due to the marked lag in the ion temperature increase since the time available during expansion is insufficient for thermal equilibration between the electrons and ions. In his calculation, no significant pellet compression could take place because the rapid heating throughout the pellet causes immediate pellet expansion.

Although conclusions showing laser energy requirements in the 1000 MJ range, similar to those obtained by

Chu, were being reached in 1969 and later in other studies, intensive analysis of the possible use of uncompressed pellets continued. Particular attention was given to the mechanism of thermal conduction for obtaining efficient laser coupling into a pellet at solid density, assuming that the pellet was overdense to the laser radiation and hence could not be directly heated by the laser. This possibility will now be reviewed in some detail.

C. Thermal conduction heating of uncompressed spheres

Published work by Shearer and Barnes (1970), Zakharov *et al.* (1970), and Bobin *et al.* (1971) showed that lasers can be used to heat thermonuclear fuel at densities well above the critical density, where direct laser penetration and deposition cannot occur. The heating is due to the supersonic penetration of the high-density region by a thermal conduction wave with energy carried by electrons. The very high thermal conductivity at thermonuclear temperatures allows the thermal wave to move ahead of the hydrodynamic rarefaction wave, causing strong heating of material which has not yet been affected by the rarefaction wave. In this region, which is both dense and hot, the rate of production of thermonuclear energy peaks. Ahead of the conduction wave, the material is compressed by a shock driven by the pressure in the laser deposition regions, but is still relatively cold. Behind the rarefaction wave, the material is hot, but the density drops rapidly due to hydrodynamic expansion. In this region, the rapid thermal conduction keeps the electrons nearly isothermal, but the ions cool by expansion, energy transfer by collision from the hot electrons being too slow to compensate for the cooling by expansion.

Let us summarize the main features of the phenomenon and exhibit the basic assumptions underlying the published work.

Consider a laser flux φ which brings the electrons in the surface of solid DT to a temperature θ_e, assumed to remain constant during the laser pulse. This temperature drives a conduction wave into the solid material, at number density n_0. The penetration distance $d_{\rm th}$ as a function of time t follows approximately on combining the energy conservation equation $\varphi t \approx n_0 \theta_e d_{\rm th}$ with Fourier's law $\varphi \simeq \kappa\theta_e/d_{\rm th}k$, where k is Boltzmann's constant, and κ is the conductivity, proportional to $\theta_e^{5/2}$ for a plasma. Thus,

$$d_{\rm th}^2 = \kappa_0 \theta_e^{5/2} t/n_0, \tag{2.17}$$

with θ_e measured in keV and

$$\begin{aligned} \kappa_0 &= 3\times 10^{27}\,\text{cm}^{-1}\cdot\text{sec}^{-1}(\text{keV})^{-5/2},\\ n_0 &= 4\times 10^{22}\,\text{cm}^{-3}. \end{aligned} \tag{2.18}$$

The exact solution of the thermal diffusion equation for a surface-heated planar medium gives a similar result for the depth of penetration of the thermal front as a function of time (see, for example, Krokhin, 1971; Bobin, 1971). A rarefaction wave also forms at the surface, penetrating at the sound velocity, with a penetration

$$\begin{aligned} d_H &= v_{\rm th}\, t\\ &= v_0[(\theta_e+\theta_i)/2]^{1/2}t \end{aligned} \tag{2.19}$$

where

$$v_0 = 3.5\times 10^7\,\text{cm/sec} \qquad (\theta \text{ in keV}).$$

The conduction wave penetrates more rapidly than the rarefaction wave until a penetration distance is reached such that

$$\dot d_{\rm th} \approx \dot d_H, \text{ or}$$
$$d_{\rm th} = (\kappa_0/2v_0 n_0)\left[\theta_e^{5/2}\Big/\left(\frac{\theta_e+\theta_i}{2}\right)^{1/2}\right]. \tag{2.20}$$

At this depth, the density may be assumed to be n_0; in the rarefaction wave, the density drops rapidly and becomes underdense to the laser wave, giving a region of laser-light absorption.

The thermal energy per unit area in the solid density heated region is

$$\epsilon_{\rm th} = \tfrac{3}{2} n_0 d_{\rm th}(\theta_e+\theta_i). \tag{2.21}$$

The fusion energy produced is

$$\epsilon_f = (n_0^2/4)(\overline{\sigma v})_i W d_{\rm th}\tau_R, \tag{2.22}$$

with the time of reaction τ_R given approximately by

$$\tau_R = d_{\rm th}/v_{\rm th} = \kappa_0\theta_e^{5/2}/v_0^2 n_0(\theta_e+\theta_i). \tag{2.23}$$

The ion temperature which determines the reaction rate $(\overline{\sigma v})_i$ is fixed by the electron temperature, the equilibration rate between electrons and ions, and the time the ions are subject at high density to the passage of the thermal wave. The equilibration rate given in Eq. (2.6) can be integrated approximately to give

$$\theta_i \cong (\tau_R/\tau_{\rm Eq.})(\theta_e-\theta_i). \tag{2.24}$$

This result together with Eq. (2.23) yields

$$\theta_i = 10^{10}[\kappa_0\theta_e(\theta_e-\theta_i)/v_0^2 n_0(\theta_e+\theta_i)]. \tag{2.25}$$

Using the values of the parameters given above and solving for θ_i gives

$$\theta_i = 0.315\theta_e. \tag{2.26}$$

Thus the ions only partially equilibrate, the ion temperature in the reaction zone remaining much lower than the electron temperature. Complete computer calculations of the structure of the conduction front give results very close to the simple analysis leading to Eq. (2.26).

Combining the above equations gives

$$\begin{aligned} \epsilon_{\rm th} &= \tfrac{3}{2}\frac{\kappa_0}{v_0}\theta_e^{5/2}\left(\frac{\theta_e+\theta_i}{2}\right)^{1/2}\\ &= 14\,600\theta_e^3\ \text{J/cm}^2\\ \epsilon_f/\epsilon_{\rm th} &= \tfrac{1}{6}(\overline{\sigma v})_i W[\kappa_0\theta_e^{5/2}/v^2(\theta_e+\theta_i)^2]\\ &= 0.646[10^{16}(\overline{\sigma v})_i]\theta_e^{1/2}, \end{aligned} \tag{2.27}$$

with $(\overline{\sigma v})_i$ evaluated at $\theta_i = 0.315\theta_e$. Examples are:

(1) $\theta_e = 10$ keV:

$$\begin{aligned} \theta_i &= 3.15 \text{ keV} \\ (\overline{\sigma v})_i &= 3.7 \times 10^{-18} \text{cm}^3/\text{sec} \\ \epsilon_{\text{th}} &= 14.6 \text{ MJ/cm}^2 \\ \epsilon_f/\epsilon_{\text{th}} &= 7.55 \times 10^{-2} \\ d_{\text{th}} &= 0.105\text{cm} \\ \tau_R &= 1.02 \text{ nsec} \end{aligned} \tag{2.27a}$$

(2) $\theta_e = 15$ keV:

$$\begin{aligned} \theta_i &= 4.72 \text{ keV} \\ (\overline{\sigma v})_i &= 1.3 \times 10^{-17} \text{cm}^3/\text{sec} \\ \epsilon_{\text{th}} &= 49.3\text{MJ/cm}^2 \\ \epsilon_f/\epsilon_{\text{th}} &= 0.325 \\ d_{\text{th}} &= 0.236\text{cm} \\ \tau_R &= 5.90 \text{ nsec} \end{aligned} \tag{2.27b}$$

(3) $\theta_e = 30$ keV:

$$\begin{aligned} \theta_i &= 9.45 \text{ keV} \\ (\overline{\sigma v})_i &= 1.0 \times 10^{-16} \text{cm}^3/\text{sec} \\ \epsilon_{\text{th}} &= 395\text{MJ/cm}^2 \\ \epsilon_f/\epsilon_{\text{th}} &= 3.54 \\ d_{\text{th}} &= 0.95\text{cm} \\ \tau_R &= 5.34 \text{ nsec}. \end{aligned} \tag{2.27c}$$

The absorbed laser energy required to produce the above results depends on the area illuminated. If the dimensions of the illuminated area are appreciably larger than the penetration depth, the lateral spreading of the conduction wave can be ignored. Thus, if the area is πd_{th}^2, the absorbed laser energy required is 505 kJ at 10 keV, 8.61 MJ at 15 keV, and 1120 MJ at 30 keV. The absorbed laser energy for which the fusion energy is equal to the absorbed laser energy is several tens of megajoules, similar to the estimate previously obtained for a uniformly heated sphere.

The inclusion of other effects, such as incomplete laser energy absorption, energy carried off in the blowoff layer penetrated by the rarefaction wave, divergence of the conduction wave, temperature and density gradients in the heated layer, all reduce the efficiency of the fusion process. Calculations by Basov and Krokhin (1970) indicated that for a pulse duration of 10^{-9} sec a laser energy of 10^5 J is required for breakeven. This is roughly consistent with the results in Eq. (2.27) only if the electron and ion temperatures are assumed to be the same and equal to 10 keV, for which condition Eq. (2.27) gives a thermal energy input of 14.6 MJ per cm^2 and a ratio of fusion to thermal energy of 0.65. Thus, if an illuminated area of 1mm^2 is assumed, as in the paper by Basov and Krokhin (1970), the laser energy requirement is 1.46×10^5 J. As has been pointed out by Haught *et al.* (1968) and Chu (1970, 1972), the inclusion of the other effects discussed above, however, increases this estimate by a factor in the range of 10^3 to 10^4.

D. Summary of results for uncompressed spheres

The uncompressed sphere heated efficiently by a short wavelength laser which can penetrate the solid density plasma or by thermal conduction by hot electrons requires approximately 1000 MJ laser input to reach a comparable fusion output. This prohibitive laser energy requirement is even further increased if the requirement of useful energy production is imposed. The energy multiplication M for practical application is determined by the efficiency of conversion of fusion energy into electrical energy and of electrical energy input to the laser into laser energy. Assuming a thermal-to-electrical conversion of 40% efficiency and 25% efficiency for the laser, the required energy multiplication for over all energy breakeven is equal to ten. Equation (2.27) shows that this increases the laser energy requirement by an additional factor of 10^3!

It is therefore clear that any expectation of producing useful fusion energy in the absence of compression is unrealistic. For a compressed sphere a new problem arises since the coupling efficiency ϵ_L to a compressed system becomes much less than unity. Results to be given later show that M/ϵ_L is, in fact, under the best conditions, equal to approximately 200, requiring that the Lawson condition be exceeded by a large factor. Under these conditions, the thermalization requirement of Eq. (2.9) is met. The large multiplication of the initial thermal energy by the fusion process, however, invalidates the assumption that the temperature remains constant during the reaction. We therefore turn next to an evaluation of the effects of compression and of fusion energy deposition on the preceding analysis. The problem of laser coupling is reviewed in detail in Sec. III and IV.

E. Uniform sphere with compression and self-heating

We now remove the assumption of no heating and return to Eq. (2.4) and Eq. (2.5), setting $\theta_e = \theta_i = \theta$. The heating equation then is

$$\begin{aligned} 3n(d\theta/dt) &= (dE/dt)_{\text{fusion, deposited}} \\ &= (n^2/4)\overline{\sigma v}(\theta) W_{\text{dep}}, \end{aligned} \tag{2.28}$$

with W_{dep} the part of the fusion energy W deposited in the fuel. The time available is determined by the temperature; to allow for the variation of sound velocity as the temperature increases, we change variable from t to $r(t)$ with dr/dt the sound velocity. Equation (2.28) then may be written

$$\int_{\theta_0}^{\theta_1} \frac{d\theta v_0 \theta^{1/2}}{\overline{\sigma v}(\theta) W_{\text{dep}}} = \frac{1}{12} \int_0^r n\, dr. \tag{2.29}$$

The ratio of fusion energy produced to initial thermal energy is

$$\frac{E_{\text{fusion}}}{E_{\text{thermal}}(0)} = \frac{W}{12\theta_0} \int_0^r n\, \overline{\sigma v}(\theta)\, dt,$$

which from Eq. (2.28) can be rewritten

$$\frac{E_{\text{fusion}}}{E_{\text{thermal}}(0)} = \frac{W}{\theta_0} \int_{\theta_0}^{\theta_1} \frac{d\theta}{W_{\text{dep}}(\theta)}. \tag{2.30}$$

The analysis may now be completed by an estimate of the energy deposited.

The deposition of energy by neutrons, due to the charged particle recoils, depends on the ratio of pellet size to neutron range. For 14 MeV neutrons, the neutron range in DT is approximately fifty times larger than the α-particle range at 5 keV electron temperature [see Eq. (2.33)]. Consequently, the α-particle heating dominates the initial ignition sequence. The neutron heating can become important for large pellets at high density. Simple estimates similar to those of this section show that this occurs in the megajoule energy input range for pellets with density of the order of 1000 grams/cm^3. This may be determined with sufficient accuracy for the present purpose by ignoring possible neutron deposition and accounting approximately for the α-particle energy. The plasma is relatively transparent to the α particles, particularly at high temperatures. The fraction of the energy deposited is approximately r/R_α for large R_α, and unity for $R_\alpha \to 0$. We interpolate roughly between these limits by assuming

$$\begin{aligned} &W_{\rm dep} = W_\alpha[r/(R_\alpha + r)] \\ &R_\alpha = \alpha\text{ - particle range} \\ &W_\alpha = \alpha\text{ - particle energy (3.6 MeV).} \end{aligned} \tag{2.31}$$

The α-particle range is determined by energy loss to electrons and to ions, the loss to electrons being dominant for electron temperatures below approximately 40 keV. In this temperature range (Sigmar and Joyce, 1971)

$$\frac{dE_\alpha}{dx} = -\frac{32\pi^{1/2}}{3} ne^4 \ln\Lambda \frac{E_\alpha^{1/2}}{\theta_e^{3/2}} \left(\frac{m_e}{m_\alpha}\right)^{1/2} \tag{2.32}$$

giving (cf. Hughes and Schwartz, 1958)

$$\begin{aligned} &R_\alpha = \lambda_0(\theta_e^{3/2}/n), \\ &\lambda_0 \cong 2 \times 10^{21}\,\text{cm}^{-2}, \qquad \theta_e \text{ in keV}. \end{aligned} \tag{2.33}$$

Thus the integral in Eq. (2.30) gives

$$\frac{E_{\rm fusion}}{E_{\rm thermal}(0)} = \frac{W}{\theta_0 W_\alpha} \int_{\theta_0}^{\theta_1} \left(\frac{\lambda_0 \theta^{3/2}}{rn} + 1\right) d\theta. \tag{2.34}$$

We now make the final approximation of this section and evaluate r and n at their initial values. This approximation neglects the hydrodynamic motion and fuel depletion during the burning of the DT. The depletion effect limits the energy multiplication M/ϵ_L to $W/6\theta_0$ = 3000 keV/θ_0. We use Eq. (2.3) for $E_{\rm fusion}/E_{\rm thermal}(0)$, and we set $W = 5W_\alpha$. The result is

$$\frac{M}{\epsilon_L} = \frac{2\lambda_0}{n_0 r_0 \theta_0}(\theta_1^{5/2} - \theta_0^{5/2}) + 5\frac{\theta_1 - \theta_0}{\theta_0}. \tag{2.35}$$

A similar approximation in Eq. (2.29) yields

$$\frac{v_0}{W_\alpha}\left(I_1 + \frac{\lambda_0}{n_0 r_0} I_2\right) = \frac{n_0 r_0}{12}, \tag{2.36}$$

with I_1 and I_2 defined by

$$\begin{aligned} I_1 &= \int_{\theta_0}^{\theta_1} \frac{\theta^{1/2}\, d\theta}{\overline{\sigma v}(\theta)}, \\ I_2 &= \int_{\theta_0}^{\theta_1} \frac{\theta^2\, d\theta}{\overline{\sigma v}(\theta)}. \end{aligned} \tag{2.37}$$

Equation (2.36) expresses $n_0 r_0$ as a function of θ_0 and θ_1 from which Eq. (2.35) gives M/ϵ_L. The corresponding laser energy requirement is

$$E_L = 4\pi(r_0^3/\epsilon_L) n_0 \theta_0. \tag{2.38}$$

From these results we readily obtain the case of weak heating, as given in Eq. (2.16), by going to the limit $\lambda_0 \to \infty$.

The temperature rise for small temperature increase, for $R_\alpha \gg r$, is

$$\theta_1 - \theta_0 = \frac{12 v_0}{25 W_\alpha \lambda_0} \left(\frac{M}{\epsilon_L}\right)^2 \frac{\theta_0}{\overline{\sigma v}(\theta_0)}. \tag{2.39}$$

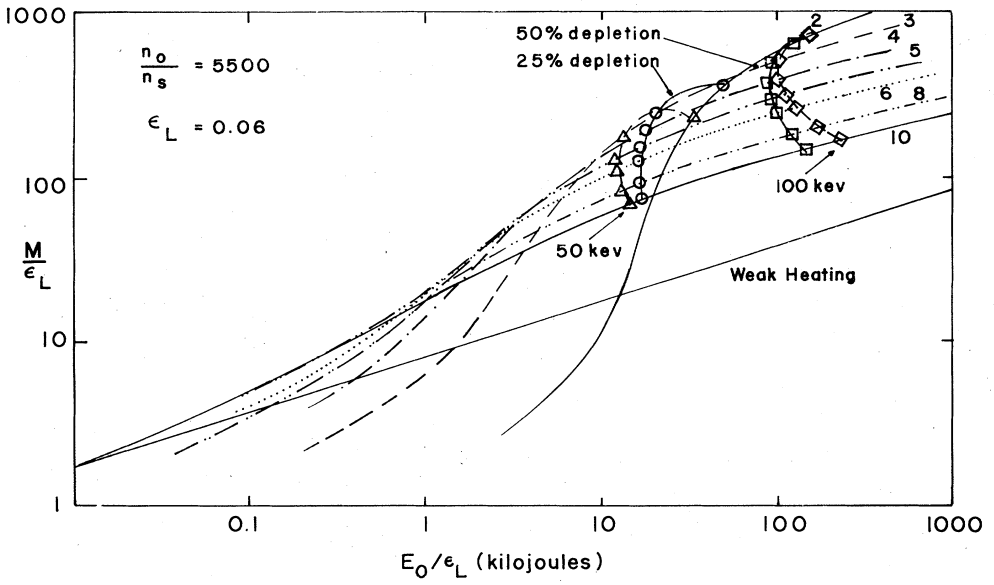

FIG. 1. Analytic results for laser energy as a function of M/ϵ_L, based on Eqs. (2.35), (2.36), and (2.37), for compression ratio of 5500, and laser coupling efficiency ϵ_L of 0.06. The points of 25% and 50% fuel depletion and of 50 and 100 keV final temperature are indicated.

At 10 keV

$$\theta_1 - \theta_0 = 0.233\left(\frac{M}{\epsilon_L}\right)^2 \text{keV} . \tag{2.40}$$

Thus appreciable heating does not occur for M/ϵ_L of order unity. For M/ϵ_L equal to 4, however, the temperature rise is about 4 keV, and the reaction rate has about doubled. This already gives substantial correction to the energy requirement; the correction is clearly very large for large energy multiplication. Under such conditions evaluation of Eqs. (2.35) and (2.36) is necessary. The results are given in Fig. 1, for several values of the initial temperature θ_0. The very large departure of the correct result from the weak heating approximation is apparent. The laser energy requirement drops by a factor of 400 for the ratio of fusion energy to initial energy M/ϵ_L equal to 100. This large drop in laser energy requirement results from the DT temperature reaching 30–50 keV where the DT reaction rate has a maximum, increasing by a factor of about 10 over the rate at 10 keV, and a factor of 100 over the rate at 4 keV. The laser, therefore, is required only to provide the relatively small ignition energy of the fuel which subsequently, through self-heating, reaches the optimum temperature range for efficient fusion energy release. The optimum initial temperature changes with energy multiplication; for small values of M/ϵ_L, the optimum is at about 10 keV, as previously pointed out for the weak heating case. For larger values of M/ϵ_L, the optimum temperature drops well below 10 keV, reaching 2 keV for M/ϵ_L greater than about 350. The achievable minimum, which in practice is of interest, depends on other loss processes which prevent heating, the most obvious being radiation loss by bremsstrahlung. The total free–free emission rate per unit volume exceeds the α-particle heating rate below about 4 keV, which gives a lower limit for the occurrence of self-heating, if the DT is transparent to the radiation. The condition for transparency is that the volume emission not exceed the surface blackbody radiation, or $V\epsilon_{ff} \leqq 4\pi r^2 \sigma T^4$, with ϵ_{ff} the emissivity, and σ the Stefan–Boltzmann constant. Using (Allen, 1955)

$$\begin{aligned} &\epsilon_{ff} = 4.9 \times 10^{-24} n^2 \theta^{1/2} (\text{erg/cm}^3\,\text{sec}), \qquad \theta \text{ in keV}, \\ &\sigma T^4 = 1.05 \times 10^{24} \theta^4 (\text{erg/cm}^2\,\text{sec}), \end{aligned} \tag{2.41}$$

we find the transparency condition

$$rn^2 \leqq 6.43 \times 10^{47} \theta^{7/2} \text{cm}^{-5} . \tag{2.42}$$

Combining this with Eq. (2.12), using $t = r/v(\theta)$, and evaluating the resulting expression at 4 keV, we obtain that for transparency

$$n/n_s \leqq 7.75 \times 10^4 (\epsilon_L/M). \tag{2.43}$$

This shows that the fuel is transparent unless very highly compressed under conditions of large energy multiplication, i.e., large M/ϵ_L. However, under the condition of interest for laser fusion, with high compression and large values of M/ϵ_L, the DT can become opaque to bremsstrahlung, and fuel heating can occur for temperatures considerably lower than 4 keV. Thus, the energy requirement given by Eq. (2.41) and Fig. 1 can be used for the lower values given for θ_0. The exact treatment of the radiation loss requires more careful analysis of the radiation problem.

F. Nonuniform compressed sphere with self-heating and propagation

In the preceding subsection (II.E), the effect of self-heating on fusion energy production was analyzed using a simple model of the processes of energy deposition and hydrodynamic expansion. We next evaluate an extremely important effect which occurs in a sphere with nonuniform initial conditions. The case of practical interest which arises is a result of shock convergence in a compressed sphere. This produces a sufficiently high central temperature to cause central ignition of the DT fuel, surrounded by relatively cold fuel in which the ignition condition is not met. In this case, the energy produced in the ignited and burning central region of the fuel, which is only partially deposited in this fuel region, can heat the surrounding cold fuel sufficiently for laser ignition to occur. This process leads to the formation of a spherically expanding burning wave which can propagate throughout the fuel causing complete ignition. The energy required to initiate the burning process is then substantially reduced from the requirement for uniform ignition.

We analyze here the condition for spherical propagation using a relatively simple model which illustrates the essential features of the process. In Sec. VII we return to the results of detailed computer studies.

The spherical expansion of the burning region of the fuel results from energy escaping from the burning fuel which is deposited in the adjacent cold layers of fuel. The energy loss can result from hydrodynamic expansion which follows the rapid pressure buildup in the ignited and burning fuel, from electron thermal conduction, or from energy deposition by the reaction products escaping from the fuel. The thermal conduction is subsonic for the temperature ranges of interest in the ignition and propagation phase of the burning front, provided that the fuel density is of the order of magnitude of 10^3gm/cm^3. The latter process usually dominates, the propagation of the burning front being sufficiently supersonic to advance more rapidly into the cold fuel than the hydrodynamic disturbance from the pressure increase of the thermal conduction front. The rate of advance of the burning front then follows from energy conservation, ignoring the hydrodynamic motion. The rate of energy production in a uniformly burning region at density n_0 is

$$\dot{U}_f = \tfrac{4}{3}\pi r^3 \overline{\sigma v} W_\alpha (n_0^2/4), \tag{2.44}$$

ignoring the neutron energy which is only weakly deposited in the burning region until the region increases in size and becomes an appreciable fraction of the neutron mean free path. The rate of change of internal energy in the expanding region, assuming negligible energy in the cold fuel and uniform density, is

$$(d/dt)(\tfrac{4}{3}\pi r^3 n_0 \theta_0) = (4\pi/3) n_0 r^3 \dot{\theta} + 4\pi n_0 r^2 \theta \dot{r}. \tag{2.45}$$

Energy conservation therefore gives for the propagation velocity of the burning front

$$\dot{r} = (n_0 \overline{\sigma v} W_\alpha / 12\theta_0) r - \tfrac{1}{3} r(\dot{\theta}_0/\theta_0). \tag{2.46}$$

The temperature in the burning fuel increases rapidly

from the α-particle heating until the increase in α-particle range with increasing electron temperature causes the α particles to escape into the surrounding cold fuel. The consequence is that the temperature adjusts itself so that the α-particle range is approximately equal to the radius of the burning region. Thus

$$r \cong R_\alpha = \lambda_0 \theta_0^{3/2}/n_0. \tag{2.47}$$

This equation breaks down if the electron temperature exceeds roughly 40 keV, the contribution of the ions no longer being negligible. The propagation of the burning front then is changed and a more detailed analysis is required. The computer analyses described in Sec. VI and VII are, of course, essential to follow the propagation quantitatively. Equation (2.47) shows that

$$\dot{\theta}_0/\theta_0 \cong \tfrac{2}{3}(\dot{r}_0/r_0). \tag{2.48}$$

The ratio of the velocity of the burning front to sound velocity, $v_s = v_0\theta^{1/2}$, is therefore

$$\dot{r}/v_s \cong 3\overline{\sigma v} W_\alpha \lambda_0/44 v_0. \tag{2.49}$$

With the values previously given for v_0 and λ_0, Eq. (2.49) gives

$$\dot{r}/v_s = 1.37(10^{16}\,\text{sec/cm}^3)\overline{\sigma v}. \tag{2.50}$$

The burning front advances supersonically ($\dot{r}/v_s \approx 2$), therefore, if the reaction rate is about $2 \times 10^{-16}\,\text{cm}^3/\text{sec}$ which occurs at 15 keV. At a lower temperature the hydrodynamic expansion dominates, and additional energy production in the burning region is required to maintain energy balance. At a higher temperature the burning front becomes strongly supersonic, $\dot{r}$ reaching a peak of about $10v_s$ at temperatures between 40 and 50 keV. The front also accelerates further as the neutron heating becomes important.

We now use the preceding results for the condition for supersonic propagation of the burning front. To determine the condition for this required temperature of 20 keV or greater to be reached in a central region of radius r_0 and density n_0 initially heated to θ_0, we use the results of Sec. II C. Equation (2.36) gives the condition

$$n_0 r_0 = \frac{6v_0}{W_\alpha}\left[I_1 + \left(I_1^2 + \frac{W_\alpha \lambda_0 I_2}{3v_0}\right)^{1/2}\right]. \tag{2.51}$$

Evaluating this at $\theta_0 = 4$ keV and $\theta_1 = 2$ keV, we obtain

$$(n_0/n_s)r_0 = 2.81. \tag{2.52}$$

The initial thermal energy to produce central ignition then is

$$\begin{aligned} E_{\text{th}} &= 4\pi n_0 r_0^3 \theta_0 \\ &= 7.99 \times 10^6 (n_s/n_0)^2\,\text{kJ}. \end{aligned} \tag{2.53}$$

The initial energy in the rest of the fuel which is ignited by the expanding burning wave is determined by the temperature and density. The minimum energy is given by the degeneracy energy of the electrons if the temperature is much less than the degeneracy temperature. The degeneracy energy of fuel with radius R is

$$\begin{aligned} E_{\text{deg}} &= \tfrac{4}{3}\pi R^3 n_0 \epsilon_{\text{deg}}\,, \\ \epsilon_{\text{deg}} &= 2.68(n_0/n_s)^{2/3}\ \text{ev/electron}\,. \end{aligned} \tag{2.54}$$

Thus

$$E_{\text{deg}} = 80.5 R^3 (n_0/n_s)^{5/3}\,\text{kJ}. \tag{2.55}$$

After ignition, the fuel burns at a temperature of 40–150 keV, depending on the dimension of the fuel. The fuel depletion is determined in the absence of hydrodynamic motion by

$$\dot{n} = -\overline{\sigma v}(n^2/2), \tag{2.56}$$

giving

$$n/n_0 = 1/\left(1 + \frac{\overline{\sigma v}}{2} n_0 t\right). \tag{2.57}$$

The fusion yield is

$$\begin{aligned} E_f &= \frac{4}{3}\pi R^3 (n_0 - n)\frac{W_{\text{fus}}}{2}, \\ &= \frac{4}{3}\pi R^3 \frac{n_0^2}{4} W_{\text{fus}} \frac{\overline{\sigma v} t}{1 + n_0 \frac{\overline{\sigma v}}{2} t}. \end{aligned} \tag{2.58}$$

For the time t we assume the hydrodynamic disassembly time

$$t = R/v_s(\theta_{\text{burn}}) \tag{2.59}$$

and assume burning at 80 keV for which $v_s = 3.47 \times 10^8\,\text{cm/sec}$ and $\overline{\sigma v} \cong 10^{-15}\,\text{cm}^3/\text{sec}$. The result is

$$E_f = \frac{1.75 \times 10^7 (n_0/n_s)^2 R^4}{1 + 0.0648 R n_0/n_s}\,\text{kJ}. \tag{2.60}$$

For fixed compression ratio, Eq. (2.52) and Eq. (2.55) determine R as a function of the initial internal energy. Equation (2.60) then determines the fusion yield. Results are given in Fig. 2 as a function of initial internal energy for several values of the compression. At low initial energy the maximum yield ratio occurs for high compression. The optimum drops for large initial energy for which the ignition energy is small compared with the degeneracy energy, leading to lower compression requirements. For initial internal energies in the one to ten kilojoule range, the energy multiplication for compressions of 3×10^3 to 10^4 is several thousand.

III. LASER PLASMA COUPLING

A. Classical coupling

The laser coupling efficiency as defined earlier is the combined efficiency of the energy deposition from the laser beam into the DT plasma and the subsequent energy transfer from the laser deposition region into the dense reacting region of the DT pellet. These problems can clearly be treated separately since the direct laser absorption may be of order unity without necessarily implying that the energy absorbed is transferred efficiently to the dense pellet.

The laser light incident on solid DT interacts with the free electrons which then cascade rapidly, giving a plasma at solid density which, as the ionization passes a few

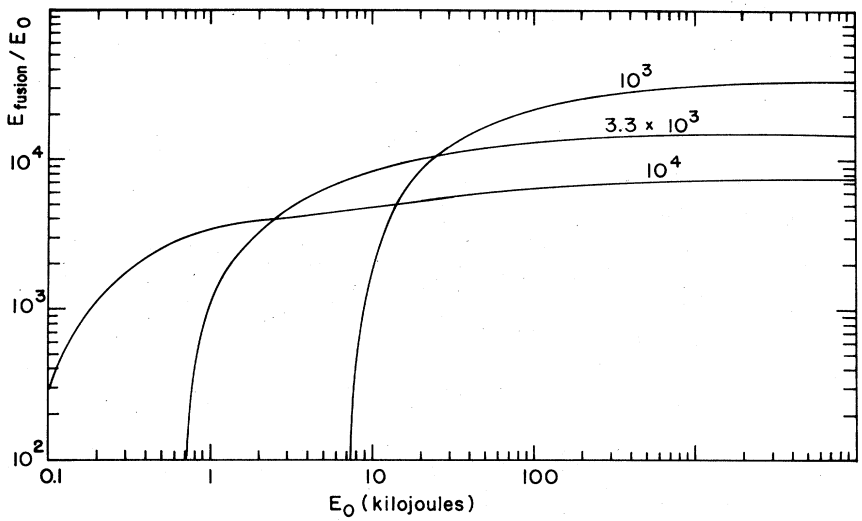

FIG. 2. Analytic estimate of fusion energy production in cold DT fuel ignited by a spherically propagating burning wave. Eq. (2.53) gives the ignition energy, Eq. (2.55) the degeneracy energy, and Eq. (2.60) the fusion energy. The initial energy E_0 is the sum of the ignition and degeneracy energy. The laser energy required to give this initial energy depends on the efficiency of laser energy deposition and of hydrodynamic transfer to the compressed fuel, and typically is a factor of ten to twenty larger than E_0. The curves are labeled by the compression ratio relative to solid DT (0.19 gm/cm³).

percent, becomes opaque to the laser radiation. The laser flux, then, is mostly reflected at the initial density discontinuity, the relatively low absorption being due to the penetration of the laser wave into the overdense plasma a distance of the order of the laser wavelength in the plasma. At one micron wavelength, and one kilovolt temperature, a fraction of one percent of the laser energy is absorbed at the solid surface. The surface temperature rises rapidly and a thermal conduction wave starts to penetrate the dense plasma. The resulting temperature gradient leads to a high pressure gradient and a hydrodynamic rarefaction wave also starts to move into the heated surface. The high thermal conductivity in the hot plasma maintains nearly isothermal conditions in the expanding plasma which expands from the overdense surface. Further absorption can now take place because of the increased amount of plasma at densities below the critical density. The depth of the isothermal layer becomes of the order of the initial sphere radius for a 1mm sphere and a temperature of a few kilovolts in about 1 nsec. The effective depth then increases only slowly with time, because of the spherical divergence of the plasma expansion. The general features of the early stages of energy deposition, plasma motion, and hydrodynamic shock formation are shown schematically in Fig. 3 and 4.

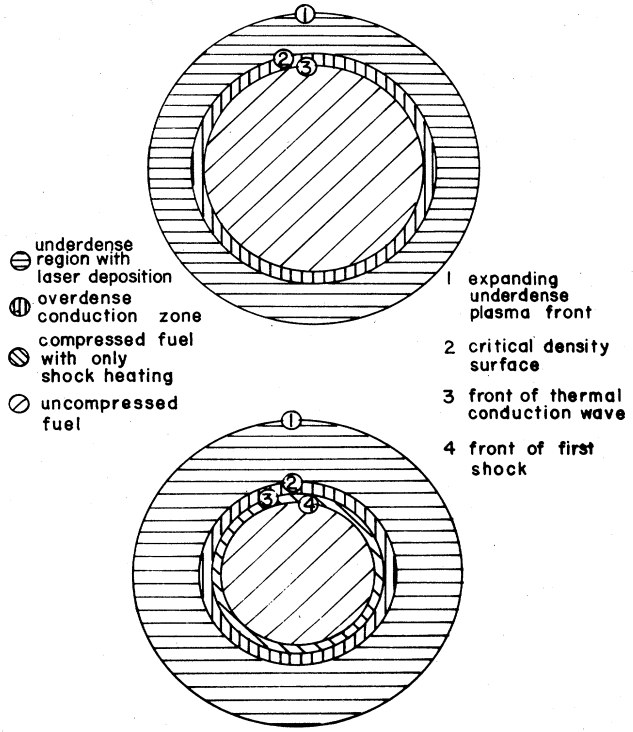

FIG. 3. A view of a fusion fuel quantity after formation of an underdense absorbing zone with the first shock not yet separated from the thermal point.

FIG. 4. A view of an intermediate stage in implosion with the first shock well separated from the thermal conduction front.

The classical laser energy deposition is the result of absorption of energy in the radiation field by electrons during electron–ion collisions. The absorption coefficient for this free-electron–free-electron transition or inverse bremsstrahlung is (cf. Heitler, 1954)

$$k_{ff} = 4.97 g Z^2 n_e n_i / (n_c^2 \lambda_\mu^2 \theta_e^{3/2}), \tag{3.1}$$

where the electron temperature θ_e is in keV, the laser wavelength λ_μ in μm, and the critical density

$$n_c = 10^{21} \lambda_\mu^{-2} \text{ cm}^{-3}. \tag{3.2}$$

The factor g which distinguishes Eq. (3.1) from Kramers' semiclassical result is a quantum mechanical correction introduced by Gaunt (1930) and ranges from 5 to 10 for laser-produced plasmas. For a DT pellet and 1μ radiation, the absorption coefficient at the critical density, where most of the energy is deposited, is about equal to $30/\theta_e^{3/2}$. Thus a pellet with an absorbing layer of a few hundred microns depth at $n_e \approx n_c$ will absorb laser energy strongly only for θ_e less than about 1 keV. For higher temperatures, the classical absorption drops rapidly. Comparison of the loss due to bremsstrahlung with that due to blackbody radiation, $I_{bb} = 5.7 \times 10^{-5} T^4$ ergs cm^{-2} sec^{-1}, shows further that the latter loss mechanism is negligible for laboratory-sized plasmas; the plasma is optically thin.

In addition to the classical absorption process, it is now believed, on the basis of intensive theoretical work,

computing studies, and limited experimental evidence, that strong nonclassical absorption occurs for laser power flux densities in excess of 10^{11} or 10^{12} watts/cm^2. The processes which may give rise to this will now be reviewed in detail.

B. Parametric excitation of instabilities

The parametric excitation of plasma instabilities by intense coherent light has been the subject of intensive study over the past eight years. The concept of parametric amplification dates back to Lord Rayleigh (1883) and subsequently has found extensive application in electronic devices (Louisell, 1960) and nonlinear optics (Shen and Bloembergen, 1965). Its more recent application to laser-produced plasmas has led to the prediction of a large number of possible plasma instabilities. Some lead to anomalous electron and ion heating; others to the scattering of electromagnetic energy out of the plasma. These collective phenomena are therefore of paramount importance in laser-driven fusion feasibility studies; and their effect on plasma heating must be taken into account over and above classical collisional heating (inverse bremsstrahlung), particularly as the latter process becomes ineffective at high temperatures.

The possibility of a parametric plasma instability was first noted by Silin (1964), and subsequently by DeBois and Goldman (1967). Silin's analysis was based on the hydrodynamic equations for a cold plasma. He ignored the effect of pressure gradients, damping, and coupling to the ion–acoustic wave. These deficiencies were overcome by DuBois and Goldman's Green's function analysis which demonstrated that coupling of the excited high-frequency Langmuir wave to the low-frequency ion-acoustic wave led to the lowest threshold for the parametric instability. The calculation of Lee and Su (1966) verified that these results could also be obtained from a fluid model with phenomenological damping constants. In yet another approach, Jackson (1967), in a kinetic theory treatment based on the Vlasov equation, recovered the results derived by the Green's function and hydrodynamic techniques for the growing ion-acoustic and electron plasma waves. This calculation also predicted the excitation of two unstable plasma modes with frequencies near the electron plasma frequency when allowance was made for the spatial variation of the pump field. Thus, we reach the paradoxical conclusion that calculations based on the fluid model (collision dominated) and the Vlasov equation (collisionless) yield essentially the same results for the growth rates and thresholds of the plasma instabilities, so long as dissipation in the continuum theory is treated microscopically. Nishikawa (1968) developed a general framework for the parametric interaction of electromagnetic waves with plasmas, illustrating his results by a comparison with the experiment of Stern and Tzoar (1966). He also drew attention to a purely growing mode, the oscillating two-stream instability, which can be excited in the dense-to-superdense regions of the plasma.

Most of the above studies are restricted to the dipole or long wavelength approximation and thus refer only to instability heating of electrons and ions near the critical surface, where the wavelength of the pump greatly exceeds the electron excursion distance. In a recent avalanche of publications, brought about by increased interest in laser-driven fusion, a numer of authors have investigated the excitation of unstable modes in the underdense region of a homogeneous plasma. Gorbunov (1968), utilizing one-dimensional fluid and kinetic descriptions, calculated thresholds and growth rates for backward stimulated Brillouin scattering (SBS) in the weak and strong coupling limits. Briefly, the incident electromagnetic field induces electron oscillations through the Lorentz force. The electrons are initially driven along the electric field vector but then develop a longitudinal component through the $V \times B$ interaction. Due to their large mass, the ions do not respond directly to the driving beam. Thus, local charge imbalances are generated which tend to be restored to neutrality by the opposing Coulomb interaction. On a macroscopic scale, the density oscillations are coupled to the pump field by the electrostrictive force density which varies essentially as the gradient of the intensity. For suitable phase matching between the incident and scattered waves, growth is induced in slowly moving density waves above a threshold intensity determined by Langmuir and acoustic wave dissipation. This instability can be excited in the underdense region of the plasma, resulting in a partially reflecting induced dielectric mirror which can lead to substantial reflection of the incident radiation, thereby possibly seriously reducing the fraction of laser energy which reaches the critical density surface.

By a similar process, the nonlinear wave mixing can also lead to the excitation of a high-frequency plasma wave. This stimulated scattering of the light wave by a Langmuir wave, or stimulated Raman scattering (SRS), can, as will be shown later, only occur at densities less than one-fourth the critical density, which constitutes a kind of critical surface for SRS. In a homogeneous plasma it has a lower threshold than SBS, although it is more readily quenched by macroscopic density gradients. Nevertheless, simulation experiments have shown that, as for SBS, back-scattered SRS poses a serious threat to laser-driven fusion by heating the electrons in the corona and correspondingly diminishing the laser energy deposition in the bulk of the plasma.

The instabilities discussed hitherto may also conveniently be thought of as the induced decay of an incident photon into various elementary excitations. Thus the "parametric decay" instability corresponds to the decay of a photon into a plasmon and phonon. Further possibilities are photon $\rightarrow$ plasmon + plasmon, or $\rightarrow$ plasmon + photon (SRS), or $\rightarrow$ photon + phonon (SBS). In the linearized theory, each of these processes modifies the dispersion function differently.

All of the studies referred to above suffer from the major defect that they are based on an oversimplified analysis of the linearized dispersion relation in which no allowance is made for spatial gain. It is well known that this yields information only on the possible excitation of instabilities and not on their character, i.e., whether they are convective or absolute. This knowledge is, of course, of great importance in determining meaningful thresholds for unstable modes in an expanding plasma. Without it we could not determine the time spent by the instability in the interaction region, or the effective interaction length.

The analysis of the dominant instabilities in a laser-driven plasma will therefore be preceded by a brief recapitulation of the salient features of instability analy-

sis, developed principally by Sturrock (1958), Fainberg, Kurilko, and Shapiro (1961), Polovin (1961), and Bers and Briggs (1963). We adopt the linearized two-fluid hydrodynamical equations supplemented by Maxwell's relations, subject to the conditions that the electron excursion length is much smaller than the minimum transverse length over which there is a change in the ion density. Dissipation effects are described by phenomenological damping constants. Temperature gradients are ignored, an assumption which is in reasonable agreement with computer studies for laser-produced plasmas. Finally some calculations will be reproduced which attempt to allow for macroscopic density gradients.

C. Instability analysis

A problem that often arises in a linearized theory is solving the equation

$$D[-i\nabla, i(\partial/\partial t)]u(\mathbf{r}, t) = S(\mathbf{r}, t), \tag{3.3}$$

where $S(\mathbf{r}, t)$ is the source function. For an infinite system, utilization of Fourier transforms and the Green's function formalism reduces this to evaluating the double Fourier integral (in one dimension)

$$u(z, t) = \iint_{-\infty}^{\infty} \exp[i(kz - \omega t)]\frac{\bar{S}(k, \omega)}{D(k, \omega)} dk\, d\omega, \tag{3.4}$$

where $\bar{S}(k, \omega)$ is the space–time Fourier transform of S. To simplify the argument we assume that the source function is of finite spatial and temporal extent so that S contributes no singularities—in fact, for asymptotic considerations we may as well take S to be a δ function so that $\bar{S}(k, \omega) = 1$. The dispersion function $D(k, \omega)$ is, of course, just the reciprocal of the Fourier transform of the Green's function.

The dispersion relation $D(k, \omega) = 0$ expresses k (or ω) as a function of ω (or k) which usually has many branches. These may be used to determine whether temporally unstable modes, Im $\omega > 0$ for real k, or spatially unstable modes, Im $k < 0$ for real ω, can be excited. They do not, however, provide the information about the pulse shape of a growing disburbance required for applying infinite medium results to finite systems. The integral in Eq. (3.4) must then be evaluated approximately for large t. To satisfy the causality condition, the ω contour is to be chosen such that it passes above all solutions of the dispersion equation. In the limit of large t, the dominant contribution to the integral is that due to the singularity with max Im (ω). Since it is always possible to choose a reference frame moving at a speed, V, say, in which a convective instability is absolute, it is convenient to make the Galilean transformation $z = Vt$, or $\omega = \omega - Vk$. Integrating first over ω by the Cauchy residue theorem, we reduce Eq. (3.4) to

$$u(Vt, t) = 2\pi i \sum_r \int_{-\infty}^{\infty} \left[\frac{\exp(-\tilde{\omega}t)}{\partial \tilde{D}/\partial \tilde{\omega}}\right]_{\tilde{\omega}=\tilde{\omega}_r(k)} dk, \tag{3.5}$$

where $\tilde{D}(k, \tilde{\omega}) = D(k, \tilde{\omega} + Vk)$, and the summation is over the poles $D[k, \omega_r(k)] = 0$. The k integration can be carried out by the method of steepest descents by deforming the path of integration such that it passes through the saddle point(s) given by $\partial \tilde{D}/\partial k = 0$. This imposes the condition that the double root in the k plane must have resulted from the coalescing (pinching) of roots which for Im $\omega \to -\infty$ lie on opposite sides of the real axis. Physically, this means that it should always be possible to apply a spatial impulse whose growth rate exceeds that of any unstable mode in the system, so that the resulting waves decay away from the origin.

In sum, the instability analysis requires solving the coupled equations

$$D(k, \omega) = 0, \tag{3.6}$$

$$\partial D/\partial k + V(\partial D/\partial \omega) = 0, \tag{3.7}$$

for the untransformed variables k, ω; and the condition for an absolute instability in a stationary system is that the "frame" velocity V be zero. Typically the dependence of growth rate on V varies with the coupling to the driving force as in Fig. 5. Clearly, the threshold for the convective instability (P_1) is generally lower than that for the absolute instability which grows throughout the system: P_2 for a medium expanding at speed s, P_3 for a medium at rest. This distinction will turn out to lead to significantly higher thresholds for plasma instabilities than those previously quoted in the literature.

The practical application of this prescription is often quite involved, and the work of Sturrock (1958) and Briggs (1964) should certainly be consulted for further details. One method for solving Eqs. (3.6) and (3.7), developed by Hall and Heckrotte (1968), starts with the determination of max Im (ω) for real k from Eq. (3.6), and reduces the problem of determining the dependence of growth rate on "observer" speed V to the solving of coupled first-order differential equations. We have adopted instead the more direct approach of satisfying the equation

$$|D|^2 + \mu\left|\frac{\partial D}{\partial k} + V\frac{\partial D}{\partial \omega}\right|^2 = 0, \tag{3.8}$$

by a powerful minimization routine based on a method described by Powell (1964). It will be noted that the solutions of this equation satisfy Eqs. (3.6) and (3.7) simultaneously. The parameter μ is adjusted to weight equally the dispersion function and its derivative. This procedure has the practical advantage of being self-contained and obviates the necessity for a separate search for the zeros of D.

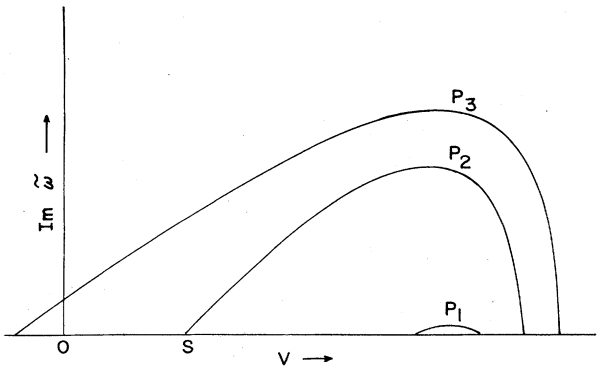

FIG. 5. Typical variation of temporal gain with "observer" speed V, comparing the levels of excitation P for convective and absolute instabilities.

D. Linearized plasma equations

We will write the basic equations such that all special cases to be discussed subsequently are included. Gravitational effects, macroscopic temperature, and density gradients are ignored. Further, the plasma is assumed to be of infinite extent, fully ionized, and macroscopically neutral, containing on the average n_0 electrons and ions per cm^3. Damping terms are inserted phenomenologically: their values are to be obtained from microscopic kinetic theory (cf. Oster, 1960) and include collisional as well as Landau damping.

In the fluid model, the physical parameters of a laser-driven plasma vary with an applied electromagnetic field according to the following conservation equations of hydrodynamics (cf., for example, Spitzer 1961): The momentum equation is

$$\left(\frac{\partial}{\partial t} + 2\Gamma_\mu + \mathbf{V}_\mu \cdot \nabla\right)\mathbf{V}_\mu = \frac{e_\mu}{m_\mu}\left(\mathbf{E} + \frac{\mathbf{V}_\mu}{c} \times \mathbf{H}\right) - \frac{\nabla p_\mu}{m_\mu N_\mu} \tag{3.9}$$

and the matter equation is

$$\partial N_\mu/\partial t = -\nabla \cdot (N_\mu \mathbf{V}_\mu) \tag{3.10}$$

in which the subscript μ refers to the electron or ion species, Γ_μ is a phenomenological damping factor which in general includes collisional as well as Landau damping, $\mathbf{V}_\mu$ is the particle velocity, e_μ and m_μ the particle charge and the particle charge and mass, respectively, P_μ the hydrodynamic pressure, and N_μ the number density of particle μ. The change in the plasma parameters induced by the incident radiation alters the current density $\mathbf{j}$ which drives the electric and magnetic fields $\mathbf{E}$ and $\mathbf{H}$ according to the Maxwell equations. In Gaussian units,

$$\nabla \times \mathbf{E} = -1/c(\partial \mathbf{H}/\partial t), \tag{3.11}$$

$$\nabla \times \mathbf{H} = (1/c)(\partial \mathbf{E}/\partial t) + (4\pi/c)\mathbf{j}, \tag{3.12}$$

$$\nabla \cdot \mathbf{H} = 0, \tag{3.13}$$

$$\nabla \cdot \mathbf{E} = 4\pi \sum_\mu e_\mu N_\mu, \tag{3.14}$$

where

$$\mathbf{j} = \sum_\mu e_\mu N_\mu \mathbf{V}_\mu. \tag{3.15}$$

In the small signal approximation these equations may be solved iteratively by expressing each variable as the sum of a large zero-order term and a small perturbation. We write,

$$N_\mu = n_0 + n_\mu, \tag{3.16}$$

$$\mathbf{V}_\mu = \mathbf{V}_{0\mu} + \mathbf{v}_\mu, \tag{3.17}$$

$$\mathbf{E} = \mathbf{E}_0 + \mathbf{E}_1, \tag{3.18}$$

$$\mathbf{H} = \mathbf{H}_0 + \mathbf{H}_1, \tag{3.19}$$

$$P_\mu = P_{0\mu} + p_\mu. \tag{3.20}$$

The relatively large mass of the ions leads to simplifications; it is therefore convenient to derive the equations for the electrons and deduce therefrom the simpler ion equations.

Let a laser beam linearly polarized along the x axis be described by the infinite plane wave

$$\mathbf{E}_0 = \bar{E}_0 \sin(k_L z - \omega_L t)\hat{\mathbf{x}}, \tag{3.21}$$

propagating in the z direction with wave number k_L and frequency ω_L. In the absence of zero-order density gradients, and with $m_i \gg m_e$, Eq. (3.9) yields to zero order for the electrons

$$\mathbf{V}_{0e} \equiv \mathbf{V}_0 = \bar{\mathbf{V}}_0 \cos(k_L z - \omega_L t), \tag{3.22}$$

where $\mathbf{V}_0 = -e\mathbf{E}_0/m_e\omega_L$ as we may neglect $\mathbf{V}_{0i}$. The damping factor $2\Gamma_e$ has been ignored since $\omega_L \gg \Gamma_e$. In the plasma, ω_L and k_L are related by the zero-order dispersion relation which follows by first combining Eqs. (3.11), (3.12), (3.14), and (3.15) to obtain the wave equation

$$\nabla^2 \mathbf{E} - \frac{1}{c^2}\frac{\partial^2}{\partial t^2}\mathbf{E} = 4\pi \sum_\mu e_\mu \nabla N_\mu + \frac{4\pi}{c^2}\sum_\mu e_\mu \frac{\partial}{\partial t}(N_\mu \mathbf{V}_\mu) \tag{3.23}$$

and then substituting for E_0 in its zero-order component. This yields

$$c^2 k_L^2 = \omega_L^2 - \sum_\mu \omega_\mu^2 \equiv \omega_L^2 \epsilon \tag{3.24}$$

which defines the dielectric constant for transverse oscillations and where $\omega_{e,i}^2 = 4\pi n_0 e^2/m_{e,i}$ is the square of the electron (ion) plasma frequency for a macroscopically neutral plasma of particle density n_0. From Eq. (3.9), the perturbed electron velocity $\mathbf{v}_e$ and density n_e are, to first order, related to the perturbed fields $\mathbf{E}_1$ and $\mathbf{H}_1$ by

$$\left(\frac{\partial}{\partial t} + 2\Gamma_e + \mathbf{V}_0 \cdot \nabla\right)\mathbf{v}_e = -\frac{e}{m_e}\mathbf{E}_1 - \left(v_{ex}\frac{\partial \mathbf{V}_0}{\partial z} + \frac{eV_0}{m_e c}H_1 y\right)\frac{\mathbf{k}_L}{k_L} - \frac{s_e^2}{n_0}\nabla n_e. \tag{3.25}$$

The precise relation between pressure and density depends, of course, on the plasma state, i.e., whether it is isothermal or adiabatic. For isothermal conditions

$$\nabla p_e = m_e s_e^2 \nabla n_e, \quad \nabla p_i = m_i s_i^2 \nabla n_i, \tag{3.26}$$

where $s_\mu^2 = \theta_\mu/m_\mu$ and θ_μ is the temperature in energy units. These results differ from those for adiabatic conditions by the ratio of the specific heats (three for one degree of freedom). In the following, the actual numerical factor is assumed to be contained in the appropriate thermal speed.

The longitudinal and transverse components of $\mathbf{v}_e$, v_{ez} and v_{ex} thus satisfy the coupled equations

$$\left(\frac{\partial}{\partial t} + 2\Gamma_e + \mathbf{V}_0 \cdot \nabla\right)v_{ex} = -\frac{e}{m_e}E_{1x} - \frac{s_e^2}{n_0}\frac{\partial n_e}{\partial x} \tag{3.27}$$

and

$$\left(\frac{\partial}{\partial t} + 2\Gamma_e + \mathbf{V}_0 \cdot \nabla\right)v_{ez} = -\frac{e}{m_e}E_{1z} - v_{ex}\frac{\partial V_0}{\partial z} - \frac{eV_0}{m_e c}H_1 y - \frac{s_e^2}{n_0}\frac{\partial n_e}{\partial z}. \tag{3.28}$$

We will assume that the wavelength of the excitation is much larger than the Debye wavelength $\lambda_D = (\theta_e/4\pi n_0 e^2)^{1/2}$. The ion wave damping must then include wavenumber-dependent Landau damping, while the dissipation in the electron wave may be taken to be collision dominated, except for low densities. From microscopic theory (see, for example, Krall and Trivelpiece, 1973), we have for $\omega_e \gg kV_e$

$$2\Gamma_i = \nu_{ie} + k\beta^2\left(\frac{\pi\theta_e}{8m_i}\right)^{1/2} \times\left\{\left(\frac{\theta_e}{\theta_i}\right)^{3/2}\exp\left(-1/2\frac{\theta_e}{\theta_i}\beta\right) + \left(\frac{m_e}{m_i}\right)^{1/2}\right\}, \quad (3.29)$$

$$2\Gamma_e = \frac{m_i}{m_e}\nu_{ie} + \sqrt{\frac{\pi}{8}}\frac{\omega_e}{|k^3\lambda_D^3|}\exp\left[-\frac{1}{2k^2\lambda_D^2} - \frac{3}{2}\right], \quad (3.30)$$

where $\beta = (1 + k^2\lambda_D^2)^{-1}$, and ν_{ie} is the ion–electron collision frequency.

The various perturbed quantities in Eq. (3.25) may be eliminated in favor of $\mathbf{v}_e$: E_{1x} and E_{1z} by the perturbed wave equation, n_e by the equation of continuity. This reduces the problem to that of solving two coupled differential equations linking v_{ex} and v_{ez}. It is then straightforward, though algebraically tedious, to derive the dispersion equation $D(\omega, k) = 0$ relating the frequency ω and wave vector k of the driven modes by taking the Fourier transforms in space and time of these equations and imposing the condition for nontrivial solutions. For the full four-mode interaction, this leads to a six by six determinant for $D(\omega, \mathbf{k})$, which reduces to a four by four determinant for the three-wave parametric scheme in which one of the sidebands is suppressed. The reduction to three-mode interaction is adequate provided the phase shift of the unstable mode is much less than its frequency, so that the contribution from the suppressed sideband is far off resonance.

We discuss the various instabilities according to their domain of excitation in the plasma. The oscillating two-stream and the ion–acoustic wave decay instability are excited near the critical density surface, while stimulated Brillouin and Raman scattering can occur in the underdense region.

The above formalism is sufficiently general for a study of the full two-dimensional problem. It is readily adapted, at least in principle, to treat arbitrary polarization of the incident radiation, and can also be used to determine the angular profile of the scattered radiation. The two-dimensional problem is discussed in more detail by Jorna (1973). In the present article, however, we restrict attention to much simpler one-dimensional applications.These include the transversely driven instabilities and the backscattering modes, which are of greatest current interest to laser-driven fusion.

To facilitate comparison with results quoted in the literature, plasma values will be used for quantities which depend on the incident field intensity. They are related to their vacuum counterparts by the flux (φ) conserving condition $\varphi_{\text{vac}} = \varphi_{\text{medium}}\sqrt{\epsilon}$. This corresponds to the so-called "swelling" of the electromagnetic waves when, in WKBJ language, a turning point is approached. Since in this region the field is approximated by an Airy function, it may also be termed the Airy function enhancement. The factor $1/\sqrt{\epsilon}$ is particularly significant in the oscillating two-stream and ion-acoustic instabilities which are excited near the critical density surface, where it reduces the vacuum threshold power flux densities by one to two orders of magnitude.

E. Instabilities excited near the critical density surface

The external field may be treated as spatially homogeneous (the dipole approximation) for instabilities excited near the critical density surface, defined by $\omega_e = \omega_L$. This follows directly from the zero-order dispersion relation Eq. (3.24) with $\omega_L \simeq \omega_e$ and $\omega_e \ll \omega_i$.

Equation (3.25) simplifies considerably with the neglect of the spatial derivative of V_0 and the correspondingly decreased coupling of the electrons driven along the field vector to the ions oscillating along the direction of energy propagation. The equations of motion take on a particularly convenient form for the electron and ion densities. Eliminating $\mathbf{E}_l$ from Eq. (3.25) by taking its divergence, we obtain with the aid of Poisson's equation and the equation of continuity

$$\left(\frac{\partial}{\partial t} + 2\Gamma_e + \mathbf{V}_0\cdot\nabla\right)\left(\frac{\partial}{\partial t} + \mathbf{V}_0\cdot\nabla\right)n_e = \omega_e^2(n_i - n_e) + s_e^2\nabla^2 n_e. \quad (3.31)$$

The corresponding ion equation follows by analogy, with the simplification due to the large ion mass, of negligible ion quivering velocity. Hence,

$$\left(\frac{\partial^2}{\partial t^2} + 2\Gamma_i\frac{\partial}{\partial t} + \omega_i^2 - s_i^2\nabla^2\right)n_i = \omega_i^2 n_e. \quad (3.32)$$

The pump field is specified by Eq. (3.22) with $k_L = 0$, so that $\mathbf{V}_0 = \bar{\mathbf{V}}_0\cos(\omega_L t)$. We can therefore readily obtain from the Fourier transforms of Eqs. (3.31) and (3.32) and the convolution theorem, coupled algebraic equations for $\bar{n}_e(\mathbf{k}, \omega)$ and $\bar{n}_i(\mathbf{k}, \omega)$ defined by

$$\bar{n}_\mu(\mathbf{k}, \omega) = \frac{1}{(2\pi)^4}\int_{-\infty}^{\infty}\int_{-\infty}^{\infty} n_\mu(\mathbf{r}, t)\exp[-i(\mathbf{k}\cdot\mathbf{r} - \omega t)]\,d\mathbf{r}\,dt. \quad (3.33)$$

If the ions are taken to be static in Eq. (3.31) for the electrons and only the slowly varying part of the driving term is retained in Eq. (3.32), it was shown by Aliev and Silin (1965) and in more detail by Kaw and Dawson (1969) that the low-frequency mode can be expanded in terms of the Bessel functions $J_p^2(\mathbf{k}\cdot\bar{\mathbf{V}}_0/\omega_L)$. A much simpler analysis suffices, however, for the present case where the phase velocity of the scattered wave is much larger than the electron quivering velocity, i.e., $\omega_L \gg \mathbf{k}\cdot\mathbf{V}_0$. It is clear that the wave mixing due to the nonlinear coupling of the plasma and the pump leads to the possible excitation of the four basic frequencies, ω_L, $\omega_L \pm \omega$, ω, and an infinite number of harmonics. This is reflected in the hierarchy of coupled equations for $\bar{n}_e(\mathbf{k}, \omega \pm n\omega_L)$. Equations (3.31), (3.32), and (3.33) yield the following recurrence relation for $\bar{n}_e(\mathbf{k}, \omega)$ with $k_L = 0$

$$\left\{L(k, \omega) - \tfrac{1}{2}\bar{\mathbf{V}}_0^2 k_x^2\right\}[\bar{n}_e(\mathbf{k}, \omega)/-\bar{\mathbf{V}}_0\cdot\mathbf{k}] = (\omega + \tfrac{1}{2}\omega_L)\bar{n}_e(\mathbf{k}, \omega + \omega_L) + (\omega - \tfrac{1}{2}\omega_L)\bar{n}_e(\mathbf{k}, \omega - \omega_L) \quad (3.34)$$

with the abbreviations

$$L(k,\omega) = -\omega^2 - 2i\Gamma_e\omega - \omega_e^2[(\omega_i^2/\Omega_i) - 1] + s_e^2k^2, \quad (3.35)$$

$$\Omega_i = -\omega^2 - 2i\Gamma_i\omega + \omega_i^2 + s_i^2k^2. \quad (3.36)$$

The hierarchy of transforms is truncated by neglecting terms involving $\bar{n}_e(\mathbf{k},\omega \pm n\omega_1)$ with $n \geq 2$, consistent with the small signal expansion. If these terms are retained, the dispersion relation also contains contributions of $O(V_0^4)$ which we are neglecting here. A shift by $\pm\omega_L$ in the frequency ω in Eq. (3.34) yields the further approximate relations

$$[L(k,\omega \pm \omega_L) - \tfrac{1}{2}\tilde{\mathbf{V}}_0^2\,k_x^2][\bar{n}_e(\mathbf{k},\omega \pm \omega_L)/-\bar{\mathbf{V}}_0\cdot\mathbf{k}] = (\omega \pm \tfrac{1}{2}\omega_L)\bar{n}_e(\mathbf{k},\omega), \quad (3.37)$$

where the higher harmonic terms have again been neglected. Elimination from Eq. (3.34) of the frequency shifted transforms by means of Eq. (3.37) leads to nontrivial solutions for $\bar{n}_e(\mathbf{k},\omega)$, provided

$$D(k,\omega) \equiv \omega^2 - s_a^2k^2 + 2i\Gamma_i\omega - \frac{1}{4}\frac{\omega_i^2\omega_L^2}{\omega_e^2}(\bar{\mathbf{V}}_0\cdot\mathbf{k})^2 \times\left[\frac{1}{\omega_+^2 - \omega_R^2 + 2i\Gamma_e\omega_+} + \frac{1}{\omega_-^2 - \omega_R^2 + 2i\Gamma_e\omega_-}\right] = 0, \quad (3.38)$$

where $\omega_\pm = \omega \pm \omega_L$. We have introduced the sound speed s_a defined by

$$s_a^2 = s_i^2 + (m_e/m_i)s_e^2, \quad (3.39)$$

and the modified plasma frequency

$$\omega_R^2 = \omega_e^2 + s_e^2k^2. \quad (3.40)$$

Equation (3.38) has been analyzed extensively by Nishikawa (1968), and also by Kaw and Dawson (1969). We discuss here the two main cases:

1. the modified oscillating two-stream instability, and
2. the ion-acoustic or "parametric decay" instability.

1. Modified oscillating two-stream instability

The possible excitation of a purely growing mode was noted by Nishikawa (1968) and by Kaw and Dawson (1969). For this absolute instability Re $\omega = 0$, while the second mode is driven at the pump frequency ω_L. Neither denominator in Eq. (3.38) can be assumed to be off resonance, so that the interaction must be described by full four-wave coupling.

The minimum threshold value for $\bar{V}_0^2$, $(\bar{V}_0^m)^2$, say, determined by setting $\omega = 0$ in Eq. (3.38), follows from the minimization with respect to Nishikawa's parameter $\delta = \omega_L - \omega_R$ of

$$\bar{V}_0^2 = -4(s_a^2\omega_e^2/\omega_L\omega_i^2)(\delta + \Gamma_e^2/\delta). \quad (3.41)$$

This occurs for $\delta = -\Gamma_e$ when

$$(\bar{V}_0^m)^2 = 8s_e^2[1 + (T_i/T_e)](\Gamma_e/\omega_L). \quad (3.42)$$

which is independent of ion wave dissipation. Consequently, this mode can be excited for an incident radiation energy which is much less than the electron thermal energy (since $\Gamma_e \ll \omega_L$).

The temporal gain near threshold, obtained by linearizing Eq. (3.38) in ω, is given by (cf. Nishikawa, 1968)

$$\text{Im}\,\omega = s_a^2k^2\Gamma_e\left(\frac{P_0}{P_0^m} - 1\right)/(s_a^2k^2 + 2\Gamma_i\Gamma_e) \quad (3.43)$$

in terms of the incident and threshold power flux densities, where $P_0 = c\bar{E}_0^2/8\pi$. Far above threshold, the damping constants may be ignored and the optimum growth rate occurs for the frequency $\omega_L = \omega_R - \text{Im}\,\omega$ with

$$\text{Im}\,\omega = (\omega_i^2k^2P_0/2\omega_R\,cn_0m_e)^{1/3}, \quad (3.44)$$

which varies as the one-third power of the incident energy flux.

As remarked earlier, the power flux densities in the above expressions must be multiplied by the factor $1/\sqrt{\epsilon}$ if they are to refer to the vacuum rather than to the plasma values.

Determination of the optimum value of the wave number k depends on the damping. Nishikawa (1968) finds that maximum growth rates for this mode are obtained for relatively long wavelengths ($k\lambda_D \ll 1$) if the damping is collision dominated.

The oscillating two-stream instability could effectively enhance the plasma resistivity, except that the optimum interaction takes place in the critical to supercritical density region ($\omega_L < \omega_R$) where the penetration of the incident radiation is greatly reduced.

2. Acoustic instability

Inspection of Eq. (3.38) also shows a resonance at Re $\omega \simeq s_ak$ in the acoustic propagator. This corresponds to the excitation of a phonon and a plasmon of frequency $\sim \omega_R$. For small phase mismatch $\omega_L - \omega_R - s_ak$, the contribution at $\omega_L + \omega$ may be neglected as being off resonance. The problem now reduces to that of three-mode parametric amplification. The lowest threshold occurs for perfect phase matching in which case Eq. (3.38) reduces to

$$D(k,\omega) \equiv (\omega^2 - s_a^2k^2 + 2i\Gamma_i\omega)(\omega - \delta + i\Gamma_e) + (\omega_i^2\omega_L/8\omega_e^2)(\bar{\mathbf{V}}_0\cdot\mathbf{k})^2 = 0, \quad (3.45)$$

where $\delta = \omega_L - \omega_R$. Thus, for Re $\omega \simeq s_ak$ and $\omega_L = s_ak + \omega_R$,

$$(\bar{V}_0^m)^2 \simeq 16s_e^2\left(1 + \frac{T_i}{T_e}\right)\left(\frac{\Gamma_i}{s_ak}\right)\left(\frac{\Gamma_e}{\omega_L}\right), \quad (3.46)$$

which differs from the threshold for the oscillating two-stream instability by a factor $2\Gamma_i/s_ak$, and again indicates an electron excitation energy much less than the electronic thermal energy. Near $\bar{V}_0 = \bar{V}_0^m$ the growth rate is approximately given by

$$\text{Im}\,\omega = \left(\frac{\Gamma_i\Gamma_e}{\Gamma_i + \Gamma_e}\right)\left(\frac{P_0}{P_m} - 1\right), \quad (3.47)$$

for a plasma with $s_ak > \Gamma_{e,i}$, though it should be realized that even for $T_e/T_i \simeq 5 - 10$, $\Gamma_i \simeq s_ak$ and can still be comparable to Γ_e. For a more detailed analysis the work of Nishikawa (1968) should be consulted.

The growth rate for negligible damping follows readily from Eq. (3.45) by setting $\omega = s_ak + i\gamma_0$ and $s_ak = \delta$.

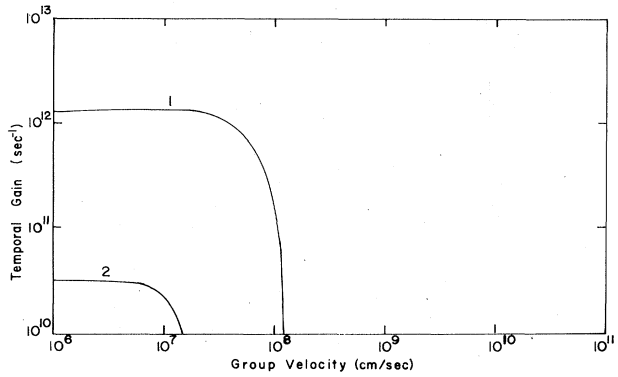

FIG. 6. Temporal gain vs convective speed for the ion-acoustic instability at a power flux density of $P_L = 10^{14}$ W cm^{-2}, and for 1: $k_X = 9.5 \times 10^4$ cm^{-1}, 2: $k_x = 1.2 \times 10^5$ cm^{-1}.

This yields

$$\gamma_0 = \frac{1}{4}(V_0/s_e)[\omega_L \omega_a/(1 + T_i/T_e)]^{1/2}, \tag{3.48}$$

where $\omega_a \equiv s_a k$.

The propagation speed V_m corresponding to the mode with Max[Im ω] is readily calculated from the dispersion relation by the prescription given previously, i.e , $\partial D/\partial k + V \partial D/\partial \omega = 0$ with real k satifying $D(k, \omega) = 0$. Near threshold

$$V_m \simeq s_a[1 + (\Gamma_i/\Gamma_e)]^{-1}, \tag{3.49}$$

so that the ion-acoustic instability is an absolute instability in a plasma expanding at sound speed. Figure 6 shows the dependence of temporal gain on "observer" speed V for a radiation power flux density of $10^{14} W$ cm^{-2} coupled to a DT plasma with $T_e = 1$ keV and $T_i = 0.1$ keV. The calculations are based on the k-dependent dissipation factors given earlier and illustrate the sharp variation of gain with wave number, whose optimal value in this case is given by $k\lambda_D \sim 0.07$. Equation (3.45) shows that far above threshold when damping may be ignored, the growth rate exhibits the characteristic cube root dependence on the incident power flux density.

In early discussions (Kaw and Dawson, 1969) it was speculated that this parametric decay instability might be an effective mechansm for direct heating of the ions at temperatures where collisional heating has become inefficient. The Manley-Rowe relations indicate, and computer simulation studies confirm, that most of the energy goes into the electrons, raising some to very high nonthermal energies. These so-called "hot" electrons exchange little energy with the rest of the plasma and may, in fact, be responsible for the undesirable preheating of the solid core discussed elsewhere in this article. The simulation experiments of Bodner *et al.* (1973) do, however, indicate the occurrence of instability heating of the ions by their interaction with the turbulent plasma. The importance of this decay mode for fusion may be diminished by the excitation of back-scattering instabilities at subcritical densities.

F. Subcritical density instabilities

In the subcritical density region of the plasma, $\omega_e < \omega_L$, so that the spatial variation of the driving field can no longer be ignored. The Lorentz force now has an additional component which couples the transversely driven electrons to the ion and electron waves propagating along the direction of (normal) incidence. Above a certain threshold, low- and high-frequency instabilities develop accompanied by a scattered electromagnetic wave with a frequency and wave number given by the phase-matching conditions $\omega_L = \omega_1 + \omega_2$, $\mathbf{k}_L = \mathbf{k}_1 + \mathbf{k}_2$. In quantum terminology, these processes, which have been named stimulated Brillouin scattering (SBS) and stimulated Raman scattering (SRS), correspond to the decay of a photon into a phonon and a photon, or into a plasmon and a photon. A mode in which the photon decays into two plasmons is a third possibility, but this process requires a two-dimensional treatment since the Langmuir waves do not propagate parallel to the driving light wave.

As has already been pointed out, the backward scattering instabilities are of particular importance to laser-driven fusion, the more so because of their apparently low thresholds.

The dispersion relation for these phenomena is most conveniently derived by first separating Eq. (3.25) into its transverse and longitudinal components Eqs. (3.27) and (3.28) and then eliminating $\mathbf{E}_l$ in favor of the perturbed velocity by means of the perturbed wave equation, Eq. (3.23). We obtain

$$\left[\Box^2\left(\frac{\partial}{\partial t} + 2\Gamma_e\right) - \frac{\omega_e^2}{c^2}\frac{\partial}{\partial t}\right]v_{ex} + \Box^2\left(V_0\frac{\partial v_{ex}}{\partial x}\right) = \frac{\omega_e^2}{n_0}\left[\frac{1}{c^2}\frac{\partial}{\partial t}(n_e V_0) - \frac{\partial}{\partial x}(n_i - n_e)\right] - \frac{s_e^2}{n_0}\Box^2\frac{\partial n_e}{\partial x}, \tag{3.50}$$

$$\left[\Box^2\left(\frac{\partial}{\partial t} + 2\Gamma_e\right) - \frac{\omega_e^2}{c^2}\frac{\partial}{\partial t}\right]v_{ez} + \Box^2\left(V_0\frac{\partial v_{ez}}{\partial x} + v_{ex}\frac{\partial V_0}{\partial z} + \frac{eV_0}{m_e c}H_l y\right) = -\frac{\omega_e^2}{n_0}\frac{\partial}{\partial z}(n_i - n_e) - \frac{s_e^2}{n_0}\Box^2\frac{\partial n_e}{\partial z}, \tag{3.51}$$

where the d'Alembertian

$$\Box^2 \equiv \nabla^2 - (1/c^2)\partial^2/\partial t^2, \tag{3.52}$$

Fourier decomposition of these equations coupled with the continuity equation leads to a six by six determinant for the dispersion relation in two dimensions which will be discussed elsewhere (Jorna, 1973).

For backward scattering there is no transverse variation, and Eqs. (3.50) and (3.51) simplify to

$$\left[\Box^2\left(\frac{\partial}{\partial t} + 2\Gamma_e\right) - \frac{\omega_e^2}{c^2}\frac{\partial}{\partial t}\right]v_{ex} = \frac{\omega_e^2}{n_0 c^2}\frac{\partial}{\partial t}(n_e V_0), \tag{3.53}$$

$$\left[\Box^2\left(\frac{\partial}{\partial t} + 2\Gamma_e\right) - \frac{\omega_e^2}{c^2}\frac{\partial}{\partial t}\right]v_{ez} = -\frac{\omega_e^2}{n_0}\frac{\partial}{\partial z}(n_i - n_e) - \frac{s_e^2}{n_0}\Box^2\frac{\partial n_e}{\partial z} - \Box^2\left(v_{ex}\frac{\partial V_0}{\partial z} + \frac{eV_0}{m_e c}H_l y\right). \tag{3.54}$$

The perturbed densities may be eliminated by the equation of continuity, and the perturbed magnetic field may

be eliminated by Eq. (3.11) and the wave equation, Eq. (3.23). Taking Fourier transforms of the resulting equations, we obtain ($\omega_\pm = \omega \pm \omega_L, \mathbf{k}_\pm = \mathbf{k} \pm \mathbf{k}_L$)

$$\mathfrak{L}_1(k,\omega)\bar{v}_{ex}(\mathbf{k},\omega) = -\frac{\omega_e^2 \overline{V}_0}{2c^2}\left[\frac{(k_z - k_L)}{\omega_-}\bar{v}_{ez}(\mathbf{k}_-,\omega_-) + \frac{(k_z + k_L)}{\omega_+}\bar{v}_{ez}(\mathbf{k}_+,\omega_+)\right], \tag{3.55}$$

$$\mathfrak{L}_2(k,\omega)\bar{v}_{ez}(\mathbf{k},\omega) = -\frac{1}{2}f(k,\omega)\overline{V}_0\left\{\left[k_L + \frac{\omega_e^2(k_z - k_L)}{c^2 f(k_-,\omega_-)}\right]\bar{v}_{ex}(k_-,\omega_-) - \left[k_L - \frac{\omega_e^2(k_z + k_L)}{c^2 f(k_+,\omega_+)}\right]\bar{v}_{ex}(k_+,\omega_+)\right\}, \tag{3.56}$$

where

$$\mathfrak{L}_1(k,\omega) = f(k,\omega)(-1 - 2i\Gamma_e/\omega) + (\omega_e^2/c^2), \tag{3.57}$$

$$\mathfrak{L}_2(k,\omega) = \omega^2\mathfrak{L}_1(k,\omega) + k_z^2\left[\omega_e^2\left(\frac{\omega_i^2}{\Omega_i} - 1\right) + s_e^2 f(k,\omega)\right], \tag{3.58}$$

$$f(k,\omega) = -k^2 + (c^2)^{-1}\omega^2, \tag{3.59}$$

and Ω_i is given by Eq. (3.36). The dispersion relation follows on combining Eqs. (3.55) and (3.56) with their frequency-shifted analogues and truncating the resulting hierarchy of equations by neglecting the higher harmonic terms. The result is (cf. Gorbunov, 1968)

$$\mathfrak{L}_2(k,\omega) = \frac{1}{4}\omega_e^2 k_z f(k,\omega)\frac{\overline{V}_0^2}{c^2} \times\left[\left(k_L + \frac{\omega_e^2(k_z - k_L)}{c^2 f(k_-,\omega_-)}\right)\frac{1}{\mathfrak{L}_1(k_-,\omega_-)} - \left(k_L - \frac{\omega_e^2(k_z + k_L)}{c^2 f(k_+,\omega_+)}\right)\frac{1}{\mathfrak{L}_1(k_+,\omega_+)}\right]. \tag{3.60}$$

This expression has the characteristic form for four-wave interaction. $\mathfrak{L}_2$ contains the plasma oscillations (ion-acoustic and Langmuir waves), while the coupling factor is multiplied by the Maxwell propagators for the up- and downshift scattered waves.

1. Stimulated Brillouin scattering

The dispersion relation for stimulated Brillouin scattering (SBS) follows from Eq. (3.60) with $\omega^2 \ll \omega_e^2$. We reduce the interaction to three-mode parametric coupling by assuming perfect phase matching and suppressing the wave upshifted in frequency. This yields for the Stokes component (since $k_x = 0$, we drop the subscript z in k_z) near the point of resonance of the Maxwell propagator where $c^2 f(k_-,\omega_-) \simeq \omega_e^2$

$$(\omega^2 - s_a^2 k^2 + 2i\Gamma_i\omega)\left[\omega - \frac{c^2}{\omega_L}\left(kk_L - \frac{1}{2}k^2\right) + i\Gamma_e'\right] = -\omega_i^2 k^2 \overline{V}_0^2/8\omega_L \equiv -\Omega^3, \tag{3.61}$$

with $\Gamma_e' = \Gamma_e^h\omega_e^2/\omega_L^2$, in agreement with Bodner and Eddleman (1971). Here Γ_e^h is the high-frequency damping decrement of the Langmuir waves. An estimate for the threshold of the phonon excitation follows readily on setting $\omega = s_a k + \delta$ with $0 < |\delta| \ll s_a k$. We find for the back-scattered mode ($k \simeq 2k_L$)

$$\omega \simeq s_a k + i\Gamma_i[(P_0/P_0^m) - 1], \tag{3.62}$$

with a threshold for $\overline{V}_0^2$ given by

$$(\overline{V}_0^m)^2 = 16 s_e^2\left(1 + \frac{T_i}{T_e}\right)\frac{\Gamma_i}{s_a k}\frac{\Gamma_e^h}{\omega_L}. \tag{3.63}$$

The growth rate in the absence of damping follows straightforwardly from Eq. (3.61) with $\Gamma_e^h = \Gamma_i = 0$, and $\omega = s_a k + i\gamma_0$. For $k \simeq 2k_L$,

$$\gamma_0 \simeq \frac{1}{4}\frac{\overline{V}_0}{s_e}\frac{\omega_e}{\omega_L}\left[\frac{\omega_L\omega_a}{1 + T_i/T_e}\right]^{1/2}. \tag{3.64}$$

These expressions are similar to those for the ion-acoustic instability Eq. (3.46), and might lead to the conclusion that both instabilities can be excited concurrently and independently. There are important differences, however. First, the SBS threshold depends inversely on $k_L = \omega_L\sqrt{\epsilon}/c$ and decreases away from the critical density surface. Thus, if SBS develops optimally, a partially reflecting layer is generated in the subcritical density region of the plasma sending photons of frequency $\omega_L - s_a k$ back out of the plasma, thereby reducing the energy reaching the critical density surface. Any heating of the ions would be of marginal importance because of the low densities involved. The second difference concerns the nature of the instability in an expanding plasma. The threshold given by Eq (3.63) is that for a convective instability propagating near threshold at a large fraction of the speed of light (Brueckner and Jorna, 1973). This conclusion follows from a determination of the propagation speed V in

$$\partial D/\partial k + V(\partial D/\partial\omega) = 0, \tag{3.65}$$

for the solution Eq. (3.62). With $\omega = s_a k + \delta$ and D given by Eq. (3.61), Eq. (3.65) yields approximately

$$(V - s_a)\left[\omega - \frac{c^2}{\omega_L}\left(kk_L - \frac{1}{2}k^2\right) + i\Gamma_e'\right] + (\delta + i\Gamma_i) \times\left[V - \frac{c^2}{\omega_L}(k_L - k)\right] = 0, \tag{3.66}$$

or for the back-scattering mode

$$V \simeq s_a - [c\sqrt{\epsilon}/2(1 + \Gamma_e'/2\Gamma_i)]. \tag{3.67}$$

If we assume $\Gamma_e = 4\Gamma_i$, $V \sim -4 \times 10^9$ cm sec^{-1} for $n = 1/2n_c$, and $V \sim -3 \times 10^9$ cm sec^{-1} for $n = \frac{3}{4}n_c$. For a typical interaction length of 100μm the growth time is about 1 psec which is clearly too short for development of the convective instability. An absolute instability is approached for very small k_L, but here the threshold is correspondingly increased.

Far above threshold the damping terms may be neglected in Eq. (3.61) and the growth rate is given by Im ω where

$$\omega = \exp(i\pi/3)\Omega, \tag{3.68}$$

exhibiting the characteristic one-third power dependence on the incident power flux density of the modified decay instability. The propagation speed of the fastest temporally growing mode can again be calculated from Eq. (3.65). We find $V \sim -\frac{1}{3}c\sqrt{\epsilon}$ or $V \sim -c/6$ for $n = \frac{3}{4}n_c$ for a 1 keV DT plasma.

It is evident that Eq. (3.63) is not a meaningful threshold for a finite plasma expanding at a speed $\mathfrak{M}s_a$ where $\mathfrak{M}$ is the Mach number. Instead, the threshold must be determined for the excitation which in the frame of the expanding plasma is an absolute instability (cf. Section III.C). Thus, Eqs. (3.61) and (3.65) must be solved with $V = \mathfrak{M}s_a$ and a pump intensity for which $\mathrm{Im}(\omega - Vk) = 0$. Figures 7(a) and 7(b) show the results of numerical calculations for a DT plasma with $T_e = 1$ keV and $T_i = 0.1T_e$ obtained by solving Eq. (3.8), for various power flux and plasma densities. By the present criterion, we expect the onset of the absolute instability to be at approximately 10^{14} W cm^{-2}, several orders of magnitude higher than that for the convective instability. The effective intensity at which SBS should manifest itself is still higher and depends on the magnitude of the initiating fluctuation and the size, L, say, of the region over which phase matching can be maintained. Let us assume that the instability builds up from thermal noise and that ξ e foldings are required for the perturbed quantities to be observable. The effective interaction time may be approximated by $\tau(\text{psec}) \sim 5L(\mu m)/\mathfrak{M}$. For reasonable values, $\xi \sim 30$, $\mathfrak{M} = 3$, and $L = 100\mu m$, say, the growth rate must be at least 2×10^{11} sec^{-1} at $V = 10^8$ cm/sec^{-1}. Figures (7a) and (7b) indicate that this raises the threshold for SBS to about 10^{15} W cm^{-2} for a DT plasma. Higher Z plasmas should have somewhat lower effective thresholds due to decreased damping.

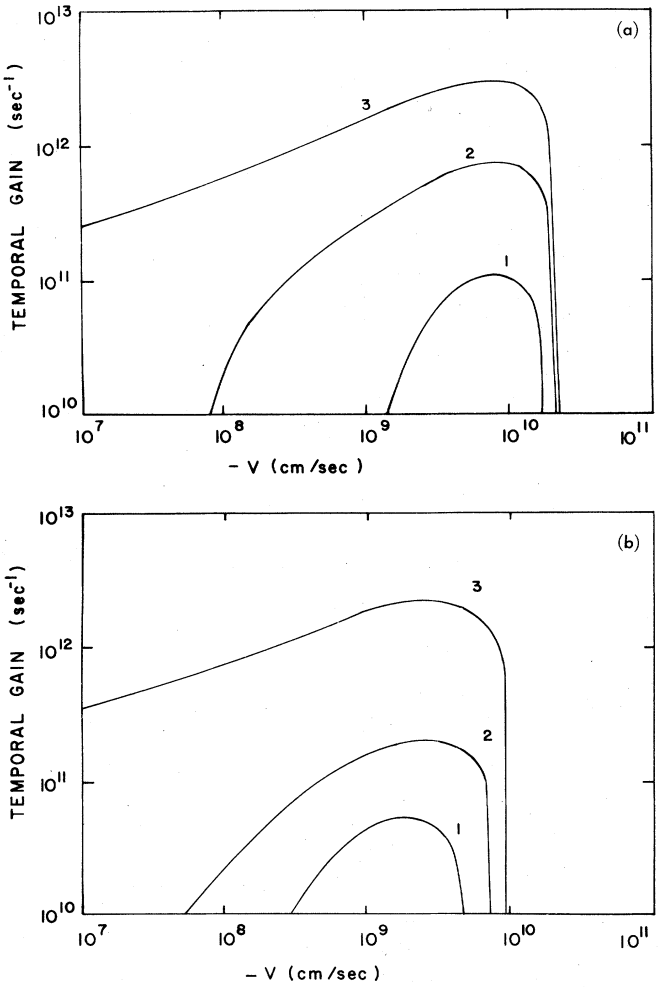

FIG. 7. Temporal gain vs convective speed for stimulated Brillouin scattering: (a) $n = 0.5n_c$; power flux densities in W cm^{-2}, 1: 4×10^{12}, 2: 5×10^{13}, 3: 10^{15} (b) $n = 0.9n_c$; power flux densities in W cm^{-2}, 1: 3×10^{12}, 2: 10^{13}, 3: 10^{15}.

2. Two plasmon decay and stimulated Raman scattering

The decay of a photon into a plasmon and a scattered photon is also described by Eq. (3.60), but now the region of interest is Re $\omega \simeq \omega_R$ and $\omega^2 \gg \omega_i^2$. With these assumptions, the dispersion relation becomes (again, the anti-Stokes wave is suppressed)

$$(\omega^2 - \omega_R^2 + 2i\Gamma_e\omega[\omega^2 - 2\omega\omega_L - c^2(k^2 - 2kk_L) - (2i\Gamma_e^h/\omega_-)(c^2k_-^2 - \omega_-^2)] = \frac{1}{4}\omega_e^2 V_0^2 k^2. \tag{3.69}$$

The threshold equation for an infinite medium follows on setting $\omega = \omega_R + \delta$, $|\delta| \ll \omega_R$, and is given by

$$(\delta + i\Gamma_e)[\delta + i\Gamma_e^h\omega_R^2/(\omega_R - \omega_L)^2] = -[\omega_e^2 V_0^2 k^2/16\omega_R(\omega_L - \omega_R)]. \tag{3.70}$$

This yields

$$(V_0^m)^2 = 16\Gamma_e\omega_R^3\Gamma_e^h/k^2(\omega_L - \omega_R)\omega_e^2, \tag{3.71}$$

subject to the resonance condition

$$\omega_R^2 - 2\omega_R\omega_L = c^2k(k - 2k_L). \tag{3.72}$$

The temporal gain near threshold is given by

$$\mathrm{Im}\ \omega = \Gamma_e\left(\frac{P_0}{P_0^m} - 1\right)\Big/\left[1 + \left(\frac{\omega_R - \omega_L}{\omega_R}\right)^2\frac{\Gamma_e}{\Gamma_e^h}\right]. \tag{3.73}$$

The resonance condition imposes stringent restrictions on the range of densities over which this instability can be excited. Let the matching wave number $k = \zeta k_L$ and set $\omega_L/\omega_R = \alpha \simeq \omega_L/\omega_e$. This assumes that $s_e^2k^2 \ll \omega_e^2$ which is satisfied provided the density is not too low. Eq. (3.72) is then satisfied for

$$\zeta = 1 \pm [\alpha(\alpha - 2)/(\alpha^2 - 1)]^{1/2}, \tag{3.74}$$

which shows that $\zeta \to \pm\infty$ for $\alpha = \pm 1$ and further that there are no values of ζ for the range $1 \leq \alpha < 2$. Consequently, there exists a critical region for this mode at the density $n = \frac{1}{4}n_c$. Also, as k increases from the matching value $k = k_L$, the corresponding density satis-

fying the resonance condition decreases sharply away from $\frac{1}{4}n_c$.

At the critical surface $n = \frac{1}{4}n_c$ the decay products in two dimensions are two plasmons, each with a frequency $\sim\omega_R$. In the backscattering case this is the cut-off density for a photon decaying into a plasmon and a photon. The propagation speed at maximum temporal growth follows on solving the saddle-point equation for V keeping k real. Differentiations of Eq. (3.69) with respect to k yields, near threshold, that $V \simeq s_e^2/c \simeq 10^8$ cm sec^{-1} for $n = n_c/4$ and $\theta_e = 1$ keV. This indicates an absolute instability in a plasma expanding at a few times sound speed. Figure 8(a) shows the results of numerical calculations for a DT plasma with $\theta_e = 10\theta_i = 1$ keV. If 30 e foldings are required for the instability to manifest itself in a plasma expanding at three times the sound speed, the graph shows the threshold must be increased from 10^{12} W cm^{-2} given by Eq. (3.71) to 10^{14} W cm^{-2}. Analogously with the "parametric decay" instability, there is a further enhancement due to the WKBJ factor at the transition point. By Landau damping, the plasma oscillations heat the electrons in the underdense region in a non-Maxwellian way, which can again result in the generation of undesirable "hot" electrons.

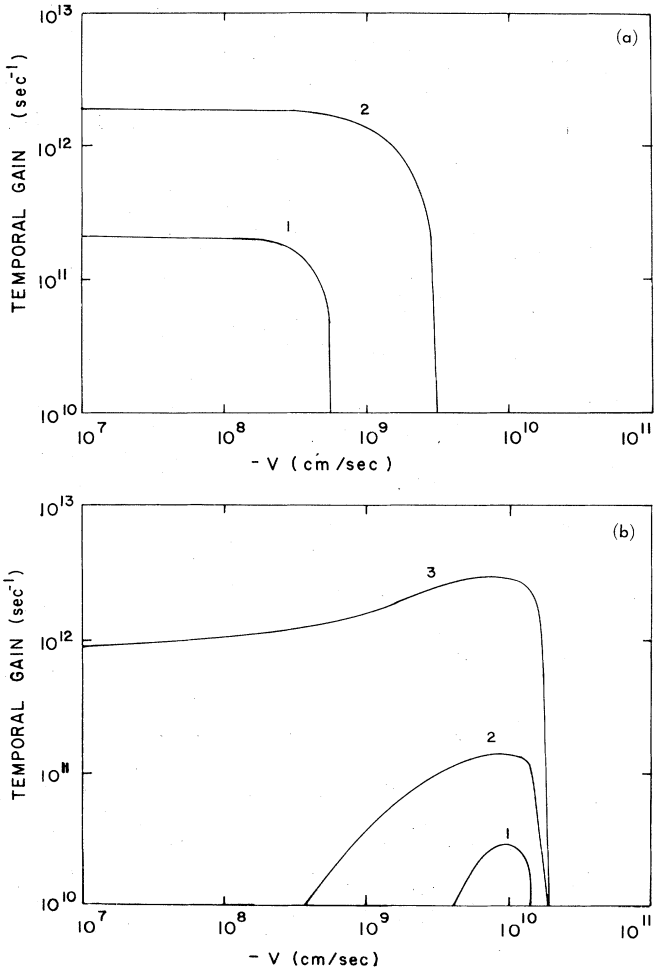

FIG. 8. Temporal gain vs convective speed for $\frac{1}{4}n_c$ and Raman modes (a) $n = \frac{1}{4}n_c$; power flux densities in W cm^{-2}, 1: 8.5×10^{13}, 2: 10^{14}, stimulated Raman scattering (b) $n = 1/5n_c$; power flux densities in W cm^{-2}, 1: 10^{11}, 2: 5×10^{11}, 3: 10^{14}.

For densities less than $\frac{1}{4}n_c$, the matching condition $\omega_L = \omega_R + \omega_2$ yields a dispersion for the ω_2 mode given by $\omega_2 = (\omega_e^2 + c^2k_2^2)^{1/2}$, $k_2 = k_L - k \neq 0$. The excitations are now a plasmon and a scattered photon, a process which may be termed stimulated Raman scattering. Since the threshold, Eq. (3.71), decreases with density, this mode is most readily excited at low densities. Well above threshold ($|\delta| \gg \Gamma_e$), however, the temporal gain becomes

$$\text{Im } \omega = \frac{1}{4}\left(\frac{\omega_e^2 k^2 \overline{V}_0^2}{\omega_R(\omega_L - \omega_R)}\right)^{1/2} \sim \frac{\overline{V}_0}{c}\sqrt{\omega_e \omega_L}, \quad (3.75)$$

which falls off at lower densities.

These results for SRS cannot be applied to a finite medium because for $n < n_c/4$ the saddle-point relation near threshold gives a propagation speed which is a sizeable fraction of c. Instead, the threshold for the absolute instability must be determined. Figure (8b) shows the results of detailed numerical calculations based on Eq. (3.69) and Eq. (3.7) for a DT plasma with $\theta_e = 10\theta_i = 1$ keV. For $n = n_c/9$, for example, the threshold for the convective instability is 10^{11} W cm^{-2} in agreement with Eq. (3.71), while for the absolute instability in a plasma expanding at a speed of 10^8 cm sec^{-1} it is larger than 10^{12} W cm^{-2}. If the further requirement of 30 e foldings is imposed, the effective threshold becomes about 10^{13} W cm^{-2} for $n = n_c/9$.

It is interesting to note the correspondence between the ion-acoustic instability and the two-plasmon decay mode as they relate to SBS and SRS, respectively. The ion-acoustic instability is excited at the critical density n_c, while SBS occurs for $n_0 < n_c$. Similarly, the two-plasmon decay mode is excited at its "critical" density $\frac{1}{4}n_c$, while SRS occurs only for $n < \frac{1}{4}n_c$.

G. Stabilizing mechanisms

The growth rates and thresholds of the instabilities discussed so far are based on the linearized equations for a homogeneous plasma. The finite extent of the interaction has been taken into account through an effective interaction time determined by the propagation speed of the instability. We have seen that in some instances this raises considerably the expected threshold over the homogeneous value. A linear mechanism which can further increase thresholds has been suggested by Perkins and Flick (1971), and Rosenbluth (1972). Since a plasma has zero-order density gradients,[1] the wave numbers of the elementary excitations depend on density so that in general the resonance condition can only be satisfied locally. The growth rate is now set by the magnitude of the inhomogeneity which determines the size of the region over which the phase mismatch is still reasonably small. This process can lead to reduced growth rates and correspondingly higher thresholds.

The following argument yields the main conclusion; for details, the work of Rosenbluth (1972) should be consulted. Assume that the amplitudes of the excited fields are slowly varying functions of time and space.

[1]This density variation was, of course, already implicit in the previous discussions on subcritical density instabilities. There, however, we assumed that this did not affect the resonance conditions.

Equations (3.9) to (3.15) then yield for the amplitudes, a_1 and a_2, say, of the decay products the following approximate equations (See, for example, Tsytovich, 1970):

$$\partial a_1/\partial t + V_1(\partial a_1/\partial z) + 2\Gamma_1 a_1 = \gamma_0 a_2^* \exp\left(i\int_0^z \kappa(z)\,dz\right), \tag{3.76}$$

$$\partial a_2^*/\partial t + V_2(\partial a_2^*/\partial z) + 2\Gamma_2 a_2^* = \gamma_0 a_1 \exp\left(i\int_0^z \kappa(z)\,dz\right). \tag{3.77}$$

The coupling factor γ_0 is taken to be the growth rate in the absence of damping for the homogeneous medium, and has been given earlier for the various processes. The phase mismatch $\kappa(z) = k_L - k_1 - k_2$ is defined such that $\kappa(0) = 0$, $V_1 = \partial\omega_1/\partial k_1$, and $V_2 = \partial\omega_2/\partial k_2$ are the group velocities, and Γ_1 and Γ_2 the damping constants. If we now assume that there are no normal temporal modes and that the effective threshold much exceeds $\gamma_0^2 = \Gamma_1\Gamma_2$, the problem reduces to that of solving approximately the Weber parabolic cylinder equation (cf. Miller, 1965)

$$\partial^2 A_2/\partial z^2 - ik'z(\partial A_2/\partial z) - (i\kappa + \gamma_0^2/V_1V_2)A_2 = 0, \tag{3.78}$$

for $A_2 = a_2^* \exp[-i\int_0^z \kappa dz]$, where it is assumed for simplicity that $\kappa = k'z$. Substituting in Eq (3.78)

$$A_2 = \int_{\mathfrak{IC}} S(p)e^{-pz}\,dp, \tag{3.79}$$

we obtain

$$\frac{d}{dp}(pS) = \frac{-1}{ik'}\left(p^2 - \frac{\gamma_0^2}{V_1V_2} - ik'\right)S \tag{3.80}$$

or

$$S(p) = \exp(-\tfrac{1}{2}p^2/ik')\,p^{\gamma_0^2/ik'V_1V_2} \tag{3.81}$$

provided $\gamma_0^2 > |V_1V_2k'|$. The boundary terms are zero and the solution properly behaved if for $\mathfrak{IC}$ we choose the Hankel contour $\infty - (0+)$ as defined by Whittaker and Watson (1927), say. The asymptotic behavior of A_2 is determined by expanding the integrand around the saddle point at $p_0 = -\frac{1}{2}ik'z \pm [-\frac{1}{4}(k'z)^2 + \gamma_0^2/V_1V_2]^{1/2}$. Exponential growth occurs, therefore, over the range $0 \leq |z| \leq z_t = 2\gamma_0/k'(V_1V_2)^{1/2}$. The net gain over this interval in the intensity $I = A_2A_2^*$ from some initial value I_0 is

$$I = I_0 \exp(2\pi\gamma_0^2/V_1V_2k'), \tag{3.82}$$

so that the modified threshold condition is $2\pi\gamma_0^2 > V_1V_2k'$.

To illustrate, $k' \sim \partial k_L/\partial z \sim k_0 n_0/n_c L\sqrt{\epsilon}$, where k_0 is the vacuum wave number of the incident radiation, and $L \equiv [(1/n_0)dn_0/dz]^{-1}$ is the scale length of the inhomogeneity. Equation (3.82) can now be combined with the expressions for γ_0 to yield modified thresholds for the various elementary processes discussed previously. The results are conveniently expressed in terms of V_0, the electron quivering velocity in the photon field. We find $V_0^2 k_\alpha L > V_\alpha^2$. In this expression, $V_\alpha \simeq s_e$ for the ion-acoustic instability, the two-plasmon decay excitation, and SBS, and $V_\alpha = c$ for SRS; k_α is the photon wave number, except for the ion-acoustic instability when k_α is the acoustic wave number. As a numerical example, consider SBS in a 1 keV DT plasma with $\theta_e = 10\theta_i = 1$ keV so that $s_e^2 = \theta_e/m_e = 1.76 \times 10^{18}$ (cm/sec^{-1})^2. For $L = 100\mu m$ and a photon wave number of 10^5 cm^{-1}, the inhomogeneity threshold is $V_0^2 \simeq 10^{17}$(cm/sec^{-1})^2, corresponding to a power flux density in the plasma of about 3×10^{14} W cm^{-2}. While this is several orders of magnitude higher than the homogeneous infinite plasma value, it is quite comparable to the threshold for the absolute instability.

The application of the above analysis should be qualified by the following considerations. First, the growth rate γ_0 follows from the equations for an infinite homogeneous plasma by ignoring dissipation and by further assuming that γ_0 is much less than the frequency of the excited wave. The former assumption is justified *a posteriori* by the elevated effective threshold, but the latter may be invalid in some applications, particularly in the case of phonon excitation ($\gamma_0 \not< s_a k$) with scale lengths of the order of mm. In fact, we have seen for phonon excitation that, at high intensities, the growth rate no longer varies linearly with the proper flux density but, rather, with its one-third power (cf. also, Galeev *et al.* 1973). In view of the discussions on absolute instabilities, it is also not clear that the proper identification of the group velocities V_1 and V_2 can always be made without a detailed analysis of the dispersion relation. This is closely connected with the problem of the unique determination of the wave number of the excitation. We saw, for instance, that for SBS the mode growing at a rate γ_0 convected at a speed which was a sizable fraction of the speed of light. This would, of course, result in a still higher threshold. Finally, any application of these linear theory results to instabilities which are excited near the critical density surface must be viewed with some skepticism, as these are transversely propagating modes whose group velocity in the direction of ∇n_0 is zero in the one-dimensional problem.

Since the parametric instabilities require for their excitation a strongly phase-correlated driving beam, their growth rates should be reduced by any mechanism which lessens the space-time coherence of the laser beam. One method for achieving this would be to heat the plasma by a large number of mode-locked pulses. Another approach involves frequency broadening (Bodner, 1973). Yamanaka *et al.* (1973) have indeed found that a broad band laser system heats the plasma more effectively than the conventional narrow band system.

Other stabilizing schemes which have been suggested involve nonlinear interactions. An example is the analysis by Valeo, Oberman and Perkins (1972) (see also DuBois and Goldman, 1972) of the nonlinear wave-kinetic equation for the ion-acoustic instability. For strong acoustic damping, the unstable plasma waves are stabilized by coupling to stable plasma waves through ion nonlinear Landau damping. The resulting plasma waves of smaller wave number then decay by collisions. These calculations assume three-mode coupling, equal ion and electron temperatures, and weak turbulence which lessens their significance for laser fusion conditions. In fact, the stimulated decay waves will in turn be coupled by the pump, a process which ultimately results in the incident energy being distributed over a whole spectrum of excitations.

It has also been proposed that some nonlinear interaction process may result in an effective electron collision frequency, ν^* say, sufficiently large to stabilize the para-

metric instability, i.e., such that $\gamma_0^2 = \Gamma_i \nu^*$. This would lead to $\nu^* = \omega_L \omega_a E_0^2/32\pi n_c T_e \Gamma_i$ which would correspond to strong absorption of the incident radiation.

Stimulated Raman scattering may be limited by Landau damping of the Langmuir waves, which sets in for $k\lambda_D \gtrsim 1/3$. For back scattering $k \sim 2k_L$, predicting stabilization at electron temperatures $\theta_e \sim 0.03 m_e c^2 n_0/\epsilon n_c$. The upper limit on k for ion-acoustic waves is higher, so that these continue to be excited down to considerably shorter wavelengths, and this is not an effective saturation mechanism for Brillouin back scatter.

It appears, therefore, that of the back scatter instabilities SBS must be regarded as the more serious, not only because of its lower threshold, but also because of the apparent lack of strong saturation mechanisms. There is, however, a need for a realistic nonlinear analysis for laser fusion problems, as even the more elaborate calculations only apply for weak turbulence and/or plane geometries.

H. Resonant absorption

The calculations so far have not allowed for the effect of polarization on the energy absorption. Zhekulin (1934) found for radio waves incident at angle θ_0 on a stratified isotropic ionosphere that the electric field components propagate independently through such a medium. The calculation of the component perpendicular to the plane of incidence is analogous to that for a normally incident beam, and exhibits the usual Airy function enhancement at the point of reflection where the dielectric constant $\epsilon = \sin^2\theta_0$. The field components in the plane of incidence satisfy an equation which in a collisionless system has a singularity at the critical density surface leading to increased absorption. This singularity clearly disappears for normal incidence. Further, as the angle of incidence increases, the point of reflection recedes from the critical surface, thereby reducing the effect of the singularity. One might expect, therefore, that the increase in absorption at the critical surface will be largest for some intermediate angle whose value depends on the scale length of the density inhomogeneity.

Let an electromagnetic wave propagate along the z direction and be incident at angle θ_0 on an inhomogeneous plasma whose properties vary only with z, and let the plane of incidence be the y–z plane. The field components then follow from the solution of

$$\frac{d^2w}{dz^2} - \frac{1}{\epsilon(z)}\frac{d\epsilon(z)}{dz}\frac{dw}{dz} + k_L^2(\epsilon - \sin^2\theta_0)w = 0, \quad (3.83)$$

and $H_x = w(z)\exp[-i(k_L \sin\theta_0 z - \omega_L t)]$, $E_y = -i(\partial H_x/\partial z)/k_L\epsilon$, $E_z = i(\partial H_x/\partial y)/k_L\epsilon$. For $\Gamma_e \ll \omega_L$, the dielectric constant varies with z according to

$$\epsilon(z) \simeq 1 - \frac{\omega_e^2(z)}{\omega_L^2}\left(1 + i\frac{2\Gamma_e}{\omega_L}\right) \simeq 1 - \frac{n(z)}{n_c} - i\frac{2\Gamma_e}{\omega_L}, \quad (3.84)$$

if we assume a constant damping factor given by its value at $\omega_e = \omega_L$. Denisov (1956) studied the solutions of Eq. (3.83) extensively for a linear density profile $n/n_c = z/L$, say. For large angles of incidence the singular point $z_0 = L(1 - i2\Gamma_e/\omega_L)$ and the point of reflection $z_1 = L(1 - \sin^2\theta_0 - i2\Gamma_e/\omega_L)$ are sufficiently far apart in terms of the wavelength for the solution near these points to be given by distinct functions. As expected, the solution away from $z = z_0$ is an Airy function. For $z_1 < z < z_0$ the solution is essentially a modified Hankel function of the first kind of order 1. From the relations below Eq. (3.83) and the asymptotic behavior of the Hankel function it follows that at $z = z_0$ the field component E_y has a logarithmic singularity and $|E_z| \sim \sin\theta_0 |w(z_0)|/|(z - z_0)/z_0 + i2\Gamma_e/\omega_L|$. In the limit $\theta_0 \to 0$ this last result is clearly incorrect as $E_z = 0$ for normal incidence, reflecting the fact that for small angles the transition point and the singularity can no longer be treated separately. To determine the angle of incidence for which absorption at $z = z_0$ is a maximum, Denisov (1956) obtained a solution in terms of an Airy function and its derivative which approximately represents $w(z_0)$ for all angles θ_0. On the basis of that calculation $|E_z(z_0)|$ has, in a collisionless medium, its maximum value when $(k_L L)^{1/3} \sin\theta_0^{\rm opt} \simeq 0.7$. For 1.06μ radiation falling on a plasma with scale length $L = 100\mu$, this yields $\theta_0^{\rm opt} \sim 6°$ corresponding to $|E_z| \sim (\omega_L/2\Gamma_e)(2\pi k_L L)^{-1/2}$ in units of the incident field. It will be seen that this phenomenon can lead to large fields and electron velocities at $z = z_0$. This has been confirmed by the simulation studies of Freidberg *et al.* (1971) who find that the resonant mechanism leads to the formation of a strongly non-Maxwellian high-energy tail on the electron velocity distribution. The approximate electron energy, ϵ_e say, may be calculated by integrating the maximum E_z from $z = z_0$ to the point $z_0 \pm \Delta z$ where E_z drops to half its maximum value. The above expression for E_z yields $\Delta z = 2\Gamma_e z_0/\omega_L$, and allowing for the field normalization we obtain $\epsilon_e \sim (8 P_L \omega_L m_e L/n_c)^{1/2}$, where P_L is the absorbed power flux density. For 1.06μ radiation, $P_L = 10^{15}$ W/cm^2 and $L = 100\mu$, $\epsilon_e \sim \frac{2}{3}$ MeV.

I. Experiments and simulation studies

Experimental investigations on the above-named instabilities are at present scant. There is no incontrovertible evidence as yet for their excitation in laser-driven plasmas, although it is difficult to explain the reflection measurements of Shearer, Mead, Petruzzi, Swain, and Violet (1972) and of Eidman and Sigel (1972) without invoking some sort of stimulated phenomenon such as SBS. Yamanaka *et al.* (1972) found that the theoretical thresholds for the modified two-stream instability and the parametric decay instability were within the range of intensities covered in their experiments which showed anomalous absorption. They further correlated the onset of anomalous absorption with an anomaly in light reflection and with the appearance of a fast-ion group and an increase in electron temperature. These phenomena, incidentally, appeared to be closely correlated with neutron yield. The recent experiments of Bobin, Decroisette, Meyer and Vitel (1973) are also convincingly explained by coupling between parametrically excited longitudinal Langmuir waves and the pump field. These experiments all involved peak intensities of 10^{14}–10^{15} Wcm^{-2}, sufficient for parametric conversion, even allowing for macroscopic density gradients. Their counterparts are almost certainly responsible for parametric coupling of waves, enhanced heating, and anomalous reflectivity observed in microwave and ionosphere experiments carried out among others by Stern and Tzoar (1966), Gekker and Sizukhin (1969), Eubank (1971), Phelps, Rynn, and Van Hoven (1971), Dreicer, Henderson, and Ingraham (1971), and Chu and Hendel (1972), for electromagnetic excitation, and by Franklin, Hamberger, Lampis, and Smith (1971),

and Stenzel and Wong (1972) with electrostatic excitation. Where thresholds were measured they agree reasonably with calculated values, particularly in the Stenzel and Wong (1972) experiment where boundary effects for the decay waves were small, and in the experiment of Eubank (1971) if allowance is made for plasma inhomogeneity (cf. Chu, Hendel, and Dawson, 1972). The ultimate proof, however, must involve detailed substantiation of the resonance conditions and determination of the dispersion of the excited modes.

Further evidence has been provided by a number of numerical or simulation experiments. We note particularly those indicating anomalous electron heating (Kruer *et al.*, 1970), ion-acoustic decay instability (Bodner, Chapline, and de Groot, 1973), anomalous high-frequency resistivity (Kruer and Dawson, 1972), and excitation and nonlinear development of back-scattered SRS and SBS (Forslund, Kindel, and Lindman, 1972). Strong electron heating due to the initial development of SRS at $n < \frac{1}{4}n_c$ was seen followed by saturation and the subsequent excitation of the ion wave in SBS. Simulation calculations such as these are of great importance for studying the nonlinear regime, especially with respect to stabilizing mechanisms. The work of Forslund *et al.* (1972), for instance, indicates stabilization by fluid saturation when the reflected wave has grown until it is equal in amplitude to the pump wave. They also find that at high pump intensities, linear growth is quenched by wave breaking, resulting in reduced reflection. This nonlinear phenomenon can occur when the perturbed density grows to exceed the unperturbed density before fluid saturation is attained. The limitation of these studies is that they do not provide detailed information about the early, linear, phase of instability development near threshold. This is because the computer running time is limited to a few thousand laser periods. Thus, a temporal gain of $10^{12}\,\mathrm{sec}^{-1}$ is required, corresponding to intensities well above threshold.

IV. HYDRODYNAMIC ENERGY TRANSFER

The problem of laser energy deposition in the plasma, which is clearly one of the major issues in laser-driven fusion, has been extensively reviewed in the preceding section. The analysis is necessarily inconclusive since the actual magnitudes of the various coupling mechanisms are limited by nonlinear effects which are outside the scope of the usual instability theory. In addition, the time dependence and spatial scale of the laser heating process can markedly affect the instability growth. The problem of the laser–plasma interaction therefore awaits experimental resolution. For the present, we assume that the various effects lead to good energy absorption.

The absorbed laser energy appears as thermal energy of the absorbing layer, as kinetic energy of the expanding plasma, and as thermal and kinetic energy of the overdense plasma into which energy is transferred primarily by electron conduction. The penetration of energy into the overdense plasma is accompanied by a hydrodynamic rarefaction wave following the thermal conduction wave. Consequently, the energy deposited by the laser is very markedly depleted by the loss of energy to outward motion and expansion of plasma heated by the conduction wave and subsequently removed by the hydrodynamic rarefaction wave.

These effects can be estimated to give the order-of-magnitude of the energy partition among the various processes. The pressure driving the implosion arises primarily by removal of material at the surface of the dense compressed DT, as a result of energy transport from the laser deposition region to the region of compression. This region of energy flow, primarily by electron conduction, must be approximately isothermal if efficient energy transfer is occurring, although the density drops rapidly outward from the dense heated surface due to outward acceleration of the ablated material removed at the dense surface. If the temperature is sufficiently high so that the laser energy flux is efficiently transferred to the ablating surface, energy balance requires that the incident laser flux be equal to the energy in the ablated material. In one dimension and under isothermal conditions, the equations of motion and continuity are (we assume equal electron and ion temperatures)

$$\begin{aligned} m_i n\left(\frac{\partial}{\partial t} + v\frac{\partial}{\partial z}\right)v &= -2\theta\frac{\partial n}{\partial z}, \\ \partial n/\partial t + \partial nv/\partial z &= 0, \end{aligned} \tag{4.1}$$

with z the depth from the surface, and t the time. The solution is easily shown to be

$$\begin{aligned} n &= n_0 \exp(-z/c_T t), \\ v &= c_T + (z/t), \end{aligned} \tag{4.2}$$

with c_T the isothermal sound velocity $c_T^2 = (2\theta/m_i)$. The total energy per unit area in the plasma is

$$\begin{aligned} E &= \int_0^\infty dz\left[\frac{1}{2}m_i n\left(c_T + \frac{z}{t}\right)^2 + 3n\theta\right] \\ &= 8n_0\theta c_T t. \end{aligned} \tag{4.3}$$

Thus energy balance in plane geometry requires a laser energy flux

$$\varphi_L = 8n_0\theta c_T. \tag{4.4}$$

The mass flow into the rarefaction zone is $\dot{m} = m_i c_T n_0$, and the ablation pressure $p_A = 2n_0\theta$.

These equations may now be used to determine the acceleration of the surface. We treat the accelerating high density layer as a mass layer of initial mass per unit area m_0. The mass loss makes the mass a function of time,

$$m(t) = m_0 - \dot{m}t. \tag{4.5}$$

The equation of motion is

$$(m_0 - \dot{m}t)\ddot{r} = p_A \tag{4.6}$$

giving

$$\begin{aligned} v(t) &= (p_A/\dot{m})\ln[m_0/m(t)] \\ &= c_T \ln[m_0/m(t)]. \end{aligned} \tag{4.7}$$

The kinetic energy in the accelerated layer is

$$\tfrac{1}{2}m(t)v(t)^2 = \tfrac{1}{2}m(t)c_T^2\{\ln[m_0/m(t)]\}^2. \tag{4.8}$$

The laser energy is

$$E_L = \varphi_L t = 8n_0\theta c_T[(m_0 - m(t))/\dot{m}] = 4c_T^2[m_0 - m(t)]. \quad (4.9)$$

The ratio of energy in the accelerated layer to the incident laser energy is then

$$\frac{\frac{1}{2}m(t)v(t)^2}{E_L} = \frac{1}{8}\frac{m(t)}{m_0 - m(t)}\left(\ln\frac{m_0}{m(t)}\right)^2. \quad (4.10)$$

The maximum energy transfer occurs at $m_0/m(t) \cong 5$, so that

$$[\tfrac{1}{2}m(t)v(t)^2/E_L]_{\max} = 0.081 \quad (4.11)$$

The above estimate is based on simplifying assumptions and has neglected the spherical nature of the motion. More detailed calculations for the actual process using the numerical methods described in Sec. VI give a similar result, the energy transfer being at best about 10% and more typically about a factor of two lower. Thus the efficiency factor ϵ_L is between 0.05 and 0.10.

V. COMPRESSION

A. Introduction

The preceding analysis shows that the production of useful amounts of fusion energy can result only if the pellet is highly and efficiently compressed. The compression must also be carried out under conditions which bring the central region of the pellet to ignition temperature and density but which leave the rest of the compressed pellet as cold as possible. The latter condition is essential to minimize the over-all energy requirements.

The problem of compression centers around the hydrodynamics of convergent shocks and of providing the pressure at the pellet surface which is required to produce the desired hydrodynamic motion. The pressure variation is in turn determined by the absorbed laser flux and the energy transfer from the deposition region into the ablating pellet surface. These processes therefore depend critically on a correct description of the laser deposition process and the energy flow into the dense pellet. Finally, the compression may be limited by departures from spherical symmetry produced by nonuniform laser illumination, intrinsic pellet asymmetries, or by hydrodynamic instability causing amplification of small disturbances in the pellet motion.

In Secs. III and IV we have exhaustively examined the problem of laser coupling to the plasma and given an outline of the limits set by hydrodynamic transfer into the dense pellet core. In subsection V.B we review the general features of the hydrodynamics. In subsection V.C we describe the structure of a single shock in spherical geometry and show how the fusion energy produced can be determined analytically. In subsection V.D we review the theory of shock sequences in plane geometry as an introduction to the more difficult problem of shock sequences in spherical geometry, which is reviewed in subsection V.E. We then turn in subsection V.F to the difficult issues of anomalous energy transport into the pellet. Finally, in subsection V.G we discuss the origins and effects of asymmetry in the pellet compression.

B. General features of the hydrodynamics

The conditions to be achieved in the compressed pellet are qualitatively clear from the analysis in Section II. The center of the compressed pellet must be brought to the ignition temperature of a few keV while the rest of the pellet is highly compressed at the lowest possible temperature. Very high compression is desirable to maximize the reaction rate after the pellet has ignited. Too high compression however requires excessive work done against the degeneracy pressure of the electrons. Excessive compression is also unnecessary since the pellet yield is eventually limited by fuel depletion.

The driving pressure producing the pellet compression results from the ablation of the dense pellet surface, which is produced by the flow of energy from the laser deposition region, the energy being carried by hot electrons. If the electron distribution is Maxwellian and the electron mean free path short, relative to the depth of the overdense plasma, the electron energy is carried by classical electron conduction which can be described by the standard diffusion equation of heat flow. Since the conductivity of the electrons is proportional to $(\theta_e)^{5/2}$, the temperature in the conduction region is a steeply rising function of distance from the thermal front, with most of the conduction region being approximately isothermal.

Since the compression is ablation-driven, with the velocity of material removal at the dense pellet surface determined essentially by the local speed at the thermal front, the time available for the hydrodynamic motion is less than the sound transit time to the pellet center through the relatively cold plasma ahead of the conduction front. The motion of the pellet surface must therefore be supersonic with respect to the cold plasma, and shocks necessarily form. The shock heating, however, must be minimized since the shocks heat the plasma irreversibly, increasing the final work which is required to reach the desired compression. The strength of the shocks which form is determined by the pressure at the conduction front, which is fixed by the temperature in the conduction region. The temperature is determined by the laser flux which is absorbed near the critical density surface.

The problem of minimizing the shock heating while at the same time driving the pellet to high compression is qualitatively clear but the highly nonlinear nature of the process makes analysis difficult. The problem is, however, ideally suited to computer study which is the basis of the quantitative results to be given later. The next subsection analyzes the relatively simple case of a single shock in spherical geometry.

C. Compression and fusion yield in a single convergent shock

The first published suggestion of the possibility of obtaining increased fusion yield by producing pellet compression in a convergent shock is that of Daiber, Hertzberg, and Wittliff (1966). They did not analyze the problem of laser energy deposition, or of the thermal conduction process and pellet ablation driving the implosion, or of the energy loss into the ablated plasma. Their results are, however, of considerable interest since they

were among the first to suggest using a laser as a hydrodynamic driver of pellet compression rather than as a plasma heater. Their analysis was based on the compression produced by uniform pressure applied to the pellet surface which produces a single shock. This case is of interest since the results for fusion yield and shock energy can be obtained analytically from the well known results of Guderley (1942), provided that the perturbation of the hydrodynamic process by the fusion reaction is ignored. This is approximately valid under the conditions which can be produced by a single shock, if the fusion yield is not appreciably larger than the hydrodynamic energy.

In a strong spherically convergent shock, a self-similar solution holds which gives the shock position as a function of time as

$$r = \xi(-t_0)^n, \tag{5.1}$$

with time measured from the time the shock reaches the center of convergence. For an ideal gas with $\gamma = 5/3$ and in spherical geometry, $n = 0.6884$ (Sigmar and Joyce, 1971). The parameter ξ in Eq (5.1) determines the shock strength. The scaled density, scaled temperature, and scaled pressure at a radius r are functions only of the reduced time t/t_0, i.e.,

$$\begin{aligned} \rho/\rho_0 &= f_\rho(t/t_0), \\ p/\rho_0 u_0^2 &= f_p(t/t_0), \\ \theta &= mp/2\rho = (mu_0^2/2) f_\theta(t/t_0), \end{aligned} \tag{5.2}$$

(we assume equal electron and ion temperatures) with

$$\begin{aligned} f_\theta &= f_p/f_\rho\ , \\ \rho_0 &= \text{initial density}, \\ p_s &= \text{pressure in initial shock} \\ &= (2/(\gamma+1))\rho_0 u_0^2. \end{aligned} \tag{5.3}$$

The functions f_ρ, f_p, and f_θ are (from Goldman, 1973) given in Figs. 9(a), 9(b), and 9(c). Figure 9(a) shows that the passage of the first converging shock gives a density increase of a factor of four (for a gas with $\gamma = 5/3$) followed by adiabatic compression to a density ratio of about 15. The shock then is reflected at the center and on returning gives a further shock compression to a maximum density ratio of 33. This is the maximum compression that can be achieved in spherical geometry by passage of a single shock. From Eq. (5.1), the shock velocity is

$$u_0 = n\xi^{1/n} r^{(n-1)/n}. \tag{5.4}$$

The fusion yield is

$$E_{\text{fusion}} = 4\pi \int_0^{r_{\max}} r^2\, dr \int_{t_0}^{t_{\max}} dt \frac{n(r,t)^2}{4} \overline{\sigma v}(\theta(r,t)) W \tag{5.5}$$

where $W = 17.6$ MeV for the DT reaction. The fusion yield sharply peaks for small r and near the time of maximum compression, so that the upper limits of integration in Eq. (5.5) can be set equal to ∞. Using Eq. (5.1) and Eq. (5.2), we rewrite Eq. (5.5) as

$$E_{\text{fusion}} = \pi n_0^2 W \int_0^\infty r^2\, dr \left(\frac{r}{\xi}\right)^{1/n} \int_{-1}^\infty dx f_\rho^2(x) \overline{\sigma v}[\theta(r,x)]. \tag{5.6}$$

The fusion energy is to a very good approximation produced by the compression and heating due to the reflected shock. In addition, the temperature in the reflected shock is a slowly varying function of x, although a rapidly varying function of r. Thus, Eq. (5.6) can be accurately approximated by

$$E_{\text{fusion}} = \pi n_0^2 W \xi^{-1/n} \int_0^\infty r^{2+1/n}\, dr\, \overline{\sigma v}(\theta(r, x_1)) \int_{x_1}^\infty dx f_p^2(x), \tag{5.7}$$

with x_1 the scaled time of the reflected shock. In Eq. (5.7) the temperature following the second shock is given as a function of radius by

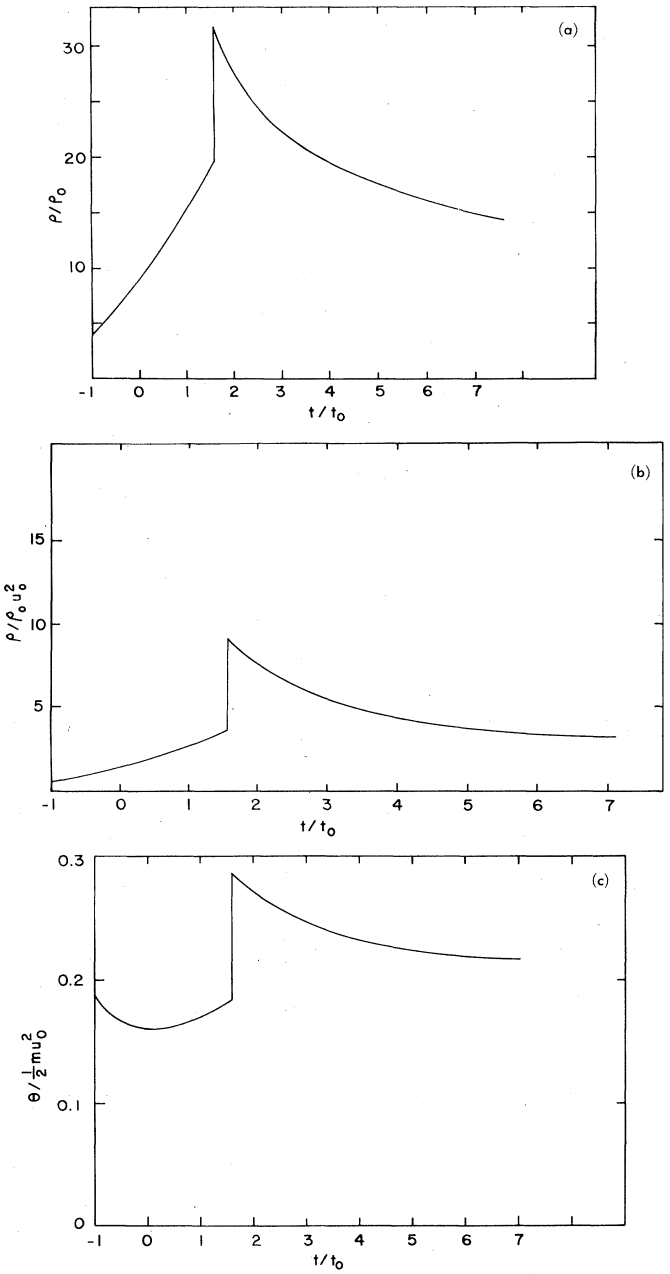

FIG. 9. Distributions of density ρ, pressure p, and temperature θ for a converging shock wave (Goldman, 1972).

$$\theta(r, x_1) = (m/2)[p_s(r)/\rho_0] f_\theta(x_1) = \frac{m}{\gamma + 1}(n\xi^{1/n} r^{1-1/n})^2 f_\theta(x_1). \tag{5.8}$$

In Eq. (5.7), changing variables from r to θ, we find

$$E_{\text{fusion}} = \pi n_0^2 W \xi^{-1/n} I_1 \left(\frac{1}{\lambda}\right)^{(3n+1)/2(n-1)} \frac{n}{2(1-n)} \times \int_0^\infty \theta^{(n+3)/2(n-1)} d\theta \overline{\sigma v}(\theta), \tag{5.9}$$

with

$$\lambda = \frac{m}{\gamma + 1} n^2 \xi^{2/n} f_\theta(x_1), \quad I_1 = \int_{x_1}^\infty dx f_\rho^2(x).$$

The integral over θ in Eq. (5.9) may be evaluated by a saddle-point approximation. The reaction constant $\overline{\sigma v}$ in the few keV temperature range is (Wandel *et al.*, 1959)

$$\overline{\sigma v} = (\sigma_0/\theta^{2/3}) \exp(-B/\theta^{1/3}). \tag{5.10}$$

Thus the integral over θ in Eq. (5.9) may be written

$$\int_0^\infty d\theta \exp(-f(\theta)), \tag{5.11}$$

with

$$f(\theta) = k \ln \theta + B\theta^{-1/3}, \quad k = (n+3)/2(1-n) + 2/3. \tag{5.12}$$

The saddle point is at

$$\theta_s = (B/3k)^3 = 0.92 \text{ keV}. \tag{5.13}$$

The saddle-point approximation gives

$$\int_0^\infty d\theta \exp[-f(\theta)] = \sqrt{\frac{2\pi}{f''(\theta_s)}} \exp(-f(\theta_s)).$$

Returning to Eq. (5.9), we find

$$E_{\text{fusion}} = \pi n_0^2 W I_1 \frac{n}{2(1-n)} \sqrt{\frac{6\pi}{k}} \overline{\sigma v}(\theta_s) \times \left(\frac{\theta_s}{mn^2} \frac{\gamma + 1}{f_\theta(x_1)}\right)^{(3n+1)/2(n-1)} \xi^{4/(1-n)}. \tag{5.14}$$

The corresponding value of the radius at which θ equals θ_s is, using Eq. (5.8),

$$r_s = \left(\frac{\theta_s(\gamma + 1)}{mn^2 f_\theta(x_1)}\right)^{n/2(n-1)} \xi^{1/1-n}. \tag{5.15}$$

With this result, we can also put Eq. (5.14) into the form

$$E_{\text{fusion}} = \left\{\frac{4}{3}\pi \frac{n_0^2 \overline{\sigma v}(\theta_s)}{4} W r_s^3 t_0(r_s)\right\} \frac{3n}{2(1-n)} \sqrt{\frac{6\pi}{k}} I_1. \tag{5.16}$$

The factor

$$\frac{3n}{2(1-n)} \sqrt{\frac{6\pi}{k}} I_1$$

gives the correction, arising from the shock compression, to the simple formula in the brackets { } in Eq. (5.16), which would be the result for a homogeneous plasma at density n_0 with radius r_s heated to θ_s confined for the hydrodynamic disassembly time $t_0(r_s)$. The numerical value can be determined by evaluation of the integral I_1, as defined in Eq. (5.9), using the function f_ρ given in Eq. (5.2). The result is

$$\frac{3n}{2(1-n)} \sqrt{\frac{6\pi}{k}} I_1 = 3.43 \times 10^4. \tag{5.17}$$

This large correction factor arises from an average compression of about 30, an increase in temperature and rise of reaction rate for the region $r < r_s$, from a reaction time which is about five times t_0, and from a factor of about 2 over r_s in the effective radius of the reacting fuel, r_s being the radius at which the reaction peaks.

The kinetic and thermal energy in the shock can be similarly calculated. The energy is

$$E_{\text{shock}} = 4\pi \int_0^{r_{\max}} r^2 dr \left(\tfrac{1}{2}\rho u^2 + \tfrac{3}{2}p\right) = 4\pi \int_0^{r_{\max}} r^2 dr \frac{2}{\gamma + 1} \rho_0 u_0^2 f_E(t/t_s), \tag{5.18}$$

with

$$f_E = \left(\frac{1}{2}\rho u^2 + \frac{3}{2}p\right) \Big/ \left(\frac{2}{\gamma + 1}\rho_0 u_0^2\right). \tag{5.19}$$

Using the relationship between r and t_0 given in Eq. (5.1), and Eq. (5.4) for u_0, and introducing the variable $x = t/t_0$, we obtain for Eq. (5.18)

$$E_{\text{shock}} = 4\pi[2/(\gamma + 1)]\rho_0 n^3 \xi^5 t^{5n-2} I_E, \tag{5.20}$$

with

$$I_E = \int_{1.60}^\infty \frac{dx}{x^{5n-1}} f_E(x) = 3.60. \tag{5.21}$$

To evaluate Eq. (5.20), t must be specified. To obtain an estimate we set t equal to the time at which the reflected shock reaches the radius r_s, given in Eq. (5.15), i.e., $t = 1.60 t_0(r_s)$. The result may be put into clearer form by also using the relationship in Eq. (5.15) between the temperature θ_s and the radius r_s at the saddle point of the temperature integral in Eq. (5.9). After some rearrangement of Eq. (5.20) we find

$$E_{\text{shock}} = \frac{4}{3}\pi(3n_0\theta_s) r_s^3 \frac{1}{\gamma + 1} \frac{\beta^{5n-2}}{f_\theta(1.60)} I_E. \tag{5.22}$$

Using the numerical values of the various parameters, we obtain the result

$$E_{\text{shock}} = 24.1 \frac{4}{3}\pi(3n_0\theta_s) r_s^3. \tag{5.23}$$

Eq. (5.23) shows that the energy in the shock is greater by a factor of 24.1 than that given by the thermal energy at a density n_0 and a temperature θ_s within the radius r_s. This factor arises from the compression of about 20 within this radius, and from higher temperatures than θ_s for $r < r_s$.

Equation (5.16) for the fusion yield and Eq. (5.23) for

the energy in the shock now may be combined to determine r_s as a function of $E_{\text{fusion}}/E_{\text{shock}}$, and finally E_{shock}. The result, which may be expressed in the form of Eq. (2.16) with $E_{\text{laser}} = E_{\text{shock}}/\epsilon_L$, is

$$E_{\text{laser}} = 40.9\left(\frac{n_s}{n_0}\right)^2\left(\frac{E_{\text{fusion}}}{E_{\text{laser}}}\right)^3\frac{1}{\epsilon_L^4}\ \text{MJ}. \tag{5.24}$$

In the original paper by Daiber *et al.* (1966), the energy requirement for a fusion energy equal to twice the shock energy and an initial density equal to solid density is given as approximately 2 MJ. Since the details of their calculations are not given we have not been able to determine the source of the large discrepancy between their result and that given by Eq. (5.23). They also did not determine the coupling efficiency ϵ_L.

The surprising result of the analysis leading to Eq. (5.24) is that the shock compression has not reduced the laser energy requirement from that given by Eq. (2.16), assuming that the coupling efficiency is the same. The effect of compression appears to be offset by an inefficient temperature distribution which reduces fusion energy production in most of the fuel. The compressed center which is strongly heated has too small a volume and too short a compression time to contribute appreciably to the net fusion yield.

The effective laser coupling to the shock cannot be readily estimated from the preceding analysis, since the laser absorption, surface pellet ablation, and the energy lost in the expanding plasma must be separately calculated.

Calculations by Lubin and collaborators (1971) give for DD a fusion yield of 3.7×10^9 neutrons for an absorbed laser energy of 927 J. Scaling this result to DT gives a fusion yield of 0.41 J. Equation (5.24) gives this yield for $\epsilon_L \cong 0.21$.

Calculations at KMS Fusion for a solid DT sphere with a laser pulse constant in time give $E_{\text{fusion}} = E_{\text{laser}}$ at a laser energy of about 500 MJ, although the calculation differs from the model described above in that the effect of pellet self-heating is included.

The analysis of this section and the numerical results given show that pellet compression sufficient to give an interesting fusion yield cannot be produced by a single shock. This is because a single shock in spherical geometry cannot give a compression greater than a factor of about 30, which is too small to overcome the other inefficiency factors in the laser coupling and in the hydrodynamic processes.

We turn next to shock sequences for achieving high compression.

D. Shock sequences in a plane

To clarify the problem of compression by a sequence of convergent shocks, we first review the process of compression in plane geometry for which the problem can be solved exactly. We then will turn in the next subsection to the actual case of interest in spherical geometry.

The conditions at a shock are fixed by the conservation of mass, momentum, and energy. Implicit in the assumption of a shock is the process of entropy change due to particle collisions which spread the shock discontinuity over a few mean free paths.

In a one-dimensional planar shock the jump conditions between n and $n+1$ give

$$\begin{aligned}\frac{\rho_{n+1}}{\rho_n} &= (\gamma+1)\Big/\left(\gamma-1+\frac{2\gamma p_n}{\rho_n(C_{nn+1}-v_n)^2}\right),\\ C_{nn+1}-v_{n+1} &= (\rho_n/\rho_{n+1})(C_{nn+1}-v_n),\\ p_{n+1} &= p_n+(C_{nn+1}-v_n)^2\rho_n[1-(\rho_n/\rho_{n+1})],\end{aligned} \tag{5.25}$$

with C_{nn+1} the shock velocity between the n and $n+1$ zones. Now consider the case of successive shocks such that the same density change occurs at each shock following the first shock into the stationary material at $\rho_0 = 0$ and $v_0 = 0$, i.e.,

$$\gamma p_n/\rho_n(C_{nn+1}-v_n)^2 = \lambda, \tag{5.26}$$

giving

$$\rho_{n+1}/\rho_n = (\gamma+1)/(\gamma-1+2\lambda). \tag{5.27}$$

(Note, that if $\lambda = 1$, $\rho_{n+1} = \rho_n$ and the shock is sonic.) For this case,

$$\begin{aligned}p_{n+1} &= p_n\{1+[2\gamma(1-\lambda)/(\gamma+1)\lambda]\},\\ v_{n+1} &= v_n+[2(1-\lambda)/(\gamma+1)](\gamma p_n/\rho_n\lambda)^{1/2}.\end{aligned} \tag{5.28}$$

The shock velocity is

$$C_{nn+1} = v_n+(\gamma p_n/\lambda\rho_n)^{1/2}. \tag{5.29}$$

These equations show that the pressure and density increase with n as

$$\begin{aligned}p_{n+1}/p_1 &= \{1+[2\gamma(1-\lambda)/\lambda(\gamma+1)]\}^n,\\ \rho_{n+1}/\rho_1 &= [(\gamma+1)/(\gamma-1+2\lambda)]^n,\\ \rho_1 &= [(\gamma+1)/(\gamma-1)]\rho_0.\end{aligned} \tag{5.30}$$

The material velocity is

$$\frac{v_{n+1}}{v_1} = 1+\frac{1-\lambda}{\gamma+1}\left(\frac{2\gamma(\gamma-1)}{\lambda}\right)^{1/2}\sum_{k=1}^{n-1}x^k, \tag{5.31}$$

with

$$\begin{aligned}v_1 &= \{[2/(\gamma+1)](p_1/\rho_0)\}^{1/2},\\ x &= \{[2\gamma+\lambda(1-\gamma)](\gamma-1+2\lambda)/\lambda(\gamma+1)^2\}^{1/2}.\end{aligned} \tag{5.32}$$

The sum in Eq. (5.31) gives

$$\frac{v_{n+1}}{v_1} = 1+\frac{1-\lambda}{\gamma+1}\left(\frac{2\gamma(\gamma-1)}{\lambda}\right)^{1/2}\frac{x^n-1}{x-1}. \tag{5.33}$$

Equations (5.30) and (5.33) combine to give v_n as a function of p_n, i.e.,

$$\begin{aligned}\frac{v_n}{v_1}-1 &= \frac{1-\lambda}{\gamma+1}\left(\frac{2\gamma(\gamma-1)}{\lambda}\right)^{1/2}\frac{1}{x-1}\left[\left(\frac{p_n}{p_1}\right)^{g_1}-1\right],\\ g_1 &= \ln x/\ln\left(1+\frac{2\gamma(1-\lambda)}{\lambda(\gamma+1)}\right).\end{aligned} \tag{5.34}$$

Similarly,

TABLE I. Effective gamma for compression.

λ	ρ_{n+1}/ρ_n	g_2
0.15	2.76	2.06
0.25	2.29	1.89
0.50	1.60	1.74
0.75	1.23	1.68
1.00	1.00	1.67

$$p_n/p_1 = (\rho_n/\rho_1)^{g_2},$$
$$g_2 = \ln\left[1 + \frac{2\gamma(1-\lambda)}{\lambda(\gamma+1)}\right] \Big/ \ln\left(\frac{\gamma+1}{\gamma-1+2\lambda}\right). \quad (5.35)$$

The effective gamma for the compression is g_2, which reduces to γ if the density change at successive shocks is small, i.e. $\lambda \to 1$. For density increases, some typical values of g_2 are given in Table I. Thus the compression is not far above adiabatic even with the density doubling at each shock.

If the successive shocks are weak, $\lambda \to 1$ and Eq. (5.34) and Eq. (5.35) can be expanded in powers of $1-\lambda$. The result is

$$g_1 = \frac{\gamma-1}{2\gamma} + \frac{\gamma-1}{3\gamma(\gamma+1)}(1-\lambda)^2 + O(1-\lambda)^3,$$
$$g_2 = \gamma + \frac{\gamma(\gamma-1)}{3(\gamma+1)}(1-\lambda)^2 + O(1-\lambda)^3. \quad (5.36)$$

Thus, for λ close to 1, the compression following the first shock is adiabatic, and Eq. (5.34) reduces to

$$\frac{v_n}{v_1} - 1 = \frac{\gamma+1}{\gamma-1}(2\gamma(\gamma-1))^{1/2}\left[\left(\frac{p_n}{p_1}\right)^{(\gamma-1)/2\gamma} - 1\right], \quad (5.37)$$

for $\gamma = 5/3$,

$$\frac{v_n}{v_1} - 1 = \frac{8}{3}(5)^{1/2}\left[\left(\frac{p_n}{p_1}\right)^{1/5} - 1\right]. \quad (5.38)$$

Equation (5.38) shows that the material velocity increases only slowly with the driving pressure. For a pressure increase of 100 over p_1, the material velocity is 10 times the velocity after the first shock.

The above equations hold only if the successive shocks do not overtake each other. If the nth shock is formed at t_n, the condition for non-overtaking by time t is

$$v_n(t - t_n) \leq v_{n-1}(t - t_{n-1}). \quad (5.39)$$

Treating n as a continuous variable, Eq. (5.39) gives the condition

$$\frac{dv_n}{dn}\Big/\frac{dt_n}{dn} \leq v_n/(t - t_n) \quad (5.40)$$

or

$$v_n/v_1 \leq t/(t - t_n). \quad (5.41)$$

Thus, all shocks arrive at the same point at time t if started at the time given by Eq. (5.41). The required driving pressure is

$$\frac{p(t_n)}{p_1} = \left[\frac{3}{8(5)^{1/2}}\left(\frac{t_n}{t - t_n}\right) + 1\right]^5. \quad (5.42)$$

E. Shock sequences in spherical geometry

As is apparent from the preceding analysis of shocks in plane geometry, compression larger than that which can be reached in a single shock can be produced if the fuel is subject to a rising pressure, or equivalently, to a succession of shocks of increasing strength which are adjusted in time so that the successive shocks do not overtake each other before arriving at the center of convergence. In either case, the compression and temperature histories after the passage of the first shock follow approximately an adiabat until the shock reaches the center of convergence where the kinetic energy of motion is converted into internal energy and a reflected shock forms. The final temperature necessary to initiate the fusion reaction is determined for a given final compression by the first shock strength. It is particularly important to avoid excessive early heating of the DT by the initial shock or by successive shock coalescence, since the final temperature reached by the hydrodynamic compression may be too high. The optimum occurs when the DT, after final compression, reaches the minimum temperature required for ignition. If a proper pressure history is achieved, the achievable compression is limited finally only by the degeneracy pressure of the electrons or possibly by ignition of the fuel before the maximum compression has been reached.

As an example, if DT is initially compressed without excessive shock heating, the energy required at high compression is the work done against the degeneracy pressure of the electrons. The degeneracy energy per electron is $2.68(n/n_s)^{2/3}$ electron volts. Thus at a compression of 300, the energy is 120 eV/electron. Compression of a 1/2 mm radius sphere, initially at solid density, to this density therefore requires an energy in compression of 515 J. If a strong shock is now applied to the compressed DT, further compression and heating will result. The peak compression of 33 by the final reflected shock will bring the final compression ratio to a peak of about 10^4. The temperature of five kilovolts required for fuel ignition gives a pressure peak of 8×10^6 Mbars. For this to be achieved over a 5 μm dimension requires an initial driving pressure at the surface of the precompressed pellet of about 10^4 Mbars, the increase to 8×10^6 Mbars resulting from the convergence and the formation of the reflected shock. The pressure of 10^4 Mbars requires an energy flux to the surface of the dense pellet of about 4×10^{16} W/cm^2. The actual problem of shaping the pressure and hence the laser flux profile is qualitatively clear but can be solved quantitatively only by computer study.

The problem of fuel compression can also be solved by the use of a spherical shell of DT fuel of relatively large radius. The increase in the volume change of the fuel on compression increases the hydrodynamic work resulting from a given applied pressure, allowing a drop in driving pressure for a given fuel mass. The shock strengths are accordingly lower and an optimized pressure and compression history may be realized more easily for a shell than for a uniform sphere. The shell acceleration also reduces the required range of laser powers very markedly, particularly for relatively thin shells. The flux optimization problem is again soluble only by extensive computer analysis.

The fuel compression which can in practice be achieved at fuel temperatures in the desired range of

many kilovolts is sensitive to other details of the desired density and temperature profiles, which will be discussed later. The hydrodynamic studies in spherical geometry using the numerical methods described in Sec. VI, which include the laser energy deposition and energy partition processes described earlier, show that central densities peaking at several thousand gm/cm³ are achievable. Departures from spherical symmetry, and anomalies in the energy transfer processes may, however, in practice reduce the compression. These problems are described next.

F. Preheat by fast electrons

At high laser power the laser energy deposition is probably by anomalous absorption and strong electron heating is expected together with departures of the electron distribution from Maxwellian. The magnitude of the electron heating can be estimated from a simple model proposed by Morse and Nielson (1972). Detailed calculations of energy deposition show approximate agreement with the result of this model.

The laser flux φ_L, which under conditions of anomalous absorption is deposited close to the critical density surface, is removed by an inward flux φ_{hot} of fast electrons. The imposition of charge neutrality requires that an outward flux φ_{cold} of cold electrons balance the fast electron current. For one dimension, with $n(v)$ = constant, $v < v_{\max}$, the fluxes are

$$\begin{aligned} \varphi_{\text{hot}} &= n_H(m/8)v_H^3, \\ \varphi_{\text{cold}} &= n_C(m/8)v_C^3. \end{aligned} \tag{5.43}$$

Current conservation requires $n_H v_H = n_C v_C$. The sum of the electron densities may be taken equal to the critical density n_{crit}. The result is

$$\varphi_L = \frac{m}{8} n_H v_H^3 \left[1 - \frac{n_H^2}{(n_{\text{crit}} - n_H)^2}\right]. \tag{5.44}$$

According to the results of computer simulation studies, the fluxes adjust themselves to minimize the fast electron flux, which occurs at $n_H = \frac{1}{3}n_{\text{crit}}$, $n_C = \frac{2}{3}n_{\text{crit}}$, giving

$$\begin{aligned} \varphi_L &= (m/32)n_{\text{crit}} v_H^3 \\ &= \tfrac{3}{4}\varphi_{\text{hot}}. \end{aligned} \tag{5.45}$$

The resulting maximum electron energy is

$$\begin{aligned} E(v_H) &= \tfrac{1}{2}mv_H^2 \\ &= 5(\varphi_L \lambda_\mu^2)^{2/3}\ \text{keV}. \end{aligned} \tag{5.46}$$

(Here φ_L is in units of 10^{14} w/cm², λ in μm). The electron energy can therefore become very high, particularly for 10 μm radiation, for laser power flux densities in the range of 10^{16}–10^{17} W/cm².

The fast electron flux from the deposition region can markedly affect the heating and compression of the pellet, preventing high compression from being achieved if substantial preheating of the pellet occurs. The principal heating is from the unscattered electron flux. Scattered electrons usually lose sufficient energy to reduce their range and prevent them from penetrating the pellet further. The unattenuated flux at the pellet center, with R the radius of the dense pellet core, is

$$\begin{aligned} \varphi_H(0) &\simeq \tfrac{4}{3}\varphi_L \int_0^{v_H} \exp\left[-\frac{R}{\lambda_e(v)}\frac{dv}{v_H}\right] \\ &\simeq \tfrac{1}{3}\varphi_L \frac{\lambda_e(v_H)}{R} \exp\left[-\frac{R}{\lambda_e(v_H)}\right]. \end{aligned} \tag{5.47}$$

For the reasons discussed in earlier sections, only 5 to 10% of the laser energy is effective in the hydrodynamic compression of the pellet core. The hot electron flux, therefore, may significantly perturb the compression unless the electron flux throughout most of the dense pellet core is less than roughly 1% of the laser flux at the critical density surface. This requires that the hot electron mean free path $\lambda_e(v_H)$ be much less than the pellet radius. To obtain a quantitative estimate we assume that $R/\lambda_e(v_H)$ is equal to four, which according to Eq. (5.47) gives a flux $\varphi_H(0)$ at the pellet center equal to $1.4 \times 10^{-3}\varphi_L$. The Coulomb cross section for the fast electrons is approximately 6×10^{-19} cm²/E (keV)² giving a mean free path

$$\lambda_e = 6.7 \times 10^{-6} \frac{E(\text{keV})^2}{\rho(\text{gm/cm}^3)}\ \text{cm}. \tag{5.48}$$

Thus, for pellet preheat to be prevented, the laser flux must satisfy the approximate inequality

$$\varphi_L < [(R\rho)^{3/4}/\lambda_\mu^2]1.2 \times 10^{16}\ \text{W/cm}^2. \tag{5.49}$$

In the final stages of compression the product of radius and density ranges from 1 to 10 gm/cm², and the laser flux ranges from 3×10^{15} to 5×10^{16} W/cm², depending on the pellet configuration. The lower flux value is typical of a relatively thin fuel shell and the higher value is typical of an initially uniform pellet. The condition Eq. (5.49) therefore cannot be met for 10 μm radiation, except possibly in the last stages of compression of a relatively thin fuel shell giving a relatively high fusion yield.

For 1 μm radiation, inequality Eq. (5.49) can only be marginally satisfied for a typical flux and compression. If this problem is present for DT spheres values, it may be alleviated by the use of fuel shells which allow a large reduction in laser power. The electron mean free path may also be markedly reduced by the introduction of a small admixture of high-Z contaminants in the DT.

The effect of electron preheat is clearly important for certain pellet configurations, particularly for long wavelength lasers. The quantitative effect must therefore be determined by a complete calculation which includes the variation of the flux with time during the implosion, and which treats more precisely the production of fast electrons. This problem depends critically on laser coupling instabilities in the deposition region, so that an experimental study is needed to verify the general features of the theory and to determine the possible anomalies in the electron distribution which cause preheating.

G. Asymmetries in compression

While the compressions achievable in a spherically symmetric implosion may be extremely high, assuming that the pellet preheat problem can be avoided, unavoidable departures from symmetry certainly limit the compression which can in practice be achieved. As pointed

out in the introduction to this section, departures from symmetry can arise from intrinsic pellet asymmetries, from nonuniform laser illumination, and from hydrodynamic instability. We discuss these problems next.

The fusion pellets must, of course, be sufficiently symmetric so that the compression is not reduced by nonuniform motion of the pellet surface. To achieve a compression of 10^4 requires the radius to be smaller by a factor of 0.046. The initial pellet configuration should therefore be symmetric to within one or two percent. Though this requirement is severe, it is not unachievable. The problems of illumination uniformity and implosion stability appear to present more important difficulties.

The uniformity of laser energy deposition in a spherical pellet depends on the intensity and angle of incidence of the laser flux. These are determined by the intensity distribution in the laser output and by the illumination system used to deliver the laser output to the pellet surface. It is very difficult, if not impossible, to produce a laser beam which is uniform in intensity and phase across the output aperture of the laser amplifier. The focused beam therefore will be nonuniform in space and usually also in time. In addition, the application of illumination systems using multiple laser beams, beam splitters, and focusing elements, results in unavoidable flux and angle-of-incidence variation, even for uniform output from the laser (or lasers for a multiple-beam laser system). The consequence of these effects is that the pellet is exposed to a laser flux which has a relatively slow variation resulting from the optics of the illumination system, and a much more rapid variation due to interference effects and mode structure in the laser beam.

In the absence of any smoothing or averaging effects, the nonuniformity in laser flux would lead to marked temperature and hence pressure varation in the pellet surface, causing non-uniform acceleration and possibly exciting instability in the hydrodynamic motion. The effects of nonuniformity are, however, very markedly alleviated by electron conduction in the high temperature region of laser deposition. The effect may be qualitatively estimated from the expected conductivity and temperature. The diffusion equation

$$\tfrac{3}{2}n_e K(\partial T_e/\partial t) = \nabla\cdot[K(T_e)\nabla T_e] \tag{5.50}$$

shows that conduction gives approximate temperature uniformity over distances Δx and times Δt such that

$$(\Delta x)^2 \simeq K(T_e)\Delta t/n_e K. \tag{5.51}$$

The conductivity is

$$K(T_e) \simeq 3\times 10^{27} T_e^{5/2}\ \text{erg/cm sec}, \quad T_e \text{ in keV}. \tag{5.52}$$

At the critical density $n_e = n_c = 10^{21}/\lambda_\mu^2$, and Eq. (5.51) yields

$$(\Delta x) = 550\lambda_\mu[\Delta t\ (\text{nsec})]^{1/2} T_e^{5/4}\ \mu\text{m}. \tag{5.53}$$

This equation imposes a condition on the scale of the temperature nonuniformity which must be satisfied for temperature and hence pressure uniformity to be maintained. The characteristic implosion times are of the order of one nanosecond, and the electron temperature in the critical density region ranges from a few to tens of keV. Thus for 1 μm radiation the characteristic smoothing scale is of the order of thousands of microns which is typically much larger than the initial pellet radius. The smoothing scale is much larger than for 10 μm radiation where, however, the other problems of coupling instability are more serious. Qualitatively, therefore, the very rapid electron conduction leads to a very high tolerance of the pellet hydrodynamics to laser illumination nonuniformity. The effect of fine structure in the intensity distribution is particularly strongly suppressed by the rapid conduction flow.

The above effects can be readily calculated with a two-dimensional or three-dimensional hydrodynamic energy deposition and conduction code. We have calculated a number of implosions with a two-dimensional code with variations as large as a factor of two in intensity between the equator and pole of spheres and shells and found that adequate symmetry is maintained in the implosion. Since it is relatively easy to provide much more uniform pellet illumination by a variety of optical methods, we conclude that reasonable care in the design of the system will adequately meet the symmetry requirements. This apparently difficult illumination problem, therefore, is probably one of the more easily resolved issues in laser fusion.

We finally turn to the question of stability in the implosion. The implosion results from the acceleration of a dense layer of plasma under the pressure resulting from the ablation of the layer, leading to the formation of a hot low density layer of plasma. This configuration resembles two well known hydrodynamic conditions where instability occurs. The classic problem of Rayleigh–Taylor instability arises in the acceleration of a dense fluid by a fluid of lower density which is unstable against disturbances at the interface, the dense fluid falling in "spikes" between bubbles of the less dense fluid rising upward into the dense fluid. The second type of instability is the formation of convection or Bénard cells in a fluid heated from below. This, of course, is most familiar in cloud formation in the atmosphere.

The possible importance of these phenomena can be estimated from the well known results for the Rayleigh–Taylor instability (Taylor, 1950) and for the formation of Bénard cells. We give these results first and then turn to a more complete analysis of the problem. The equations to be solved are:

$$\begin{aligned}
&\rho\frac{dv_i}{dt} = -\nabla_i p + \frac{\partial}{\partial x_j}\left[\mu\left(\frac{\partial v_i}{\partial x_j}+\frac{\partial v_j}{\partial x_i}\right) - \frac{2}{3}\delta_{ij}\mu\ \text{div}\ v\right] - \rho g_i,\\
&\frac{d\rho}{dt} + \rho\ \text{div}\ \mathbf{v} = 0,\\
&\frac{d\epsilon}{dt} = \frac{p}{\rho^2}\frac{d\rho}{dt} + \frac{1}{\rho}\ \text{div}\ \mathbf{q}\\
&\qquad + (\text{second-order term in viscous dissipation}),\\
&\mathbf{q} = K\nabla\theta.
\end{aligned} \tag{5.54}$$

In these equations d/dt is the convective derivative, i.e.,

$$d/dt = (\partial/\partial t) + v\nabla. \tag{5.55}$$

The viscosity μ and conductivity K are both proportional to $\theta^{5/2}$ and independent of density. The energy source term, which is due to the laser deposition, is not included in the above equations. This is most simply included by

introducing an energy flux boundary condition at the critical density surface. We will later consider the solution of equations which include the material flow due to ablation. For the Rayleigh–Taylor and convective instabilities, the unperturbed flow velocity and the derivative of the heat flux can be set equal to zero. We also simplify the problem by assuming a constant acceleration field g in the z direction and unperturbed motion in the z direction only These approximations are valid for times sufficiently short so that the change in acceleration can be neglected, and for compressed layer thickness and perturbed wavelengths much less than the radius of curvature. The zero-order equations then are simply

$$\begin{aligned} dp_0/dz &= -\rho_0 g, \\ dq_0/dz &= 0. \end{aligned} \tag{5.56}$$

In linearizing Eqs. (5.54), we use

$$\begin{aligned} \epsilon &= 3kT/2m, \\ p &= k\rho T/m. \end{aligned} \tag{5.57}$$

The linearized Eqs. (5.54) are then

$$\rho \frac{\partial v_i}{\partial t} = -\frac{\partial p_1}{\partial x_i} - \rho_1 g \delta_{i3} + \frac{\partial}{\partial x_j}\left[\mu\left(\frac{\partial v_i}{\partial x_j} + \frac{\partial v_j}{\partial x_i}\right) - \frac{2}{3}\mu\delta_{ij}\,\mathrm{div}\,\mathbf{v}\right], \tag{5.58}$$

$$\rho\,\mathrm{div}\,\mathbf{v} + \mathbf{v}\cdot\nabla\rho + (\partial\rho_1/\partial t) = 0,$$

$$(\partial T_1/\partial t) + \mathbf{v}\cdot\nabla T = -\tfrac{2}{3}T\,\mathrm{div}\,\mathbf{v} + (1/\rho)\nabla^2(\kappa\rho T_1),$$

with $\kappa = (2/3)(m/k)(K/\rho)$ the thermal diffusivity. In Eq. (5.58), the unperturbed quantities are ρ, μ, T, κ, and the first-order perturbed quantities v_i, ρ_1, T_1, p_1. If the motion of the fluid is sufficiently subsonic, the divergence of the flow can be set equal to zero. In addition, it is usually a sufficiently accurate approximation to set the gradient of the viscosity equal to zero. We now assume that the perturbed quantities depend on t and a transverse dimension x as

$$f_1(x,z,t) = f_1(z)\exp(nt + ikx). \tag{5.59}$$

We also set $d/dz = D$ and $v_z = W$. Equations (5.58) then become

$$\begin{aligned} \rho n v_x &= -ikp_1 + \mu(D^2 - k^2)v_x, \\ \rho n W &= -Dp_1 - \rho_1 g + \mu(D^2 - k^2)W, \\ WD\rho + n\rho_1 &= 0, \\ DW + ikv_x &= \mathrm{div}\,\mathbf{v} = 0, \\ nT_1 + WDT &= (1/\rho)\nabla^2(\kappa\rho T_1). \end{aligned} \tag{5.60}$$

The Rayleigh–Taylor instability occurs in the absence of a temperature gradient. In Eqs. (5.60), the transverse velocity can be eliminated by the use of the fourth equation and the perturbed density by the use of the third equation. The equations then reduce to

$$\begin{aligned} \rho n DW &= -k^2 p_1 + \mu(D^2 - k^2)DW, \\ \rho n W &= -Dp_1 + (gW/n)D\rho + \mu(D^2 - k^2)W. \end{aligned} \tag{5.61}$$

Eliminating the perturbed pressure gives

$$[\rho n - \mu(D^2 - k^2)](D^2 - k^2)W = -[nDW + (gk^2/n)W]D\rho. \tag{5.62}$$

The solutions of this equation are determined by the boundary conditions in z.

A particularly simple configuration which exhibits the principal features of the unstable growth is two uniform fluids separated by an interface at $z = 0$. The boundary condition then is that the perturbed z velocity W vanishes far from the interface. Equations (5.61) show that W and D^2W are continuous, but that DW is discontinuous at the interface. The resulting problem can be readily solved. For long wavelengths the viscous term can be ignored and the solution is particularly simple, with the result

$$n^2 = kg[(\rho_1 - \rho_2)/(\rho_1 + \rho_2)], \tag{5.63}$$

provided the depths of the liquids are much larger than k^{-1}. The configuration is therefore unstable if $\rho_1 > \rho_2$. The growth rate increases with increasing k until the viscous effects can no longer be ignored. The maximum growth rate then occurs when the viscous drag becomes comparable with the gravitational forces on the perturbed density. Chandrasekhar (1961) gives, for a large ratio of ρ_1/ρ_2, the wave number at maximum growth $k_{\max} = 0.49(g/\nu^2)^{1/3}$ for which the growth rate is $n_{\max} = 0.46(g^2/\nu)^{1/3}$ with $\nu = \mu/\rho$.

For laser fusion applications the acceleration is about 5×10^{16} cm/sec^2, corresponding to a final implosion velocity of 5×10^7 cm/sec and an implosion time of 1 nsec. The viscous diffusivity μ/ρ for DT is about 5000 cm^2/sec at 1 keV and at the solid density of 0.19 gm/cm^3. The corresponding maximum growth rate is about 10^{10}/sec at a wave number of 600 cm^{-1}. This can seriously affect an implosion unless other effects reduce or dominate the growth.

The second instability, convective overturning or the formation of Bénard cells, again occurs in the case of no ablative flow and with the flow assumed to be divergence free. For this mode the growth is an absolute instability so that the onset can be determined by considering the linearized equations with the time derivatives set equal to zero. Equations (5.60) then simplify, after eliminating v_x, to

$$\begin{aligned} p_1 &= (\mu/k^2)D(D^2 - k^2)W, \\ -gT_1 &= (-T/\rho)Dp_1 + (T\mu/\rho)(D^2 - k^2)W, \\ WDT &= (D^2 - k^2)\kappa T_1. \end{aligned} \tag{5.64}$$

If the derivatives of μ and κ are again dropped, these equations finally combine to give

$$(1/k^2)(D^2 - k^2)^3 W = (g\rho DT/\kappa\mu T)W. \tag{5.65}$$

This equation has solutions satisfying the boundary conditions at the top and bottom of the heated layer only for a proper value of the dimensionless parameter

$$R = (g\rho DT/\kappa\mu T)a^4, \tag{5.66}$$

with a the characteristic scale of the layer. The analysis by Chandrasekhar (1961) shows that typical values of R

are of the order of 10^3. An example of a solution with vanishing even derivatives at the surfaces of the layer is $W \sim \sin(z\pi/a)$, which yields the minimum value of R_c for $ka = \pi/\sqrt{2}$, so that $R_c = 27/4\pi^4 = 657.5$. Other more constrained modes have much higher values of R. The onset of instability, which occurs for R greater than R_c, results when the energy released by the convective overturning or the rise of hot bubbles of fluid exceeds the dissipation due to the viscous drag and the cooling of the bubble by lateral conduction.

For laser-driven fusion with typical values of κ and μ at 1 keV and at solid DT densities, with DT/T set equal to a^{-1}, and an acceleration of 5×10^{16} cm^2/sec,

$$R \cong 10^9 a \text{ (cm)}^3. \tag{5.67}$$

Thus, the layer is unstable for a greater than approximately 100 μm. This is considerably greater than the depth of the thermal front over which the temperature drop occurs in a typical fusion pellet, which therefore appears to be relatively stable against convective overturning. The orders of magnitude, however, are sufficiently close to require a more complete discussion of the full problem, including the effects of ablation.

The conduction into the dense colder material produces ablation flow, and changes the unperturbed solution in a basic way. The viscous terms are generally unimportant and will be dropped in the following analysis. We have, however, included the full viscous effects in a more complete analysis which will be discussed later. In the following we will no longer assume divergence-free flow. Hence, div **v** will not be set equal to zero. With zero-order flow included, the unperturbed equations are

$$\begin{aligned} \rho v(dv/dz) &= -(dp/dz) + \rho g, \\ (\partial/\partial z)\rho v &= 0, \\ v(d\epsilon/dz) &= \frac{p}{\rho^2} v \frac{d\rho}{dz} + \frac{dq}{dz}. \end{aligned} \tag{5.68}$$

The conservation of mass flow gives $\rho v =$ constant. The momentum equation may be integrated to give

$$\rho v^2 = -p + g \int \rho \, dz + \text{constant}. \tag{5.69}$$

We have chosen the acceleration to be negative, directed into the cold material. Large positive z therefore corresponds to moving out into the high temperature and low density region of the plasma. The flow generally will go from subsonic in the cold plasma to supersonic in the hot plasma. It is therefore convenient to choose the sonic point $v_0^2 = p_0/\rho_0$ as the interface $z = 0$. Introducing the dimensionless coordinate $M = g \int_0^z \rho \, dz/\rho_0 v_0^2$, we rewrite Eq. (5.69) as

$$\rho_0/\rho = 2 - (\rho\theta/\rho_0\theta_0) + M. \tag{5.70}$$

The energy equation becomes

$$\begin{aligned} \frac{d\theta}{dM} &= \frac{2}{3}\frac{\theta}{\rho}\frac{d\rho}{dM} + \frac{2}{3}\frac{m}{v_0\rho_0}\frac{dq}{dM}, \\ q &= \frac{g\rho K}{\rho_0 v_0^2}\frac{d\theta}{dM}. \end{aligned} \tag{5.71}$$

These two equations determine θ and ρ as a function of M. Their numerical solution is relatively straightforward,

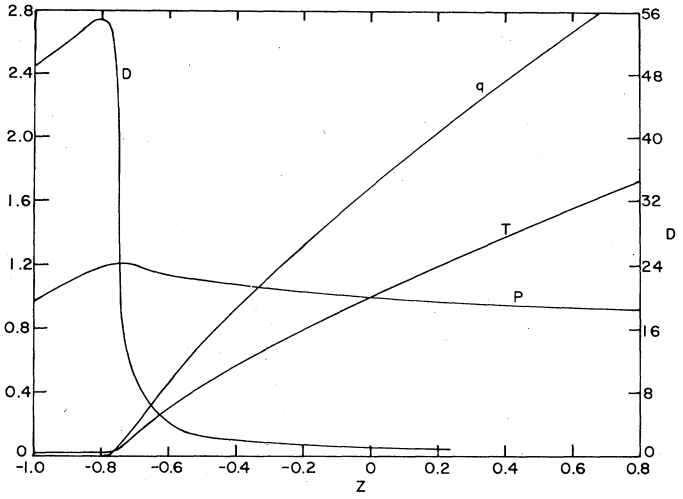

FIG. 10. Spatial variation of the zero-order density (D), pressure (p), temperature (T), and heat flux (q) in dimensionless units for the boundary conditions $q(0) = 1.69$ and $p'(0) = -0.14$.

but the sonic point must be handled with care because of the condition of continuity in the velocity. The solutions are most easily obtained by starting at the sonic point and integrating in both directions with the condition of continuity applied explicitly. The solution which decreases monotonically into the cold layer is obtained for only a properly chosen value of the heat flux at the sonic point. This determines the temperature gradient and hence the density gradient at the sonic point. The proper dimensionless constant is

$$\frac{2}{3}\frac{gK(\theta_0)}{\rho_0 v_0^5}\left(\frac{d\theta}{dM}\right)_0 = 1.69. \tag{5.72}$$

The corresponding solutions are given in Fig. 10 . The dimensional energy flux at the sonic point is

$$q_0 = [K(d\theta/dz)]_0 = \tfrac{3}{2}(1.69)\rho_0 v_0^3. \tag{5.73}$$

The isothermal sound speed in DT is equal to $3.5 \times 10^7 \theta \text{ (keV)}^{1/2}$ cm/sec, so that the heat flux at the sonic point is

$$q_0 = 1.1 \times 10^{16} \rho_0 \theta_0 \text{ (keV)}^{3/2} \text{ (W/cm}^2\text{)}. \tag{5.74}$$

To proceed with the instability analysis, we next linearize the equations around the zero-order solutions. Neglecting the viscous terms, we obtain

$$\begin{aligned} &\rho\left(\frac{\partial W}{\partial t} + v\,DW + WDv\right) + \rho_1 v\,Dv = -Dp_1 + \rho_1 g, \\ &\rho[(\partial v_x/\partial t) + v\,Dv_x] = -ikp_1, \\ &D(\rho W + \rho_1 v) + ik\rho v_x + (\partial\rho_1/\partial t) = 0, \\ &\frac{\rho_1}{m}[[(\partial/\partial t) + vD]\theta_1 + WD\theta] + \frac{\rho_1}{m} vD\theta \\ &\quad = \frac{2}{3}\frac{p}{\rho}\left[\left(\frac{\partial}{\partial t} + vD\right)\rho_1 + WD\rho\right] + \frac{2}{3}\left(\frac{p_1}{\rho} - \frac{p\rho_1}{\rho^2}\right) vD\rho \\ &\qquad + \frac{2}{3}\text{div } \mathbf{q}_1, \\ &\mathbf{q}_1 = K\nabla\theta_1 + K_1\nabla\theta. \end{aligned} \tag{5.75}$$

These equations determine the time evolution of ρ_1, θ_1, v_x, and W for fixed transverse wave number k. They can be solved as an eigenvalue problem in the time variation, subject to proper boundary conditions on the perturbed variables. We have found it simpler to integrate the time-dependent equations as an initial value problem, starting from various assumed perturbations in W and v_x. We have assumed that the perturbations vanish at the boundaries of the system which were taken to lie far from the sonic point. Of the various numerical difference schemes investigated, the simplest stable scheme was an integration in Lagrangian coordinates with the unperturbed quantities convecting through the Lagrangian mesh.

To determine the nature of the possible growing disturbances, we have integrated the equations in different approximations to identify the cause of unstable growth. If the unperturbed velocity is set equal to zero, corresponding to no ablation, and the perturbed heat flux dropped, the problem reduces approximately to the standard Rayleigh–Taylor problem. We have verified that the unstable growth which develops corresponds in growth rate to that predicted by the dispersion relation.

We next included the effect of ablation but with the perturbed heat flux set equal to zero. The growth was sharply reduced, due to rapid convection of the fluid through the narrow interface at the conduction front. The usual Rayleigh–Taylor mode exponentiates only once or twice as the fluid moves through the unstable region, which does not allow significant growth to occur.

We finally have integrated the full equations with ablation and the perturbed heat flux included. The effects of viscosity were also included but were not found to have a significant effect. The disturbances again were very weakly amplified at the conduction front, showing no appreciable unstable growth.

We conclude that the unperturbed ablative flow alone eliminates the Rayleigh–Taylor instability. The convective overturning is also absent, being suppressed both by the ablative flow and by the combined effects of high conductivity and high viscosity. These conclusions are in qualitative agreement with a conjecture due to Nuckolls *et al.* (1972) who, in a simplified model, found that the effect of the perturbed heat flux on the ablative flow led to a stabilization of the Rayleigh–Taylor growth.

We have also studied the problem using a two-dimensional code which allows for the implosion of perturbed shells and spheres. The complete hydrodynamic calculations have in no case shown amplification of initial hydrodynamic perturbations, in agreement with the prediction of the linearized equations.

H. Induced magnetic fields

Under conditions of nonuniform laser illumination of planar targets, magnetic fields have been observed (Stamper *et al.*, 1971). Rough estimates of the field strength in the plasma have shown that fields of the order of a megagauss are produced (Chase *et al.*, 1973). The occurrence of strong magnetic fields can affect the plasma behavior through hydromagnetic effects or from alterations of the plasma transport coefficients. Detailed calculations of the effects on laser heating of a planar target, using a two-dimensional code axisymmetric around the beam normally incident on the target have shown very marked effects on electron temperature and neutron production.

The magnitude of the source of the magnetic fields produced can be estimated from a simple analysis. The electron pressure produces charge separation along the pressure gradient, and hence an electric field given roughly from pressure balance, ignoring magnetic forces, by

$$e\mathbf{E}n_e \simeq -\nabla(n_e\theta), \tag{5.76}$$

where θ is the electron temperature in energy units, and n_e the electron density. The magnetic field, therefore, has a source term given by

$$\begin{aligned}\partial\mathbf{B}/\partial t &= -c\nabla\times\mathbf{E}\\ &\simeq (c/e)\nabla\times[(n_e)^{-1}\nabla(n_e\theta)]\\ &= (c/n_e e)\nabla\theta\times\nabla n_e.\end{aligned} \tag{5.77}$$

The magnetic field therefore vanishes if the temperature gradient and density gradient coincide. To estimate the magnetic field strength, we write

$$\begin{aligned}\nabla\theta &= \hat{\theta}(\theta/L_\theta),\\ \nabla n_e &= \hat{n}_e(n_e/L_\rho),\end{aligned} \tag{5.78}$$

with L_θ and L_ρ characteristic scale lengths. We also assume that the time over which the field develops and the density scale length are related by the hydrodynamic velocity v_ρ, i.e.,

$$\begin{aligned}\mathbf{B} &= \int dt\frac{c}{n_e e}(\nabla\theta\times\nabla n_e)\\ &\approx \frac{L_\rho}{v_\rho}\frac{c}{n_e e}\nabla\theta\times\nabla n_e\\ &= \frac{c}{e}\frac{\hat{\theta}\times\hat{n}_e}{L_\theta v_\rho}\theta.\end{aligned} \tag{5.79}$$

At 1 keV temperature, $v_\rho = 3\times10^7$ cm/sec and for a scale length L_θ of 50 μm, Eq. (5.79) gives

$$\mathbf{B} = 0.64\,\hat{\theta}\times\hat{n}_e\ \text{MG}. \tag{5.80}$$

This is of the correct order of magnitude for conditions of illumination asymmetry where $\hat{\theta}\neq\hat{n}_e$.

The hydrodynamic effect of the magnetic field on the plasma behavior is determined by the ratio of the particle pressure to the magnetic pressure,

$$\beta = \frac{n_e\theta}{B^2/8\pi}. \tag{5.81}$$

From Eq. (5.79), using $v_\rho \cong (\theta/m_i)^{1/2}$,

$$\beta = \frac{2\omega_i^2}{(\hat{\theta}\times\hat{n}_e)^2}\left(\frac{L_\theta}{c}\right)^2. \tag{5.82}$$

For a DT plasma and for a scale length of 50 μm with maximum asymmetry ($|\hat{\theta}\times\hat{n}_e| = 1$), β is about 60. Under these conditions, the magnetic field cannot appreciably affect the hydrodynamic motion of the plasma or the flow of energy. Extensive experience in the CTR program shows that under these conditions the magnetic field is strongly distorted by the hydrodynamic motion, the field diffusing slowly in the highly conducting plasma as the hydrodynamic motion occurs.

The effect of the magnetic field on the classical transport coefficients depends, under quiescent plasma conditions, on the ratio of the Larmor frequency to the collision rate, which is

$$\frac{\omega_L}{\nu_c} = \frac{|\hat{\theta} \times \hat{n}_e|}{n_e \sigma_c L_\theta} \left(\frac{m_i}{m_e}\right)^{1/2}, \tag{5.83}$$

with σ_c the Coulomb cross section. At 1 keV σ_c is about 10^{-18} cm^2, and for L_θ of 50 μm, ω_L/ν_c is about 13. Thus a significant reduction in transport coefficients might occur if the classical formulae were relevant, the reduction being roughly by the factor $1 + (\omega_L/\nu_c)^2$. This estimate, however, cannot be expected to hold in the strongly excited unstable plasmas characteristic of laser heating. Under these conditions, the classical diffusion coefficient $\frac{1}{3}v_e^2/\nu_c/[1 + (\omega_L/\nu_c)^2]$ is replaced by the much larger Bohm diffusion coefficient v_e^2/ω_L. For the example given above, the Bohm coefficient is about 40 times larger than classical. The discrepancy increases with increasing electron temperature.

The strong magnetic field distortion by hydromagnetic effects in a plasma with large β and Bohm diffusion are very difficult to simulate with the computer codes presently used in laser fusion analyses. In the authors' judgment, the present evidence for magnetic field effects, experimental and computational, is inconclusive. The problem, if present, is much less important if good symmetry of laser heating is achieved, which is essential for implosion symmetry.

VI. COMPUTER CODE

A. Physical model

The model considers the hydrodynamic motion of a plasma which is absorbing and emitting radiation by bremsstrahlung and free-bound electron processes, and which undergoes thermonuclear reactions. Electronic and ionic thermal conduction and electron–ion energy exchange via electron–ion collisions, thermal radiation pressure, and pressure from charged thermonuclear reactant transport are included in the model.

The difference equations used in the calculation are in the Lagrange formulation, i.e., in a reference frame moving with the plasma. The one-dimensional equations of motion and continuity in Lagrangian coordinates, and the transformation equation between Lagrangian and Eulerian coordinates are:

Equation of Motion

$$du/dt = -(1/\rho)\nabla p + F_{\text{viscous}}, \tag{6.1}$$

Transformation Equation

$$u = dR/dt, \tag{6.2}$$

Continuity Equation

$$\rho(dR^\alpha/dm) = \alpha, \tag{6.3}$$

where u is the plasma-directed velocity, ρ the density, p the pressure, R the spatial coordinate, and α a geometric parameter. (Here $\alpha = 1$, 2, or 3 for slab, cylindrical or spherical geometry. All work has been done on spherically symmetric configurations.) The quantity m is a constant of the motion (excluding mass generation or loss) in the Lagrange system and is the mass per unit area in slab geometry, the mass per unit length per radian in cylindrical geometry, and the mass per steradian in spherical geometry. Shocks are treated through inclusion of a von Neumann-Richtmyer artificial viscosity, q, if real viscous effects give insufficient spreading of the shock front. The form of F_{viscous} is discussed in Sec. VI.B8.

The pressure, p, in the momentum equation is separated into electronic and ionic contributions, p_e and p_i. Energy is transferred between internal and (directed) kinetic energy via pdV work. The internal energy per unit mass, ϵ, is assumed to be separable into electronic and ionic components, ϵ_e and ϵ_i, which are directly coupled only through electron–ion collisional energy exchange. The electron pressure, p_e, is thus assumed only to do pdV work on the electrons, and the ion pressure, p_i, to do work only on the ions. The electron and ion densities are assumed to be equal to maintain charge neutrality. Since the ions have essentially all of the mass, the viscous work, W_{visc}, is assumed to apply entirely to the ions.

Let Q_{ei} be the rate of transfer of energy from electrons to ions by electron–ion collisions (Sec. VI.B3). Energy is also transferred between electrons, via electron–ion collisions, and between ions, via ion–ion collisions, by thermal conduction. The electron and ion thermal conductivities, χ_e and χ_i, will be discussed in Sec. VI.B4. They are proportional to $T_e^{5/2}$ and $T_i^{5/2}$, respectively, in regions where degeneracy effects can be ignored.

Let $\varphi = \varphi(R)$ be the laser flux and $\mathrm{K} = \mathrm{K}(R)$ the absorptivity to the laser radiation. The energy $\varphi\mathrm{K}$ is assumed to be deposited locally in the electrons. The laser absorption process (by inverse bremsstrahlung) is discussed in Sec. VI.B2.

The electrons also lose (or absorb) energy by thermal radiation at a rate $\dot{Q}_r$. If the bremsstrahlung mean free path is sufficiently long at all frequencies, $\dot{Q}_r$ is the local free–free emissivity. If the complete pellet is not optically thin, a more detailed treatment, as discussed in Sec. VI.B7, becomes necessary.

To sum up, the model is based upon the following internal energy equations for electrons and ions:

$$\begin{aligned} \frac{d\epsilon_e}{dt} &= -p_e \frac{dV}{dt} - Q_{ei} + \varphi\mathrm{K} + \frac{\partial}{\partial m}\chi_e R^{\alpha-1}\frac{\partial T_e}{\partial R} - \dot{Q}_r + \dot{S}_e, \\ \frac{d\epsilon_i}{dt} &= -p_i \frac{dV}{dt} + W_{\text{visc}} + Q_{ei} + \dot{S}_i + \frac{\partial}{\partial m}\chi_i R^{\alpha-1}\frac{\partial T_i}{\partial R}, \end{aligned} \tag{6.4}$$

where $\dot{S}_e$ and $\dot{S}_i$ are the rates of deposition of thermonuclear energy. Thermonuclear processes are discussed in Sec. VI.B5, and transport and deposition of the energy released are discussed in Section VI.B6. The following Section, VI.B1, discusses the equations of state for the electrons and ions. A fundamental assumption made in

TABLE II. Variation of Gaunt factor with electron temperature at $\lambda = 1.06\mu$.

T(eV)	g
10	1.7
10^2	2 9
10^3	4.2
10^4	5 4
10^5	6.7

deriving the equations of state is that the ions and electrons are individually in local quasithermodynamic equilibrium, at temperatures T_i and T_e. Local thermodynamic equilibrium is also tacitly assumed in the discussions of radiative transport, collisional processes, and thermonuclear reaction rates.

B. Basic equations

1. Equation of state

A monatomic, ideal gas equation of state is assumed for all the ions. A Fermi–Thomas equation of state is used for the electrons. The total pressure, p, is the sum of the ion and electron pressures, p_i and p_e. The ion pressure is related to the ion energy density per unit mass, ϵ_i, by

$$\begin{aligned} p_i &= \tfrac{2}{3}\rho\epsilon_i = N_i kT_i \text{ dyne/cm}^2, \\ \epsilon_i &= \tfrac{3}{2}(N_0/A)kT_i = 1.247\times 10^8 T_i\,(^\circ\text{K})/\text{A erg/gm}. \end{aligned} \tag{6.5}$$

The electron equation of state is based on the finite-temperature Fermi–Thomas model as described by Latter (1944). The $(0°K)$ degeneracy curve is distorted at low density by correlation effects. The analysis of Salpeter and Zapolsky (1967) was used, along with "low pressure" data such as Bridgman's, and density and sound speed at STP, to modify Latter's degeneracy curve at lower densities.

The electron internal energy, ϵ_e, partial pressure, p_e, temperature, T_e, and entropy per unit mass, S_e, are related by the second law of thermodynamics

$$d\epsilon_e = -p_e dV + T_e dS_e, \tag{6.6}$$

where V is the specific volume (cm^3/gm). Here S_e and V are used as the independent thermodynamic variables. Adiabats in the p_e, V and ϵ_e, V space are generated by assuring that the two differentials defined by Eq. (6.6) are everywhere satisfied

$$-p_e = \left.\frac{\partial\epsilon_e}{\partial V}\right|_S, \quad T_e = \left.\frac{\partial\epsilon_e}{\partial S_e}\right|_V. \tag{6.7}$$

The region $0 < S_e < 1.75\,kZ$ is fitted under the assumption that the logarithmic derivative of temperature with respect to entropy is independent of S_e in this region, i.e., that $T = S^{\alpha(V)}$ since $T = 0$ for $S = 0$. The Latter fit is used for $S \geq 1.75kZ$.

2. Laser Absorption

The plasma absorbs energy from the laser by the mechanism of inverse bremsstrahlung (free–free transitions). The absorption coefficient, including the effects of stimulated emission, is given for $h\nu/kT \ll 1$, by

$$\mathrm{K}_a = 1.98\times 10^{-23} g \frac{\lambda^2}{T_e^{5/2}} N_e \frac{\Sigma_Z N_i(Z)Z^2}{\sqrt{1-\omega_p^2/\omega^2}}\ \text{cm}^{-1}. \tag{6.8}$$

The factor $(1-\omega_p^2/\omega^2)^{-1/2}$ accounts for the reduction of the group velocity of the wave in the region where the plasma is nearly overdense, ω_p^2 being the plasma frequency.

The Gaunt factor in the Born approximation is (cf. Wharton, 1961, pp. 319-320)

$$g = \frac{\sqrt{3}}{\pi} K_0\left(\frac{h\nu}{2kT}\right)\exp\left(\frac{h\nu}{2kT}\right), \tag{6.9}$$

where K_0 is the modified Bessel function. Two useful limiting expressions for K_0 are (see, for example, Abramowitz and Stegun, 1965)

$$\begin{aligned} K_0(x) &\sim [\ln(2/x) - 0.5772], \qquad 0 < x \leq 2, \\ e^x K_0(x) &\sim (\pi/2x)^{1/2}\left[1 - \frac{1}{8x} + O\left(\frac{1}{x^2}\right)\right], \\ & 2 \leq x < \infty. \end{aligned} \tag{6.10}$$

The variation of g with temperature for $\lambda = 1.06\ \mu$m ($h\nu = 1.17$ eV), the wavelength of the neodymium-doped glass laser, is shown in Table II. It is clear that one cannot take $g = 1$ in this regime.

If the plasma is initially overdense, the incoming light will be absorbed only as a result of the evanescent wave, which penetrates a distance of the order of a wavelength. Experiments involving the interaction of laser beams with surfaces are common and show more rapid heating than can be accounted for by this effect. The additional absorption results from the existence of a density gradient in the material. The light can then penetrate and cause additional heating in the underdense region. When this layer expands, the region moves into the material, causing increased absorption of the incident radiation. The underlying layers are heated and then also expand. Dawson *et al.* (1969) have recently given an analysis of this problem.

The inclusion of the square root factor in Eq. (6.8) when attenuation is computed is also given by the WKB solution for absorption in a critical-density plasma. Although higher order WKB corrections may be applied, they are not as important as the omission of refraction, i.e., in spherical geometry, the bending of the penetrating light beam away from the sphere. The inclusion of path curvature converts the one-dimensional problem into a two-dimensional one.

3. Collisional exchange

The rate of collisional transfer of energy (per unit mass) from ions to electrons is given by

$$Q_{ie} = -Q_{ei} = C_v^i(T_i - T_e)/\tau, \tag{6.11}$$

where T_i and T_e are the ion and electron temperatures, respectively. The equilibration time, τ, is found by averaging electron–ion collisions over a Maxwellian distribution of ions and (generally) a Fermi distribution of electrons. The result is given by Brysk (1974) as

$$\tau = 3\pi\hbar^3 m_i(1+\alpha)/(8m_e^2 e^4 Z^2 \ln\Lambda_{ei}). \tag{6.12}$$

The quantity α is the exponential of the thermodynamic potential, $\alpha = \exp(-E_F/kT_e)$, where E_F is the Fermi energy, while $\ln\Lambda_{ei}$ is the Coulomb logarithm whose classical limit is discussed by Spitzer (1961), but which is usually taken from the calculation of Hubbard and Lampe (1969).

In the classical limit of $\alpha \gg 1$, $\alpha \to \Gamma(3/2)(2m_e kT_e/\hbar^2)^{3/2}/2\pi^2 N_e$, and the equilibration time becomes

$$\tau_{\text{classical}} = \tfrac{3}{4} m_i (kT_e)^{3/2}/e^4(8\pi m_e)^{1/2} N_e Z^2 \ln\Lambda_{ei}. \tag{6.13}$$

In the degenerate limit, the result is merely Eq. (6.12) with $\alpha = 0$. The value of α is generally obtained implicitly from the Fermi distribution normalization:

$$\int_0^\infty y^{1/2}\,dy/(1+\alpha e^y) = 2\pi^2 N_e(\hbar^2/2m_e kT_e)^{3/2}. \quad (6.14)$$

The ion specific heat at constant volume, C_v^i, is taken to be that of a monatomic perfect gas

$$C_v^i = \tfrac{3}{2}(N_0 k/A), \quad (6.15)$$

where N_0 is Avogadro's number, and A the mass number.

4. Thermal conductivity

In the classical limit, where degeneracy effects can be ignored, the electron thermal conductivity becomes

$$\chi_e^{(c)} = \frac{20(2/\pi)^{3/2}(kT_e)^{5/2}k}{m_e^{1/2}e^4 Z \ln\Lambda_{ei}}\epsilon\delta_T. \quad (6.16)$$

The correction factors ϵ and δ_T are tabulated by Spitzer (1961) for $Z = 1, 2, 4, 16$, and ∞. The product $\epsilon\delta_T$ is fitted to within 15% by the approximation $\epsilon\delta_T \approx 0.472\,Z/(4+Z)$. Degeneracy effects change the form of χ_e at about the same region where $\ln\Lambda_e$ becomes of order unity. The electron conductivity of a partially degenerate plasma has been treated by Hubbard and Lampe (1969). The present calculations use a tabular fit to the Hubbard and Lampe results in the partially degenerate region.

The ion contribution to thermal conduction arises from ion-ion collisions. The ions are assumed to be described by a classical (Maxwellian) distribution:

$$\chi_i = \frac{3.28(2/\pi)^{3/2}(kT_i)^{5/2}k}{m_i^{1/2}e^4 Z^4 \ln\Lambda_i}. \quad (6.17)$$

The ionic Λ_i is always taken to be $\lambda_D/b_{(\mathrm{ion})}$, the classical value of the Debye length divided by the impact parameter. The electron and ion conductivity coefficients differ by the ratio g_e/g_i.

5. Thermonuclear processes

When the ions are sufficiently energetic, they may participate in thermonuclear reactions. The reaction products in turn contribute to the heating of the ions.

a. DT reaction

The DT reaction is

$$D + T \rightarrow \mathrm{He}^4(3.52\ \mathrm{MeV}) + n(14.07\ \mathrm{MeV}). \quad (6.18)$$

The corresponding rate equations are

$$-\frac{dN_D}{dt} = -\frac{dN_T}{dt} = \frac{dN_\alpha}{dt} = \frac{dN_n}{dt} = N_D N_T(\overline{\sigma v})_{DT}. \quad (6.19)$$

b. DD reaction

The DD reaction proceeds with approximately equal probability via two channels

$$D + D \rightarrow \begin{cases} T(1.01\ \mathrm{MeV}) + p(3.02\ \mathrm{MeV}) \\ He^3(0.82\ \mathrm{MeV}) + n(2.45\ \mathrm{MeV}). \end{cases} \quad (6.20)$$

Thus the rate equations are

$$\begin{aligned} dN_D/dt &= -N_D^2(\overline{\sigma v})_{DD} - N_D N_T(\overline{\sigma v})_{DT}, \\ dN_T/dt &= -N_D N_T(\overline{\sigma v})_{DT} + \tfrac{1}{4}N_D^2(\overline{\sigma v})_{DD}, \end{aligned} \quad (6.21)$$

where N_D and N_T are the number of deuterium and tritium ions per cm^3, respectively. The (2.45 MeV) neutron production rate is

$$dN_n/dt = N_D^2(\overline{\sigma v})_{DD}/4. \quad (6.22)$$

The tritium population builds up to a steady-state value:

$$N_T \approx \tfrac{1}{4}[(\overline{\sigma v})_{DD}/(\overline{\sigma v})_{DT}]N_D. \quad (6.23)$$

c. Reaction rates and energies

The reaction rates $(\overline{\sigma v})$ are (as the notation implies) values of the product of the cross section σ with the relative velocity v of the reacting particles averaged over Maxwellian distributions of the reacting particles at the ion temperature. For DD reactions, Post (1956) gives

$$(\overline{\sigma v})_{DD} = 2.6\times10^{-14}T_i^{-2/3}\exp(-18.76T_i^{-1/3})\ (\mathrm{cm}^3/\mathrm{sec}), \quad (6.24)$$

where T_i is in kilovolts. For DT reactions, the experimental results of Arnold *et al.* (1954) were integrated and fitted numerically. The result is

$$\begin{aligned} (\overline{\sigma v})_{DT} &= 3.8\times10^{-12}T_i^{-2/3}\exp(-19.02T_i^{-1/3})\ (\mathrm{cm}^3/\mathrm{sec}), \\ &\quad \text{for } T_i < 10\ \mathrm{keV} \\ &= 3.41\times10^{-14}T_i^{-2/3}\exp(-27.217T_i^{-2/3} \\ &\qquad + 3.638T_i^{-1/3})\ (\mathrm{cm}^3/\mathrm{sec}), \\ &\quad \text{for } T_i > 10\ \mathrm{keV}. \end{aligned} \quad (6.25)$$

The energy dependence of the cross sections is strong enough for the mean energy of the particles taking part in a reaction to differ considerably from the average energy of the Maxwellian distribution of such particles. This mean energy is computed by averaging the kinetic energy of the two reactants over their respective Maxwellian distributions times σv. If the above analytic fits are used for $\overline{\sigma v}$, the calculation can be performed analytically with the result (cf. Brysk, 1973)

$$\overline{E} = \frac{7}{3}T_i - \frac{1}{3}C_1 T_i^{2/3} - \frac{2}{3}C_2 T_i^{1/3}, \quad (6.26)$$

where C_1 is the coefficient of $T_i^{-1/3}$, and C_2 the coefficient of $T_i^{-2/3}$ in the exponent of Eq. (6.25). Some representative values of $\overline{E}$ for the DT reaction are quoted in Table III; for comparison, $3T_i$ (twice the Maxwellian mean energy per particle) is also listed.

TABLE III. Mean energy of the reactants taking part in a DT reaction.

T_i	1.00	8.0	27	64	125
$3\,T_i$	3.00	24.0	81	192	375
$\overline{E}$	8.67	44.0	107	203	353

6. Energy momentum deposition

a. Charged particle

The charged particles from the thermonuclear reactions do not necessarily deposit locally, i.e., where they were created, but can travel some distance before they are stopped. As they traverse a given path length, a certain amount of energy is lost due to collisions. This energy is then partitioned among the ions and the electrons. The code follows several angle groups in determining the net energy given to the ions and electrons in a given spatial zone. These contributions are then included in the source terms in the energy equations [Eq. (6.4)]. The stopping power formulae and energy partition factor show that the fractional energy loss per unit length is given by

$$d\epsilon_p/ds = -N_e f_p, \tag{6.27}$$

where N_e is the number of electrons per unit volume, and f_p has the dimension of area, i.e., is a cross section:

$$f_p = 2\pi e^4\left(\frac{Z_p}{W_p}\right)^2 A_p\left[\frac{\overline{Z}_i}{A_i}\frac{F_i}{\epsilon_p}\ln\Lambda_I + \frac{(2m_e k/\hbar^2)^{3/2}}{3\pi^3 N_e}A_e^{1/2} \times\left(\frac{W_p}{A_p}\right)^{3/2}\frac{\epsilon_p^{1/2}F_e\ln\Lambda_{ei}}{(1+\alpha)}\right] + \sigma_{pi}^T\epsilon_p F_i'. \tag{6.28}$$

Apart from the last factor, this quantity has been discussed by Chandrasekhar (1924). In this expression, Z_p, A_p, and W_p are the charge, mass number, and initial energy of particle p, ϵ_p is the energy in units of W_p, while $\overline{Z}_i$ and A_i are the average charge and mass number of the ion in the zone $A_e = (1836)^{-1}$. The quantity α is the Fermi normalization factor defined in Sec. VI.B3 on collisional exchange. In the classical limit $\alpha \gg 1$, the second term under the bracket, i.e , the electron contribution to the stopping power, becomes

$$\frac{4}{3\pi^{1/2}}A_e^{1/2}\left(\frac{W_p}{A_p}\right)^{3/2}\frac{\epsilon_p^{1/2}}{T_e^{3/2}}F_e\ln\Lambda_e. \tag{6.29}$$

Again, $\ln\Lambda_{ei}$ is the usual Coulomb logarithm. The factor $\ln\Lambda_I$ is an effective Coulomb logarithm for scattering of particles p with much higher velocity than the Maxwellian ions. Here $\ln\Lambda_I$ is about 10 over most of the range of interest to about 15%. The last term in Eq. (6.28) is the contribution of nuclear scattering, with σ_{pi}^T an "effective transport cross-section" for particle p in the i medium (Brueckner and Brysk, 1973). The correction factors F_e, F_i, and F_i' are unity to first order but contain an energy dependence in higher order.

When the energy of the charged particle becomes equal to the average kinetic energy in a zone, it is said to be stopped, and its mass is added to the zone in which this occurs.

Charge is conserved and charge neutrality maintained in each zone. Thus, the particle charge and an equal electron charge are removed from the birth zone and added to the stopping zone. The electron transit also carries with it an adjustment of the electron kinetic energy (average value $\frac{3}{2}T_e$ per electron, varying from zone to zone).

It is possible that a particle will escape from the plasma. The difference between the original energy and the energy deposited results in an energy loss to the system.

Unless and until we reach the final stage of intense burn (more than 10% depletion) the energy and momentum deposition by the reaction products are much smaller than the corresponding hydrodynamic quantities. What makes the energy deposition important is that a small rise in ion temperature due to the heating leads to a large increase in the fusion reaction rate.

Reactions by energetic knock-ons are important for very large systems in which the neutrons are appreciably stopped within the fusion medium. These effects are analyzed elsewhere (Brueckner *et al.*, 1974). The present discussion pertains to smaller systems where the neutron scattering is relatively weak.

While the Lagrangian description is well suited to the hydrodynamic motion, it is awkward to adjust for transport of particles between zones because of the occurrence of variables scaled with mass and the separation into internal and directed motion.

b. Neutron heating

Neutrons lose energy by elastic collision with ambient ions. The recoiling ions then slow down (as discussed in the last section), thus depositing energy in the medium. For the conditions of interest here, most of the neutrons escape unscattered, so that the number and distribution of scattering events can be calculated without allowing for attenuation of the neutron flux.

The fluence, $\Phi(r)$, at a point a distance r from the center of a shell source, of inner and outer radii R_1 and R_2, emitting $n(R)$ particles per cm^3 is, in terms of the geometry shown in Fig. 11,

$$\Phi(r) = \int_{R_1}^{R_2}\int_0^{\pi}\frac{2\pi R\sin\theta R\,dR\,d\theta n(R)}{4\pi(R^2+r^2-2rR\cos\theta)} = \int_{R_1}^{R_2}\frac{R}{2r}\ln\left[\frac{(R+r)}{|R-r|}\right]n(R)\,dR\,\frac{\text{particles}}{\text{cm}^2}. \tag{6.30}$$

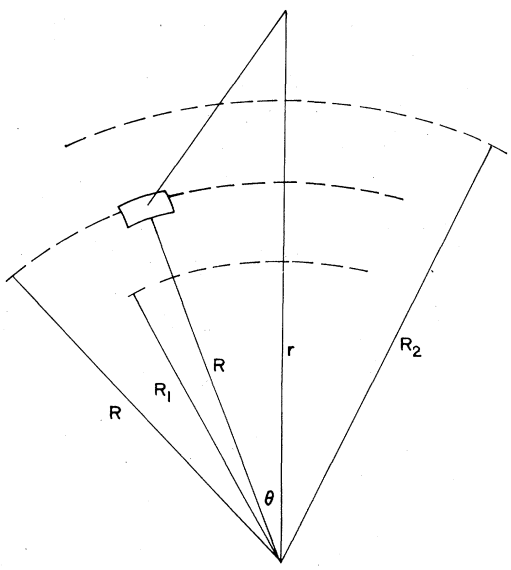

FIG. 11. Geometry for calculation of neutron deposition.

The number of scattering events per gram occurring in a shell of density ρ gm/cm^3 and atomic number A with bounding radii r_A and r_B is given by

$$n_s = \int_{r_A}^{r_B} \Phi(r)\sigma(N_0/A)\rho r^2\,dr \Big/ \int_{r_A}^{r_B} \rho r^2\,dr \qquad (6.31)$$

where σ is the neutron scattering cross section (in cm^2), and N_0 is Avogadro's number. Under the assumption that $n(R)$ and $\rho(r)$ are constant within a spherical zone, the double integral can be evaluated. For each zone, the scattering events due to neutrons originating in all zones are added up, yielding an effective source term for fast ions. The fast ions are assigned their initial energy, W_p, the mean energy obtained from the collision kinematics, namely νE with E the neutron energy and

$$\nu = 2M_nM_p/(M_n + M_p)^2 \qquad (6.32)$$

where M_n is the neutron mass, and M_p the ion mass. The slowing down and energy deposition of the recoil ions are then followed in the same fashion as for the charged reaction products. In practice, the neutron fluence integration is performed first, and the tracking of all charged particles (whether reaction products or neutron secondaries) is then done concurrently.

c. Energy partition

The first term in the expression for f_p in the energy loss formulae [Eq. (6.28)] represents the loss due to collisions with the ions, while the second term accounts for loss due to collisions with the electrons. As the reaction particle, e.g., an α-particle or a D or T neutron knock-on, traverses a zone, it gives up some of its energy to the electrons and some to the ions. These energy depositions are then incorporated into the energy source term in the electron and in the ion energy equations. If the reaction product is stopped within a zone, the energy is partitioned between electrons and ions. The treatment of this partitioning is complicated by the existence of two temperature distributions, one for the electrons and one for the ions, in the zone (Brueckner and Brysk, 1973).

7. Radiation losses

The principal source of radiation is bremsstrahlung. In the code an approximate solution of the radiative transport equation is used to compute the radiation production and absorption. Since the radiation is isotropic, it is computed in terms of solid angle groups. For a given angle group, the free–free radiation is computed in terms of frequency groups. For a given angle and frequency, the radiation is assumed to proceed in a straight line path. The Compton shift is almost always negligible. The optical depth τ is introduced by

$$\tau = \int_s^{s'} K'_{\nu,\mu}\,ds, \qquad (6.33)$$

where $K'_{\nu,\mu}$ is the absorption coefficient for the frequency ν and angular group $\Delta\mu = \Delta(\cos\theta)$, corrected for stimulated emission, and $s' - s$ is the distance traversed in the medium. Energy loss within a zone is

$$\Delta E = \int_{\text{zone}} [B_{\nu,\mu} - I_{\nu,\mu}(s')][1 - \exp(-\tau)]\,dV, \qquad (6.34)$$

where $B_{\nu,\mu}$ is the Planck function, and $I_{\nu,\mu}(s')$ the energy transported per unit time per unit frequency interval per unit solid angle per unit area into the zone from the other zones

8. Viscosity

The equation of state used is based on modeling the electrons and ions individually as monatomic gases. The bulk viscosity, ν, of a monatomic gas is $-\frac{2}{3}\mu$, where μ is the normal viscosity. In the special case of $\nu = -\frac{2}{3}\mu$, the equation of motion of a plasma with one-dimensional symmetry is

$$\rho\ddot{r} = -\frac{\partial}{\partial r}\left(P + \frac{\frac{4}{3}\mu\dot{\rho}}{\rho}\right) - 2(\alpha - 1)\frac{\dot{r}}{r}\frac{\partial\mu}{\partial r}, \qquad (6.35)$$

where $\alpha = 1$, 2 or 3 for slab, cylindrical, or spherical symmetry.

The viscous contribution to the energy equation for the three one-dimensional geometries are:

Slab Symmetry

$$\rho\dot{e}_{\text{visc}} = \frac{4}{3}\mu(\partial\dot{r}/\partial r)^2. \qquad (6.36)$$

Cylindrical Symmetry

$$\rho\dot{e}_{\text{visc}} = \frac{4}{3}\mu\left[\left(\frac{\partial\dot{r}}{\partial r}\right)^2 - \left(\frac{\dot{r}}{r}\frac{\partial\dot{r}}{\partial r}\right) + (\dot{r}/r)^2\right]. \qquad (6.37)$$

Spherical Symmetry

$$\rho\dot{e}_{\text{visc}} = \frac{4}{3}\mu\left[r\frac{\partial}{\partial r}(\dot{r}/r)\right]^2. \qquad (6.38)$$

It is apparent that the viscous terms disappear from the spherical equations for uniform compression or expansion ($\dot{r}/r$ = constant), because volume elements are undistorted under this motion in spherical geometry.

The real viscosity of a plasma predominantly arises from momentum transfer in ion–ion collisions. In the units used in the computer code, the plasma viscosity is given by (Spitzer, 1961)

$$\frac{4}{3}\mu = 1.28 \times 10^{-7}A^{1/2}T_i^{5/2}/(Z^4 \ln\Lambda). \qquad (6.39)$$

C. Description of computer code

The energy deposition and hydrodynamic code describing the focusing of a (spherically) convergent laser pulse on a small pellet contained in a vacuum chamber is discussed in this section. The energy pulse is assumed to have vaporized and ionized the pellet by radiative heating before significant energy has been delivered, so that initially there is a plasma of uniform temperature of a few electron volts with specified density. Similar models have been discussed by Kidder (1968) and by Dawson (1964). The heating of the gas as the light propagates into it sets up a (spherically convergent) shock wave.

For ease of computation, the Lagrangian description of the hydrodynamic equations, wherein one follows the history of an element of the fluid, has been adopted. Thus, for the case of spherical symmetry, r denotes the radial coordinate of a fluid element having the initial

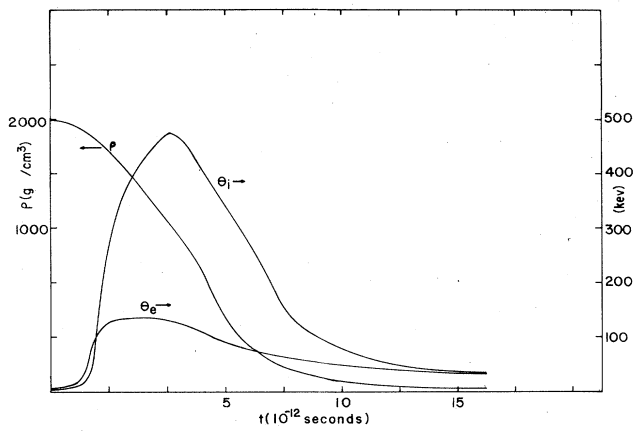

FIG. 12. Central density and temperature histories in uniformly compressed and heated DT. The initial density is 2000 gm/cm³, the initial temperature 5 keV, and the initial radius 23.4 μm. The initial energy in the fuel is 56.3 kJ and the final fusion yield 10.49 MJ. The electron temperature rise is initially more rapid than the ion temperature rise due to the stronger α-particle heating of electrons. After reaching approximately 40 keV, the ion temperature rapidly increases to several times the electron temperature as the α-particle deposition to the electrons becomes weak.

density ρ_0 gm/cm³, and $R = R(r,t)$ denotes the radial coordinate of the same element at the time t. It is assumed that the electrons and ions are individually in local quasithermodynamic equilibrium, described by Fermi–Dirac and Maxwellian distribution functions, respectively.

The plasma is divided into J–1 zones. Zone interfaces are labeled with the Lagrangian (subscripted) coordinate $j(1 \leq j \leq J)$. The temporal coordinate t is divided into distinct intervals via the (superscripted) time coordinate $n(t^n)$. Spatial coordinates are hence defined at the Lagrange interfaces (R_j). They are defined temporally at integer values of the time coordinate (R_j^n). The (directed) velocity u of the point R_j is defined at one-half integer values of the time coordinate ($u_j^{n+1/2}$). Extensive quantities such as density, pressures, and internal energies, are averaged between zone interfaces and assumed to act at the Lagrange center of the zone ($p^n_{e_{j-1/2}}$, $p^n_{i_{j-1/2}}$, $\epsilon^n_{e_{j-1/2}}$, etc.).

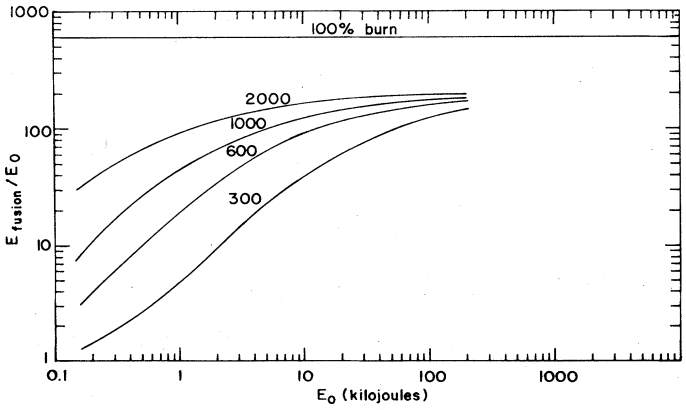

FIG. 13. Fusion energy production in uniformly compressed and heated DT. The initial temperature is 5 keV. The curves are labeled by the initial density in gm/cm³. The results are obtained with the computer code described in Sec. VI.

VII. NUMERICAL RESULTS

The code outlined in Section VI has been used to study the various phenomena described in the preceding sections. The following subsections discuss the ignition and thermonuclear burn of a uniform compressed sphere, the effect in a non-uniform sphere of propagation of a burning wave, the laser coupling efficiency, and finally some examples of complete implosion calculations showing the compression, ignition, propagation, and thermonwclear burn sequence.

A. Uniform sphere

The case of an initially uniform compressed sphere at uniform initial temperature shows the ignition and hydrodynamic sequence in the simplest configuration. Fig. 12 gives the central temperature and density histories for a typical case, starting at 5 keV electron and ion temperature. At this central temperature the thermonuclear heating rate exceeds the bremsstrahlung radiation loss

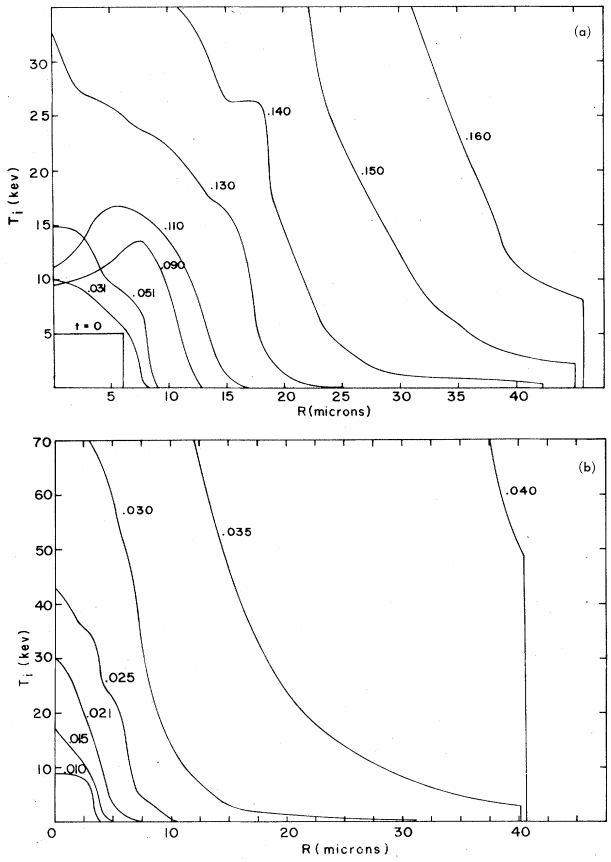

FIG. 14. (a) Propagation of burning front in initially uniformly compressed DT. The initial density is 600 gm/cm³ and the initial radius 40 μm. The central region initially heated to 5 keV has a 6 μm radius. The curves are labeled by the time in units of 10^{-10} sec. The central temperature, after an initial rise, drops as a strong shock forms and expands into the surrounding colder fuel. Subsequent recompression and further heating causes the final temperature rise. The velocity of the burning front increases with time, reaching 9×10^8 cm/sec at 0.160 time units. (b) Propagation of burning front in initially uniformly compressed DT. The initial density is 2000 gm/cm³ and the initial radius 40 μm. The central region initially heated to 5 keV has a 3 μm radius. The velocity of the burning front reaches about 5×10^9 cm/sec at 0.40 time units.

which is also suppressed by self-absorption in the compressed fuel. The calculations, therefore, have not included the effect of radiation transport, diffusion, and loss. The energy deposition by the initial particles and by deuteron and triton recoils from the fast neutrons has been included by the multiple-angle-group transport method described in Sec. VI.

The ratio of total thermonuclear yield to initial energy is given in Fig. 13 as a function of initial energy for several densities. This ratio tends toward a limiting value of approximately 200 for all initial densities and for an initial energy of several hundred kilojoules. The maximum possible yield per particle for complete fuel burnup is 8800 keV (17.6 MeV per D + T pair), and the initial energy at 5 keV is 15 keV ($\frac{3}{2}\theta$ per ion and electron). Thus the maximum possible ratio of yield to initial energy is 587. The computed limiting value of about 200 in the several hundred kilojoule range, therefore, corresponds to about 34% fuel burn.

The analytic estimate obtained in Sec. II is in semi-quantitative agreement with the computed results. Figure 1 shows an energy multiplication at a density of 1000 gm/cm^3 of about 250 at a fuel depletion of 34%, with an initial energy of 36 kJ. The result from the complete numerical calculation is a factor of about two lower in energy multiplication at this initial energy: excellent agreement considering the simple model used.

B. Nonuniform sphere with propagation

Calculations of the central ignition of a relatively cold DT sphere have also been carried out for an initial uniform density with the central temperature at 5 keV and the rest of the fuel at 500 eV. At this temperature the degeneracy energy of the electrons is appreciable, particularly at the highest compression considered. The radius of the initially heated central region was varied to determine the minimum radius at which ignition occurs. At a density of 600 gm/cm^3, for example, propagation occurred for a radius of 6 μm, corresponding to $r_0 n_0/n_s$ of 2.21 cm which is close to the analytic estimate of Eq. (2.52). Figures 14(a) and 14(b) show the development of the propagating burn front for several densities. The rapid acceleration of the front is apparent, particularly at high density where the heating by deuteron and triton recoils from the fast neutrons becomes important. The energy multiplication from the complete calculation is given in Fig. 15 for several densities. At all densities considered, multiplication approaches a value of about 1200 for initial energy of several kilojoules. This ratio is easily understood since the maximum energy per particle for 34% fuel burnup is 3000 keV and the initial energy (ignoring the small energy required for the central ignition) is 750 eV per ion and at a density of 1000 gm/cm^3 about 1250 eV per electron, including the degeneracy energy. Thus, the maximum energy multiplication is about 1500. This can be increased further only if the fuel is initially at lower temperature. The initial energy requirement, aside from the ignition energy in the central fuel region, is then only the degeneracy energy of the electrons.

The principal effect of the formation of the propagating burn front is to reduce the initial energy requirements by about a factor of ten from the case of a uniformly heated sphere. This factor is of great importance since it allows large over-all energy multiplication to be obtained, after the poor efficiency of the laser coupling to the compressed fuel is taken into account.

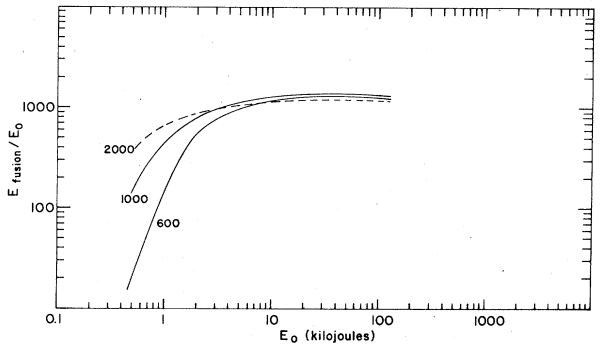

FIG. 15. Fusion energy production in uniformly compressed DT with a spherical burning wave initiated at the fuel center by a region initially heated to 5 keV. The rest of the fuel is initially at 500 eV. Details of the propagation of the burning front for two typical cases are given in Fig. (14a) and Fig. (14b). The curves are labeled by the fuel density in gm/cm^3.

C. Complete implosion calculations

The code described in Sec. VI allows a computer simulation of the complete laser fusion process. A typical calculation divides a sphere or shell into about 100 radial zones and follows the various quantities through several nanoseconds, with time-step intervals which become as small as 10^{-13} sec at the time of peak reaction. Such codes

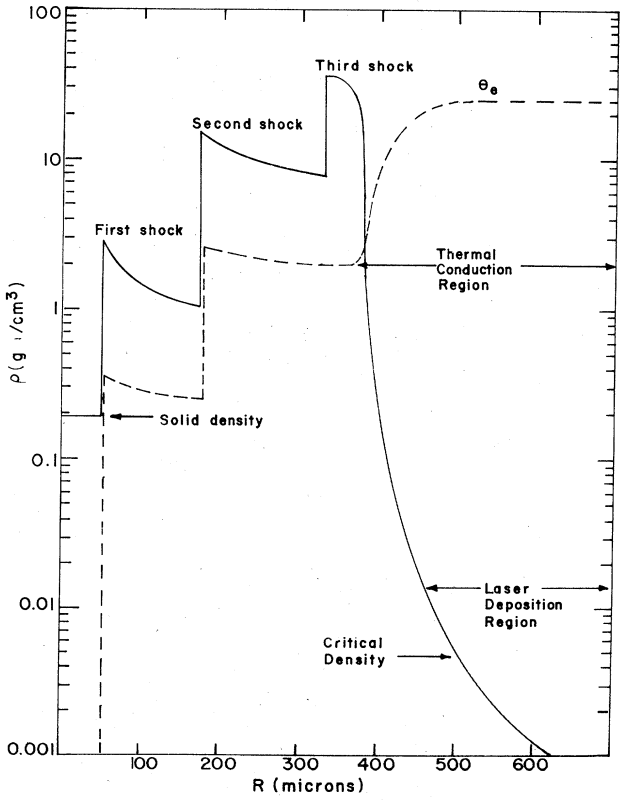

FIG. 16. A schematic diagram showing typical density and temperature profiles during implosion.

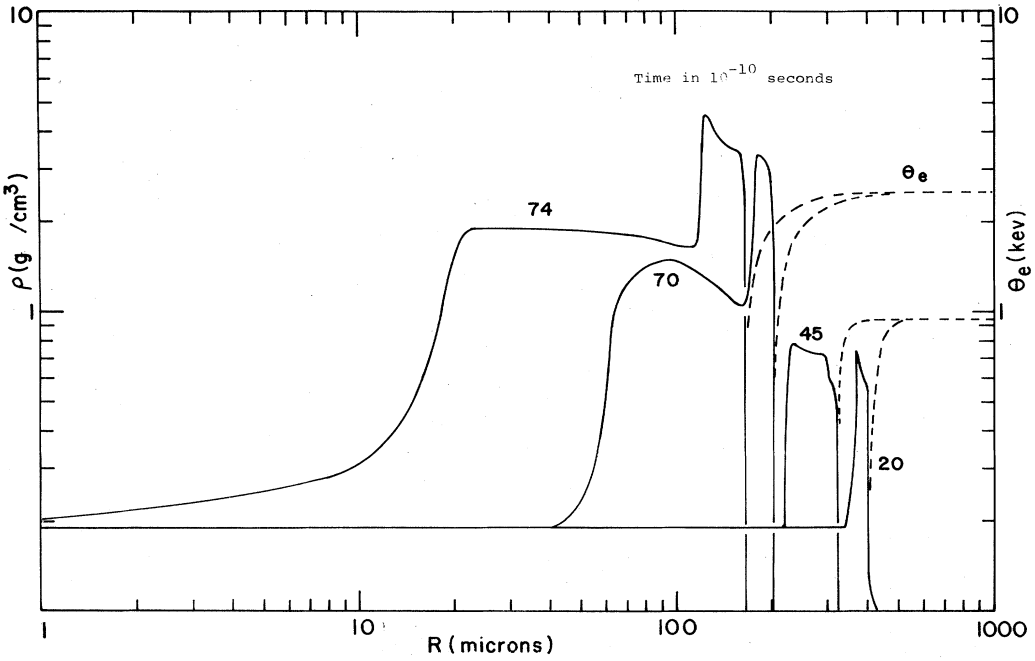

FIG. 17. Formation of shocks and thermal fronts for Case 1 (60.1 kJ input) during early stages of implosion before the final strong shock has formed.

have special features for the laser process but are otherwise of conventional structure, well known to the hydrodynamicist and numerical analyst. Codes of this type have very widespread application in aerodynamics, hydrodynamics, and high temperature gas dynamics, which have made the art of code use into a well verified and accurate method of simulation and analysis. With a typical code, a single example of laser fusion required about 30 minutes of computation on a CDC 6600 computer. A full study of one scale of size, optimizing the laser flux history, may require 30–40 computer runs. Thus, the full computer study is a problem of considerable magnitude.

The features described above may be exhibited by examination of typical computer runs. Two interesting examples are:

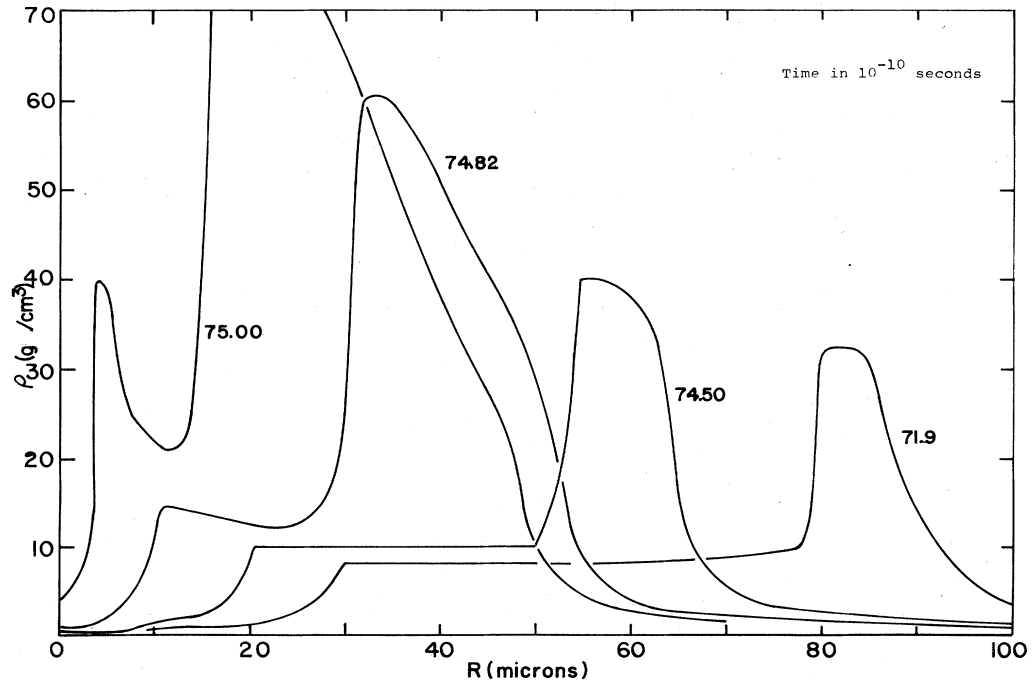

FIG. 18. Temperature and density profiles for Case 1 after third strong shock.

1. *Solid* DT *sphere, initial radius of* 1/2 *millimeter*

   Laser pulse form: 6.3×10^{11} W from 0 to 5.47 nsec; 6.3×10^{12} W from 5.47 to 7.21 nsec; linear rise from 6.3×10^{12} W at 7.21 nsec to 4×10^{14} W at 7.42 nsec.

   Absorption coefficient: 10 times classical to simulate anomalous absorption

   Laser energy absorbed: 60.1 kJ

   Central density peak (averaged over 10% of radius): 1380 gm/cm^3

   Fraction of sphere imploded to density greater than 100 gm/cm^3: 12%

   Time of central compression greater than 100 gm/cm^3: 1.8×10^{-11} sec

   Energy input into compressed DT at time of maximum compression: 2.9 kJ

   Over-all laser coupling efficiency into compressed DT: 4.8%

   Total fusion yield: 510 kJ

2. *Solid* DT *shell, outer radius of* 3.1579 mm, *inner radius of* 3.0223 mm

   Laser pulse form: Linear rise with time

   Laser energy incident: 679 kJ

   Absorption coefficient: Classical

   Total fusion yield: 51.70 MJ

Some features of the temperature and density histories are given in Figs. 16-23 .

Other computer studies carried out by us show that a total fusion yield of 51 kJ can be produced from a solid DT sphere with initial radius of 0.25 mm with a laser energy input of 7.25 kJ, i.e., a multiplication of seven. A multiplication of 21 is obtained, for a solid sphere with radius of $\frac{1}{2}$ mm, at a laser energy of 60 kJ. The computer results are surprisingly close to the results given in Fig. 1 for an assumed uniform compression by a factor of 5500. The breakeven point, with fusion energy equal to laser energy, is about 1 kJ, which is readily achievable with present glass laser technology.

VIII. ALTERNATE CHOICES OF LASER WAVELENGTH

According to the results just given, laser energy multiplication can probably be achieved with a neodymium glass laser with energy output in the kilojoule range. The over-all efficiency of the process is, however, too low to be of practical interest. The conversion of electrical energy into laser energy output for this type of laser is roughly 1%, and the conversion of fusion energy to electrical energy (at least by conventional processes) about 40%. Thus over-all energy gain can be realized only if the laser energy multiplication in the fusion process is about 250. According to the present understanding of the fusion process in DT, this multiplication will be difficult to reach with technologically feasible glass lasers.

Lasers with higher conversion efficiency, which may also be simpler than glass lasers, are of great interest. Electrically excited gas lasers have been operated with efficiency of a few tens of percent. Chemical lasers also offer in principle efficient conversion of chemical energy into laser energy output. A conversion efficiency of 25% reduces the laser energy multiplication requirement for the over-all breakeven condition to about ten, which may be achievable with a laser delivering 10 kJ to the DT pellet. A long range effort has therefore been undertaken worldwide to develop gas and chemical laser technology. No such laser in the desired pulse length and energy output range has, however, yet been operated. These lasers will probably be successfully developed before the other technological problems of laser-driven fusion reactors are solved.

The use of electrically excited gas or chemical lasers presents new problems in the theory of laser-driven fusion, since for most cases presently considered, these lasers operate at considerably longer wavelength than the

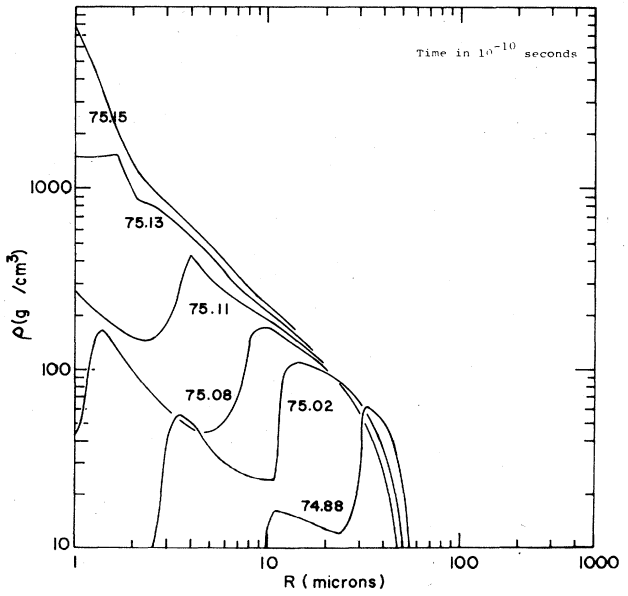

FIG. 19. Rising density profiles for Case 1 just before final convergence.

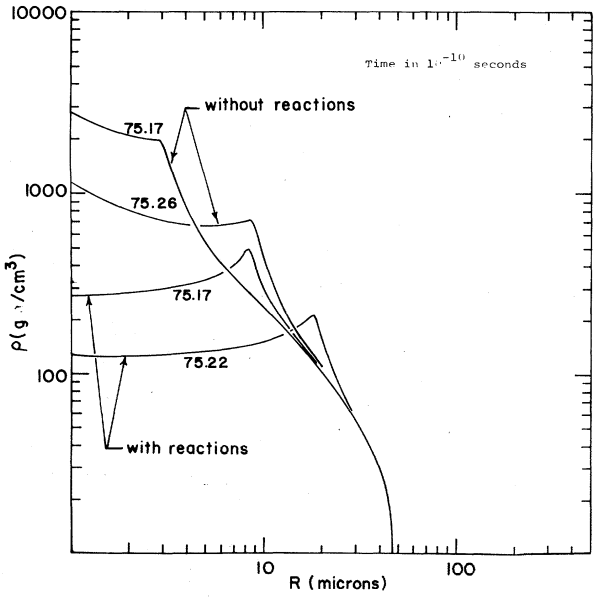

FIG. 20. Final stage of implosion for Case 1.

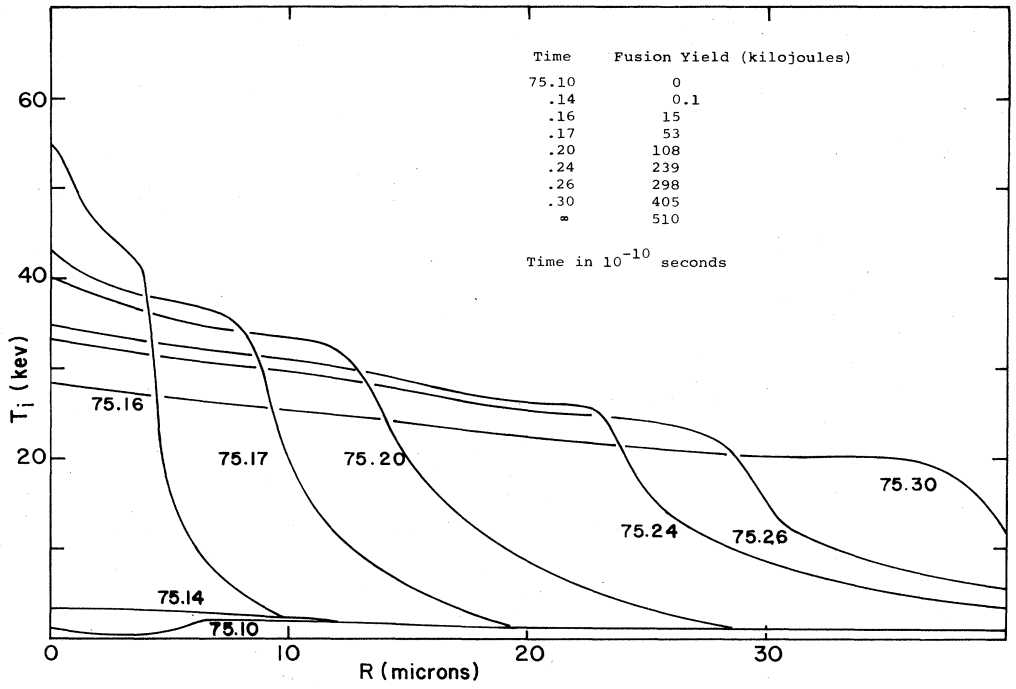

FIG. 21. Burning front for Case 1.

neodymium glass laser. The N_2–CO_2 laser, the development of which is relatively advanced, is at 10.6 μm for which the critical plasma density, into which the laser can directly penetrate, is about 1% of the critical density at 1 μm. The classical absorption coefficient is also reduced by a factor of about 100. Another problem arises from energy transfer from the laser deposition region through the overdense conduction zone. The maximum rate of energy transport per unit area out of the critical density region by electrons may easily be shown to be

$$\varphi_e = \tfrac{1}{4} n_c \theta_e^{3/2} v_e \ . \tag{8.1}$$

The critical density is

$$n_c = 10^{21}/\lambda(\mu\text{m})^2 \text{ cm}^{-3} \tag{8.2}$$

giving a flux limit

$$\varphi_e \cong 10^{14} \theta_e \text{ (keV)}^{3/2} \lambda^{-2} (\mu\text{m}) \text{ (W/cm}^2\text{)}. \tag{8.3}$$

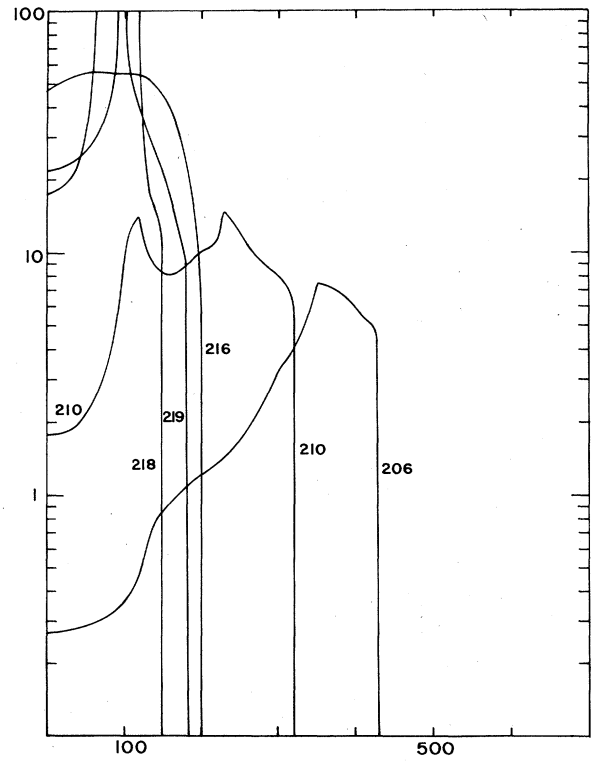

FIG. 22. Late time density profiles for DT initially in a shell of 3.15 mm outer radius and 5% shell thickness (Case 2). The curves are labeled by the time in units of 10^{-10} sec .

For the example of 60 kJ laser energy given in Sec. V, the energy input in the underdense laser deposition region reaches a maximum of approximately 10^{16} W/cm^2. This can be achieved at wavelength of 1 μm for an electron temperature of about 20 keV. At 10 μm, however, the maximum flux is far too low unless much higher electron temperatures are reached. This requirement brings the plasma condition well into the range of laser-plasma coupling instabilities. According to our present understanding, the 10 μm laser can be used successfully only if large anomalies exist both in laser-plasma coupling and in energy transport from the laser deposition region into the dense fusion pellet. These anomalies also give rise to serious electron-preheat problems, as discussed in Sec. V.F.

Lasers at wavelengths shorter than 1 μm do not presently appear to be required for tests of the principles of laser-driven fusion, but may offer advantages in eventual practical applications. In addition, the classical laser-plasma interaction at the critical density is inversely proportional to the square of the laser wavelength. If the

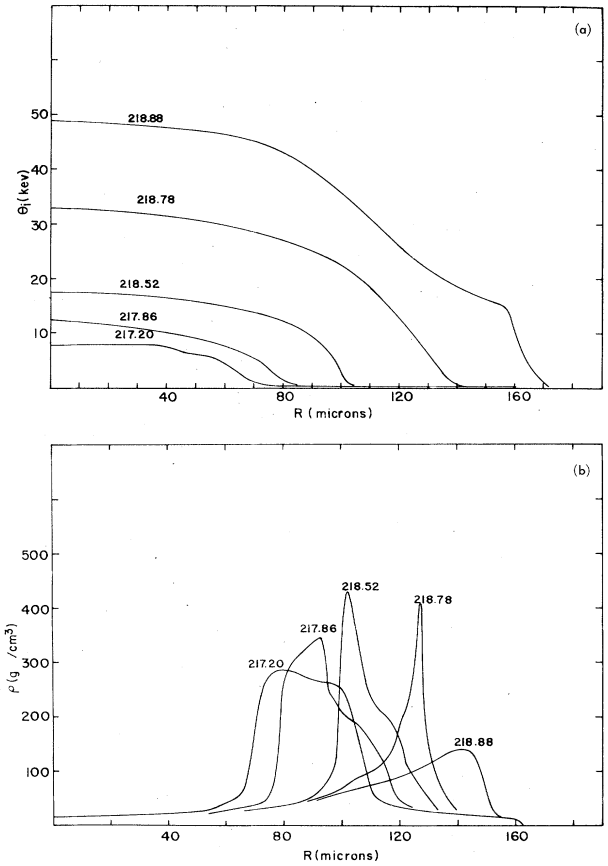

FIG. 23. Density and temperature histories after central ignition for a DT shell with initial outer radius of 3.15 mm and shell thickness of 5% (Case 2). The temperature rises rapidly in the relatively low density central region giving subsequent ignition of the highly compressed shell of fuel at larger radius. This dense shell is accelerated outward before the shell has ignited by the high pressure in the central fuel region. The curves are labeled by time measured in units of 10^{-10} sec .

plasma coupling problem is serious, use of shorter wavelengths may be necessary. This question will be much clarified by the presently planned experiments.

IX. SUMMARY AND CONCLUSIONS

Laser-driven fusion may be briefly characterized as the use of a laser as an energy source to drive the surface ablation of a spherical fuel pellet, with the rapid expansion of the ablation products providing the pressure to produce a spherical pellet implosion. Optimization of the time development of the implosion allows high compression of a pellet in which shock heating at the center of convergence of the implosion brings the DT fuel to the temperature at which the thermonuclear energy production exceeds the radiation loss rate. For a highly compressed pellet initially heated over a volume with dimensions of the α-particle range, the α-particle energy deposition produces a rapid temperature rise with a corresponding very rapid rise in the thermonuclear reaction rate. The fuel then ignites locally, with further heating bringing the temperature to several tens of kilovolts. The α-particle range now exceeds the dimension of the initial reacting region and the energy is deposited in the adjacent relatively cold fuel, causing it to ignite. The result is the formation of a spherically expanding burning front which expands into the rest of the fuel at supersonic speed, igniting the fuel before appreciable hydrodynamic motion can occur.

The uncertainties in the predictions arise principally from possible anomalies in the laser-plasma coupling which may also produce anomalies in the energy transport coefficients. Other uncertainties arise from possible loss of symmetry in the pellet compression due to intrinsic pellet asymmetries, laser illumination nonuniformity, or hydrodynamic instability in the pellet compression. The present theories and computations strongly suggest that substantial fusion energy may be produced in a laser-driven pellet implosion, but experimental confirmation is not yet available, even for some of the more elementary parts of the phenomena.

We, therefore, expect to see in 1973 and 1974 crucial tests of the laser fusion process. If these tests confirm the predictions of the present theories, study of the practical consequences for fusion power production will no doubt be greatly intensified.

ACKNOWLEDGMENTS

We gratefully acknowledge the assistance of Dr. R. Grandey, R. Janda, Dr. R. Cover, and Dr. D. Tanner with the numerical calculations, which were carried out at KMS Fusion, Inc.

REFERENCES

Abramowitz, M. and I. Stegun, Eds., *Handbook of Mathematical Functions* (U S. Government Printing Office, Washington, D. C) (1964)

Aliev, Y. M., and V. P. Silin, 1965, Zh. Eksp. Teor. Fiz. **48,** 901 [Sov. Phys. JETP **21,** 601 (1965)].

Allen, C. W., *Astrophysical Quantities* (Univ. of London, The Athlone Press) (1965)

Arnold, W. R., J. A. Phillips, G. A. Sawyer, E. J. Stoval, and J. L. Tuck, 1954, Phys. Rev. **93,** 483.

Basov, N. G., and O. N. Krokhin, 1964, Zh. Eksp. Teor. Fiz. **46,** 171 (1964) [Sov. Phys. JETP **19,** 123 (1964)]

Basov, N. G., and O. N. Krokhin, 1964, *Proceedings of the Third International Congress on Quantum Electronics* (Columbia U. P., New York).

Basov, N. G., and O. N. Krokhin, 1970, Vestn. Akad. Nauk SSSR **6,** 55.

Basov, N. G., O. N Krokhin, and G. V. Sklizkov, 1972, Heating of Laser Plasmas for Thermonuclear Fusion, *Laser Interaction and Related Phenomena,* (Plenum Press, New York), p. 389.

Bers, A., and R. J. Briggs, 1963, M. I. T. Laboratory of Electronics Quarterly Report No. 71, p. 122.

Bobin, J. L., 1971, Phys. Fluids **14,** 2341.

Bobin, J. L., D. Colombant, and G. F. Tonon, 1971, Fusion by Laser-Driven Flame Propagation in Solid DT Targets, Preprint.

Bobin, J. L., M. Decroisette, B. Meyer, and Y. Vitel, 1973, Phys. Rev Lett. **30,** 594.

Bodner, S. E., (private communication)

Bodner, S. E., G. F. Chapline, and J. DeGroot, 1973, Plasma Phys. **15,** 21.

Bodner, S. E., and J. L. Eddleman, 1971, Lawrence Livermore Laboratory Report No. UCRL-73378.

Briggs, R. J., 1964, *Electron-Stream Interaction with Plasmas* (M. I. T. Press, Cambridge, Mass.).

Brueckner, K. A. and H. Brysk, 1973, J. Plasma Phys **10,** 141.

Brueckner, K. A., H. Brysk, and R. S. Janda, 1974, Athermal Neutrons and Ions in a Fusion Plasma, submitted for publication in J.Plasma Phys.

Brueckner, K. A., and S. Jorna, 1973, Phys. Fluids **16,** 2350.

Brysk, H. 1973, Plasma Phys. **15,** 611.

Brysk, H., 1974, Electron-Ion Equilibration in a Partially Degenerate

Plasma, submitted to Plasma Phys.
Caruso, A., B. Bertotti, and P. Guipponi, 1966, Nuovo Cimento B **45,** 176
Caruso, A., and R. Gratton, 1968, Plasma Phys. **10,** 867.
Chandrasekhar, S., 1924, *Principles of Stellar Dynamics* (U. Chicago Press, Chicago), Chap. 2.
Chandrasekhar, S., 1961, *Hydrodynamics and Hydromagnetic Stability* (Clarendon Press, Oxford).
Chase, J. B., J. M. LeBlanc, and J R. Wilson, 1973, Phys. Fluids **16,** 1142.
Chu, M. S., 1970, Bull. Am. Phys. Soc. **15,** 1431.
Chu, M. S., 1972, Phys. Fluids **15,** 413.
Chu, T. K., and H. W. Hendel, 1971, Bull. Am. Phys. Soc. **16,** 1297.
Chu, T. K., H. W. Hendel, and J. M. Dawson, 1972, Comments on Plasma Physics and Controlled Fusion, **1,** 111.
Daiber, J. W., A. Hertzberg, and C. E. Wittliff, 1966, Phys. Fluids, **9,** 617.
Dawson, J. M., 1964, Phys. Fluids **7,** 981.
Dawson, J. M., P. Kaw, and B. Green, 1969, Phys. Fluids **12,** 875.
Denisov, N. G., 1956, Zh. Eksp. Teor. Fiz. **31,** 609 [Sov. Phys. - JETP **4,** 544 (1957)]
Dreicer, H., D. B. Henderson, and J. C. Ingraham, 1961, Phys. Rev. Lett. **26,** 1618.
DuBois, D. F., and M. V. Goldman, 1967, Phys. Rev. **164,** 207.
DuBois, D. F., and M. V. Goldman, 1972, Phys. Rev. Lett. **28,** 218.
Eidman, K. and R. Sigel, 1972, paper delivered at the *International Conference on the Interaction of Lasers with matter*, Marly Le Roi, 9-13 October, 1972.
Eubank, H. P., 1971, Phys. Fluids **14,** 2551.
Fader, W. J., 1968, Phys. Fluids **11,** 2200.
Fainberg, Y. B., V. I. Kurilko, and V. D. Shapiro, 1961, Zh. Tekh. Fiz. **31,** 633 (1961) [Sov. Phys.-Tech. Phys. **6,** 459 (1961)]
Forslund, D. W., J. M. Kindel, and E. L. Lindman, 1972, Phys. Rev. Lett. **29,** 249.
Franklin, R. N., S. M. Hamberger, G. Lampis, and G. J. Smith, 1971, Phys. Rev. Lett. **27,** 1119.
Freidberg, J. P., R. W. Mitchell, R. L. Morse, and L. I. Rudsinski, 1972, Phys. Rev. Lett. **28,** 795.
Galeev, A. A., G. Laval, T. M. O'Neill, M. N. Rosenbluth, and R. Z. Sagdeev, 1973, Zh. Eksp. Teor. Fiz. Pis'ma Red. **17,** 48 [JETP Lett. **17,** 35 (1973)]
Gaunt, J. A., 1930, Proc. R. Soc. A **126,** 654.
Gekker, I. E., and O. V. Sizukhin, 1969, Zh. Eksp. Teor. Fiz. Pis'ma Red. **9,** 408 [JETP Lett. **9,** 243(1969)]
Goldman, E. B., 1972, Plasma Phys. **15,** 289.
Gorbunov, L. M., 1968, Zh. Eksp. Teor. Fiz. **55,** 2298 [Sov. Phys.-JETP **28,** 1220 (1969)]
Guderley, von G., 1942, Luftfahrt-Forschung **9,** 302.
Hall, L. S., and W. Heckrotte, 1968, Phys. Rev. **166,** 120.
Haught, A. F., and D. H. Polk, 1966, Phys. Fluids **9,** 2047.
Haught, A. F., and D. H. Polk, 1966, in *Proceedings of the Conference on Plasma Physics and Controlled Nuclear Fusion Research, Culham 1965* (International Atomic Energy Agency, Vienna) (1966)
Haught, A. F., D. H. Polk, J. C. Woo, and W. J. Fader, 1968, "Production of Plasmas for Thermonuclear Research by Laser Beam Irradiation of Solid Particles." United Aircraft Corp., Semiannual Report, August, 1968 - December 31, 1968, NYO–3578-10.
Heitler, W., 1954, *The Quantum Theory of Radiation*, (Oxford U. P., Oxford), 3rd ed.
Hochstim, A. R., 1969, Ed., *Kinetic Processes in Gases and Plasma* (Academic, New York), Chap. VI.
Hubbard, W. B., and M. Lampe, 1969, Astrophys. J. Suppl. Ser. No. 163, **18,** 297.
Hughes, D. J. and R. B. Schwartz, 1958, Eds., Neutron Cross Sections, Brookhaven National Lab., Report No. 325 (U. S. Government Printing Office), p. 58.
Jackson, E. A., 1967, Phys. Rev. **153,** 235.
Johnson, R. R. and R. B. Hall, 1971, J. Appl. Phys. **42,** 1035.
Jorna, S., 1973, "Laser-Induced Instabilities in Homogeneous Plasmas," Phys. Fluids (April 1974).
Kaw, P. K., and J. M. Dawson, 1969, Phys. Fluids **12,** 2586.
Kidder, R. E., 1968, Nucl. Fusion **8,** 3.
Krall, N. A., and A. W. Trivelpiece, 1973, *Principles of Plasma Physics* (McGraw-Hill, New York).
Krokhin, O. N., 1965, Z. Angew. Math. u. Phys. **16,** 123.
Krokhin, O. N., 1971, in *Physics of High Energy Density*, edited by P. Calderola and H. Knoepfel (Academic, New York).
Kruer, W. L. and Dawson, J. M., 1972, Phys. Fluids **15,** 446.
Kruer, W. L., P. K. Kaw, J. M. Dawson, and C. Oberman, 1970, Phys. Rev. Lett. **24,** 987.
Latter, R., 1944, Phys. Rev. **99,** 1843.
Lawson, J. D., 1957, Proc. Phys. Soc. Lond. B**70,** 6.
Lee, Y. C. and C. M. Su, 1966, Phys. Rev. **152,** 129.
Louisell, W. H., 1960, *Coupled Mode and Parametric Electronics* (Wiley, New York).
Lubin, M. J. Goldman, E. B., and K. Yuan, 1971, Laboratory for Laser Energetics, Report No. 5, (University of Rochester) unpublished.
Miller, J. C. P., 1955, *Tables of Weber Parabolic Cylinder Functions* (H. M. Stationery Office, London).
Morse, R. L. and C. W. Nielson, 1972, Occurrence of High Energy Electrons and Surface Expansion in Radiantly Heated Target Plasmas, LASL Report No. LA-4986-MS.
Mulser, P. and S. Witkowski, 1969, Phys. Lett. A**28,** 703.
Nishikawa, K., 1968, J. Phys. Soc. Jap. **24,** 1152.
Nuckolls, J., L. Wood, A. Thiessen, and G. Zimmerman, 1972, Nature **239,** 139.
Oster, L., 1960, Rev. Mod. Phys. **32,** 141.
Perkins, F. W. and J. Flick, 1971, Phys. Fluids **14,** 2012.
Phelps, D., N. Rynn, and G. Van Hoven, 1971, Phys. Rev. Lett. **26,** 688.
Polovin, R. V., 1961, Zh. Tekh. Fiz. **31,** 1220 [Sov. Phys. - Tech. Phys. **6,** 889 (1962)]
Post, R. F., 1956, Rev. Mod. Phys. **28,** 338.
Powell, M. J. D., 1964, Comput. J. **7,** 155.
Raizer, Yu.P., 1965, Zh. Eksp. Teor. Fiz. **48,** 1508 [Sov. Phys.–JETP **21,** 1009 (1965)].
Lord Rayleigh, 1883, Phil. Mag. **15** (1), 229.
Rosenbluth, M. N., 1972, Phys. Rev. Lett. **29,** 565.
Rosenbluth, M. N. and R. Z. Sagdeev, 1972, Comments on Plasma Physics and Controlled Fusion **1,** 129.
Salpeter, E. E. and H. S. Zapolsky, 1967, Phys. Rev. **158,** 876.
Shearer, J. W. and W. S. Barnes, 1970, Phys. Rev. Lett. **24,** 92.
Shearer, J. W., S. W. Mead, J. Petruzzi, F. Rainer, J. E. Swain, and C. E. Violet, 1972, Phys. Rev. A**6,** 764.
Shen, Y. R. and N. Bloembergen, 1965, Phys. Rev. **137,** 1787.
Sigmar, D. J. and G. Joyce, 1971, Nucl. Fusion **11,** 447.
Silin, V. P., 1964, Zh. Eksp. Teor. Fiz. **47,** 2254 [Sov. Phys.-JETP **20,** 1510 (1965)].
Spitzer, L. Jr., 1961, *Physics of Fully Ionized Gases*, 2nd ed. (Interscience, New York).
Stamper, J. A., K. Papadopoulos, R. N. Sudan, S. O. Dean, E. A. McLean, and J. M. Dawson, 1971, Phys. Rev. Lett. **26,** 1012.
Stenzel, R. and A. Y. Wong, 1972, Phys. Rev. Lett. **28,** 274.
Stern, R. A. and N. Tzoar, 1966, Phys. Rev. Lett. **17,** 903.
Sturrock, P. A., 1958, Phys. Rev. **112,** 1488.
Taylor, G., 1950, Proc. R. Soc. A **201,** 192.
Tsytovich, V. N., 1970, *Non-Linear Effects in Plasma* (Plenum Press, New York and London).
Valeo, E., C. Oberman, and F. Perkins, 1972, Phys. Rev. Lett. **28,** 340.
Wandel, C. F., T. Hesselberg, and O. Kofoed-Hansen, 1959, Nucl. Instrum. Methods **4,** 249.
Wharton, C., in J. E. Drummond, 1961, *Plasma Physics* (McGraw-Hill, New York).
Whittaker, E. T. and G. N. Watson, 1927, *A Course of Modern Analysis* (Cambridge U.P., Cambridge, England).
Yamanaka, C., T. Yamanaka, T. Sasaki, K. Yoshida, M. Waki, and H. B. Kang, 1972, Phys. Rev. A**6,** 2335.
Zakharov, S. D., O. N. Krokhin, P. G. Kryukov, and E. L. Tyurin, 1970, JETP Lett. **12,** 36 (1970)
Zhekulin, L. A., 1934, Zh. Eksp. Teor. Fiz. **4,** 76 [Sov. Phys. - JETP **4,** 76 (1934)].